Partnership for AiR Transportation
Noise and Emissions Reduction

Environmental Cost-Benefit Analysis of Ultra Low Sulfur Jet Fuel

PARTNER Project 27 Final Report

prepared by
Christopher K. Gilmore, Steven R. H. Barrett, Steve H. L. Yim, Lee T. Murray, Stephen R. Kuhn, Amos P. K. Tai, Robert M. Yantosca, Daewon W. Byun, Fong Ngan, Xiangshang Li, Jonathan I. Levy, Akshay Ashok, Jamin Koo, Hsin Min Wong, Olivier Dessens, Sathya Balasubramanian, Gregg G. Fleming, Matthew N. Pearlson, Christoph Wollersheim, Robert Malina,, Sarav Arunachalam, Francis S. Binkowski, Eric M. Leibensperger, Daniel J. Jacob, James I. Hileman, Ian A. Waitz

December 2011

REPORT NO. PARTNER-COE-2011-006

Environmental Cost-Benefit Analysis of Ultra Low Sulfur Jet Fuel

A report to the U.S. Federal Aviation Administration Office of Environment and Energy

Christopher K. Gilmore[1], Steven R. H. Barrett[1], Steve H. L. Yim[1], Lee T. Murray[2], Stephen R. Kuhn[1], Amos P. K. Tai[2], Robert M. Yantosca[2], Daewon W. Byun[3], Fong Ngan[3], Xiangshang Li[4], Jonathan I. Levy[5], Akshay Ashok[1], Jamin Koo[1], Hsin Min Wong[1], Olivier Dessens[6], Sathya Balasubramanian[7], Gregg G. Fleming[7], Matthew N. Pearlson[1], Christoph Wollersheim[1], Robert Malina[1,8], Sarav Arunachalam[9], Francis S. Binkowski[9], Eric M. Leibensperger[10], Daniel J. Jacob[2], James I. Hileman[1], and Ian A. Waitz[1]

[1] Department of Aeronautics and Astronautics, Massachusetts Institute of Technology, Cambridge, Massachusetts, USA; [2] School of Engineering and Applied Sciences, Harvard University, Cambridge, Massachusetts, USA.[3] Air Resources Laboratory, National Oceanic and Atmospheric Administration, Silver Spring, Maryland, USA;[4] Department of Earth and Atmospheric Sciences, University of Houston, Houston, Texas, USA;[5] Department of Environmental Health, Boston University School of Public Health, Boston, Massachusetts, USA;[6] Centre for Atmospheric Sciences, University of Cambridge, Cambridge, UK;[7] Volpe National Transportation Systems Center, Cambridge, Massachusetts, USA;[8] Institute of Transport Economics, University of Muenster, Muenster, Germany;[9] Institute for the Environment, University of North Carolina at Chapel Hill, North Carolina, USA;[10] Department of Earth, Atmospheric and Planetary Sciences, Massachusetts Institute of Technology, Cambridge, Massachusetts, USA.

Steven R. H. Barrett is the corresponding author. He may be reached at sbarrett@mit.edu

Report No. PARTNER-COE-2011-006
December 2011

This work was funded by the U.S. Federal Aviation Administration Office of Environment and Energy, under FAA Cooperative Agreement No. 06-C-NE-MIT, Amendment Nos. 010, 015, 022, and 025 (with U. of Houston Subaward No. 5710002426 and U. of Cambridge Subaward No. 5710002636); and FAA Cooperative Agreement No. 07-C-NE-SU, Amendment No. 002, and FAA Cooperative Agreement No. 09-C-NE-MIT, Amendment Nos. 003 and 010. The project was managed by S. Daniel Jacob. Any opinions, findings, and conclusions or recommendations expressed in this material are those of the authors and do not necessarily reflect the views of the FAA, NASA, Transport Canada, the U.S. Department of Defense, or the U.S. Environmental Protection Agency.

The Partnership for AiR Transportation Noise and Emissions Reduction — PARTNER — is a cooperative aviation research organization, and an FAA Center of Excellence sponsored by the FAA, NASA, Transport Canada, the U.S. Department of Defense, and the U.S. Environmental Protection Agency. PARTNER fosters breakthrough technological, operational, policy, and workforce advances for the betterment of mobility, economy, national security, and the environment. The organization's operational headquarters is at the Massachusetts Institute of Technology.

The Partnership for AiR Transportation Noise and Emissions Reduction
Massachusetts Institute of Technology, 77 Massachusetts Avenue, 33-240
Cambridge, MA 02139 USA http://www.partner.aero

ENVIRONMENTAL COST-BENEFIT ANALYSIS OF ULTRA LOW SULFUR JET FUEL

A report to the U.S. Federal Aviation Administration Office of Environment and Energy by Christopher K. Gilmore[1], Steven R. H. Barrett[1*], Steve H. L. Yim[1], Lee T. Murray[2], Stephen R. Kuhn[1], Amos P. K. Tai[2], Robert M. Yantosca[2], Daewon W. Byun[3], Fong Ngan[3], Xiangshang Li[4], Jonathan I. Levy[5], Akshay Ashok[1], Jamin Koo[1], Hsin Min Wong[1], Olivier Dessens[6], Sathya Balasubramanian[7], Gregg G. Fleming[7], Matthew N. Pearlson[1], Christoph Wollersheim[1], Robert Malina[1,8], Sarav Arunachalam[9], Francis S. Binkowski[9], Eric M. Leibensperger[10], Daniel J. Jacob[2], James I. Hileman[1] and Ian A. Waitz[1].

[1] Department of Aeronautics and Astronautics, Massachusetts Institute of Technology, Cambridge, Massachusetts, USA; [2] School of Engineering and Applied Sciences, Harvard University, Cambridge, Massachusetts, USA.[3] Air Resources Laboratory, National Oceanic and Atmospheric Administration, Silver Spring, Maryland, USA;[4] Department of Earth and Atmospheric Sciences, University of Houston, Houston, Texas, USA;[5] Department of Environmental Health, Boston University School of Public Health, Boston, Massachusetts, USA;[6] Centre for Atmospheric Sciences, University of Cambridge, Cambridge, UK;[7] Volpe National Transportation Systems Center, Cambridge, Massachusetts, USA;[8] Institute of Transport Economics, University of Muenster, Muenster, Germany;[9] Institute for the Environment, University of North Carolina at Chapel Hill, North Carolina, USA;[10] Department of Earth, Atmospheric and Planetary Sciences, Massachusetts Institute of Technology, Cambridge, Massachusetts, USA.

Contents

EXECUTIVE SUMMARY

Executive Summary

Aircraft emissions can reduce air quality, leading to adverse health impacts including increased risk of premature mortality. A technically viable way to mitigate the health impacts of aviation is the use of desulfurized jet fuel, as has been done with road transportation in many jurisdictions. To attain levels of 15 ppm from the current average levels of 400-800 ppm would increase the cost of jet fuel by 1.6-6.6 ¢/gal, i.e. an increase in the cost of a gallon of just over 1% at 2011 prices. Although the environmental implications are complex, research indicates transitioning to an ultra-low sulfur jet fuel is likely to prevent 1000-4000 premature mortalities per year (if implemented globally), but may increase globally averaged climate warming caused by aviation by 1-8%.

Commercial aviation fuel (Jet A/A-1) contains sulfur at concentrations of 400-800 ppm, although there is significant variation. By contrast, US road transportation fuel is subject to an ultra-low sulfur fuel standard of 15 ppm, which is about 97% less than jet fuel. Other jurisdictions including Australia, Canada, New Zealand, Mexico, Japan, India, Argentina, Brazil, Chile, Peru and the European Union have instituted similar standards for road transportation. Marine fuels are being subjected to increasingly stringent standards too, but marine bunker fuels have higher sulfur content than aviation or road transportation fuels.

Sulfur in fuel results in the emission of SO_x (sulfur oxides) upon combustion. SO_x is predominantly a gas when emitted, but gets converted in the atmosphere to a form of fine particulate matter (i.e. small particles) called sulfate. Sulfate particles predominantly scatter solar radiation, some of it back into space, therefore offsetting a fraction of global warming, although whether this is climatically beneficial or not is a subject of continuing research. A second important effect of SO_x emissions is to increase the amount of fine particles that people inhale. There has been substantial quantitative evidence collected over decades that links human exposure to fine particulate matter to an increased risk of premature mortality and other adverse health effects. Finally, SO_x emissions result in acid rain and associated damages.

Jet fuel can be desulfurized in the same way as road transportation fuels. Jet fuel is chemically very similar to diesel and there are no significant technical challenges in doing this, although a

corrosion inhibitor/lubricity improver (CI/LI) may need to be added to the resultant fuel in order to prevent excessive component wear within engine fuel pumps. This is done routinely in the military and the cost is negligible compared to the cost of desulfurization. This hydrodesulfurization process will increase the cost of fuel by just over 1% at present-day prices, which maps to an industry total $1.3-3.8bn per year (in 2006 US$) if implemented globally, or $0.5-1.4bn per year for the US alone.

The dominant adverse environmental result of desulfurization is that removing sulfur from fuel results in increased CO_2 emissions because hydrodesulfurization involves the release of relatively small amounts of CO_2 and consumes additional energy. A second potentially adverse effect is that the reflection of solar radiation into space by sulfate particles would be reduced. In combination, these are estimated to increase the globally-averaged climate warming caused by the production and use of a gallon of jet fuel by 1-8% if it is desulfurized.

Using benefit-cost analysis techniques, the monetized climate damage due to global implementation of ultra-low sulfur jet fuel (ULSJ) is $0.1-4.3bn per year, which is a net present value with an applied 3% discount rate. The discount rate defines the charged interest rate on a value stream, be it a cost or benefit, in one year compared to the following year. This means that the higher the discount rate, the less future costs or benefits are valued relative to the base year. The magnitude of the discount rate defines the annual percentage reduction in value a cost or benefit undergoes as compared to the previous year. Of these damages, $0.01-0.7bn is incurred in the US. If only the US implements ULSJ, the damages in the US are $0.00-0.2bn per year.

ULSJ would prevent 1000-4000 premature mortalities per year globally due to a modeled reduction in ground-level fine particulate matter, of which about 5% are in the US. When US-only implementation is considered, ULSJ causes a reduction of about 80 premature mortalities per year in the US.

While a reduction in premature mortalities is relatively confidently predicted, the monetization of these mortalities depends on the approach. The US EPA recommends the use of a single (but uncertain) value of statistical life for analyses within the US. If this approach is applied to all avoided premature mortalities globally, ULSJ results in $1.2-47bn of health benefits each year

globally. In the US, global implementation of ULSJ results in $0.06-2.4bn of benefits per year. If only the US implements ULSJ, the air quality benefits in the US are $0.04-1.5bn per year.

Applying the US EPA value of statistical life globally means that there is an 84% chance that ULSJ is net beneficial, i.e. the public health benefits exceed the additional fuel production costs and climate damages. However, economists argue that there is no economic rationale for applying a single value of statistical life because incomes vary greatly around the world and so willingness to pay for reductions in mortality risk varies. If country-specific values of statistical life are used – which are derived considering country-specific income levels and are uncertain as well – then there is an 83% chance that ULSJ is not cost-beneficial on net. This is because the majority of mortality reduction occurs in developing countries where monetized health benefits outside the US are decreased due to lower income levels.

An important point is that in all these cases the uncertainties are such that the net difference between the benefits and costs of ULSJ does not statistically differ from zero. However, the most likely scenario is that ULSJ would save thousands of lives if implemented globally, increase aviation-related globally averaged climate warming by 1-8%, and increase fuel costs by at least 1%. An argument for transitioning to an ultra-low sulfur jet fuel is that the health benefits are highly likely and the industry could work to offset the additional 1-8% of increased warming by reducing greenhouse gas emissions.

REPORT

1. Introduction

1.1. Context

Aircraft emissions impact the environment by perturbing the climate[1] and reducing air quality[2], which leads to adverse health impacts including increased risk of premature mortality[2,3,4]. Aircraft landing and takeoff (LTO) emissions – i.e. emissions below 3000 ft above ground level – have been estimated to cause approximately 200 air quality-related premature mortalities per year in the US[4,5]. While engine emissions standard certification reflects only LTO activity, Barrett et al.[2] estimated that full-flight aircraft emissions result in nearly 10,000 premature mortalities per year globally, with the majority of impacts due to non-LTO emissions. With global aviation demand forecast to grow at an average of 5% per year through 2030[6], aircraft emissions and associated impacts may more than double within 20 years[3] with an even greater increase in public health impacts given population growth and changing non-aviation emissions influencing secondary particulate matter formation[7]. In this report, results are presented from a comprehensive benefit-cost analysis of transitioning to a system wide use of ultra-low sulfur jet fuel. We denote this as "ULSJ" for brevity.

In 2006, UK Jet A-1, US Jet A and US Department of Defense JP-8 fuel had an average fuel sulfur content (FSC) between 550 to 750 ppm (by mass),[8] well below the specification limit of 3000 ppm[9,10]. In 2006 the US introduced an ultra-low sulfur standard for highway diesel of 15 ppm.[11] Jurisdictions including Australia, Canada, New Zealand, Mexico, Japan, India, Argentina, Brazil, Chile, Peru and the European Union all have instituted fuel sulfur standards of 50 ppm or less effective by 2016 for road transportation. We adopt a baseline FSC for civil aviation of 600 ppm, and assess the implications of a ULSJ policy case of 15 ppm.

1.2. Overview

We approach assessing the implications of ULSJ by determining the change in emissions and costs associated with desulfurization, where costs are estimated using two approaches. Changes in emissions are propagated to three atmospheric chemistry-transport models (CTMs) to estimate the effect of ULSJ on atmospheric composition, where the policy "delta" is identified as the difference in atmospheric composition between simulations with all emissions at their nominal

values and simulations where aviation SO_x emissions have been reduced by 585/600 = 97.5%. The reduction in atmospheric sulfate loading due to lower aviation SO_x emissions is mapped to a radiative forcing (RF) and the change in lifecycle CO_2 emissions is estimated. Changes in fine particulate matter ($PM_{2.5}$) concentrations at the surface are overlaid on population density data to determine changes in human exposure to $PM_{2.5}$ by country. [This is on the basis that the majority of air quality-related health impacts are captured by considering $PM_{2.5}$.[4]] Epidemiological concentration-response functions (CRFs) relate changes in $PM_{2.5}$ exposure to expected changes in premature mortality, with consideration of variability across countries. Country-specific values of statistical life (VSL) are estimated to monetize air quality benefits of ULSJ. Short- and long-term climate impacts are monetized using a simplified impulse-response climate model and damage functions. Monetized costs, benefits and disbenefits are aggregated into an overall benefit-cost analysis.

Where possible, uncertainties in parameters are estimated and propagated throughout the analysis, for which a Monte Carlo approach is used. An important atmospheric modeling uncertainty considered in detail is that of vertical transport of pollution from cruise altitudes to the surface, which we assess by comparing model simulations to measurements of relevant tracers.

2. Methods and Assumptions

2.1. Fuel Properties

We define baseline jet fuel as having a FSC of 600 ppm and to be 86.2wt% C.[8] ULSJ fuel with a FSC of 15 ppm is assumed to be obtained from baseline jet fuel by hydrodesulfurization (HDS), requiring H_2 created from refinery operations and steam reformation of natural gas. With assumptions detailed in the technical annexes (TA), we estimate the change in operating energy inputs to produce ULSJ instead of conventional petroleum. The largest share of this is an increase of refinery and natural gas consumption of 0.018 scm/L (standard cubic meters of gas per liter of jet fuel). Accounting for both CO_2 produced from HDS – which is assumed to be vented to the atmosphere – and overall process energy efficiency, we estimate a 2% increase in lifecycle CO_2 emissions for jet fuel associated with desulfurization, with bounds of 0-4%.

ULSJ fuel has 1% lower energy density and 0.3% higher specific energy relative to baseline fuel[8] and may need a corrosion inhibitor/lubricity improver (CI/LI) additive. ULSJ fuel could also have reduced aromatic composition, relative to conventional jet fuel, and this could result in reduced black carbon emissions. Implications of these factors for emissions are neglected since they are not expected to significantly impact the overall benefit-cost analysis results.

2.2. Emissions

Baseline civil aviation emissions of NO_x, SO_x, hydrocarbons (HC), black carbon (BC) and organic carbon (OC) are calculated using the FAA's aviation environmental design tool (AEDT)[12] for 2006. We estimate total fuel burn for 2006 at 188 Tg. This corresponds to 0.11 Tg of fuel-S, of which 98% is assumed to be emitted as SO_2 and the remaining 2% as S(VI).[13] Aircraft SO_2 emissions currently account for approximately 0.5% of total SO_x emissions within the US.[14] Other assumptions are detailed in the TA and are similar to Barrett et al.[2]

Hourly emissions are gridded from raw AEDT output for each CTM applied. For the ULSJ policy case, aircraft SO_x emissions are reduced by 97.5%. In addition to the baseline and ULSJ cases, corresponding cases are also assessed where only LTO emissions are accounted, to

understand the relative contribution of LTO versus cruise emissions. Lifecycle CO_2 emissions are included in climate modeling.

2.3. Chemistry-Transport Modeling

Three CTMs are used – GEOS-Chem[15], CMAQ[16] and p-TOMCAT[17]. GEOS-Chem is driven by GEOS-5 meteorological data from the NASA Global Modeling and Analysis Office (GMAO) with 0.5°×0.667° horizontal resolution. We apply it at a horizontal resolution of 4°×5° globally, but with native 0.5°×0.667° resolution in a nested domain encompassing the contiguous US. Time-varying boundary conditions for the nested domain are taken from the global 4°×5° simulation. CMAQ is applied at a 36 km resolution for the contiguous US with time-varying boundary conditions from GEOS-Chem. A ±60% uncertainty in population-weighted $PM_{2.5}$ is applied.[2]

MM5 is used to generate meteorology for CMAQ with GEOS-5 data as boundary and initial conditions. As such meteorology for CMAQ is consistent with GEOS-Chem. p-TOMCAT is used in an ancillary way (see TA). All simulations were for 15 months, using October 2005 to December 2006 (inclusive) meteorology. The first three months are discarded as spin-up time so that steady state impacts are considered.

2.4. Climate Impacts

Warming related to (i) increased lifecycle CO_2 emissions from HDS and (ii) decreased SO_x emissions resulting in decreased direct aerosol cooling are considered. GEOS-Chem online calculations of aerosol optical depth for sulfates, nitrates, and ammonium (collectively called "sulfates") are related to radiative forcing (RF) (see TA). This short-lived sulfate RF is incorporated into the aviation environmental portfolio management tool (APMT)-Impacts Climate Module,[18] which is used to assess the difference in climate impacts of a one year pulse of emissions under the baseline and ULSJ scenarios. The forcing associated with sulfate is assumed to decay instantaneously after the one year pulse of emissions ends,[18] while the carbon cycle implemented in APMT means that the CO_2 RF survives hundreds of years after the policy year being assessed. APMT monetizes climate impacts as described in Mahashabde et al.[18]

2.5. Health Impacts

The metric chosen for health impacts is premature mortalities due to long-term exposure to $PM_{2.5}$ as this is likely to capture approximately 80% of the monetized health impacts of air pollution.[4] As done elsewhere,[19] we derive a CRF of an approximate 1% decrease in all-cause mortality in the US per 1 $\mu g/m^3$ decrease in annual average concentrations of $PM_{2.5}$, based on a Weibull distribution fit to the two major cohort studies in the US[20,21]. This value is comparable to the average value across the median estimates from experts in a recent EPA expert elicitation study[22,23]. We use lower and upper bound values of 0.4% and 1.8%, respectively, reflecting the uncertainty bounds from the Weibull distribution and comparable to the corresponding percentiles in the expert elicitation study. Results are similar to an EU expert elicitation study.[24]

Two issues arise in applying this CRF outside of the US. First, disease patterns may differ significantly from the US. To adjust for differences in contributors to baseline mortality, we assume that air quality-related premature mortalities are dominated by cardiopulmonary disease and lung cancer, an assumption that is justified within the TA. We derive disease-specific CRFs in a manner that correspond to the aforementioned all-cause mortality CRF, and apply these to other countries with different baseline disease rates. The method is detailed in the TA.

Second, the slope of the CRF may not be linear through the range of concentrations observed globally. Prior work by the WHO in the context of global burden of disease modeling[25] used a log-linear rather than linear CRF to yield lower slope at higher concentrations, providing more realistic burden of disease estimates in developing countries. As the EPA CRF described above reflects more recent interpretations of health evidence in the US, we use it for our study, but test the sensitivity of our findings to the use of the WHO methodology.

2.6. Benefit-Cost Analysis

HDS of jet fuel is considered as a cost, and monetized climate disbenefits due to reduction of sulfate (direct) cooling and increased lifecycle CO_2 are accounted for. Benefits due to reduction in premature mortality globally are monetized.

Valuation of avoided premature mortalities in the US is based on a Weibull distribution fit to 26 wage-risk and contingent valuation studies, as done elsewhere[19]. The resulting VSL distribution (in 2006US$, based on 1990 income levels) had a mean of $7.4m with lower and upper bounds of $1m and $12m, respectively. To develop appropriate VSL estimates for other countries, we used the gross national income for each country and an income elasticity range of 1-2, except where the resulting VSL would be less than the net present value of half lifetime earnings.[26] The EPA mortality lag structure is used in this analysis.[19] It assumes that 30% of avoided mortalities are seen in the year of implementation, 50% in years 2-5, and the remaining 20% spread out over years 6-20.

A range for the cost of HDS is estimated using two methods. First, historical US highway diesel prices are analyzed to determine the spread between ultra-low sulfur (<15 ppm) and low sulfur (15-500 ppm) fuel, and low sulfur and high sulfur (>500 ppm) fuel. Second, the cost of natural gas and capital investment required for HDS is estimated.

Monetized climate disbenefits are calculated by APMT-Impacts for a one-year pulse of emissions with discount rates of 2%, 3% and 7%. Discount rate choice affects the valuation of lifecycle CO_2 disbenefits and health benefits of ULSJ as it defines the charged interest rate on a value stream, be it a cost or benefit, in one year compared to the following year. This means that the higher the discount rate, the less future costs or benefits are valued relative to the base year. Discount rate is treated as a policy choice – not an uncertainty – because it is a quantitative expression of the extent to which costs and benefits in the future are valued relative to costs and benefits now.

Costs, benefits and disbenefits are aggregated using a Monte Carlo analysis with input variables assigned triangular distributions corresponding to the lower, nominal and upper values described. Results are given as an expectation with a 95% confidence interval (CI). Sensitivities to

individual parameters are calculated with all other values held at their nominal value, and main and total effect indices are calculated.

3. Results

3.1. Surface PM2.5 Impacts

Figure 1 shows results from GEOS-Chem for the change in aviation-attributable annual average surface sulfate concentration for 2006. High resolution nested GEOS-Chem results are superimposed on the US, where it can be seen that boundaries match most closely in upwind directions. Localized (negative) peaks in the US correspond to locations of airports, the impacts of which are resolved by the high resolution nested domain. Elsewhere the widespread impacts are dominated by cruise emissions, which occur primarily over North America and Europe, but impact the surface by subsidence. The largest effects are in the strongly subsiding arid regions of the subtropics. Impacts do not penetrate the intertropical convergence zone (ITCZ).

Overall ULSJ decreases the surface average sulfate concentration by 9.6×10^{-4} μg/m^3 and ammonium by 2.54×10^{-4} μg/m^3. It increases nitrate by 2.7×10^{-5} μg/m^3 due to the greater availability of ammonia to form ammonium nitrate when sulfate decreases. Within the US, the nested GEOS-Chem simulation shows a 4.1×10^{-3} μg/m^3 decrease in sulfate and a 0.4×10^{-3} μg/m^3 increase in nitrate surface average concentration.

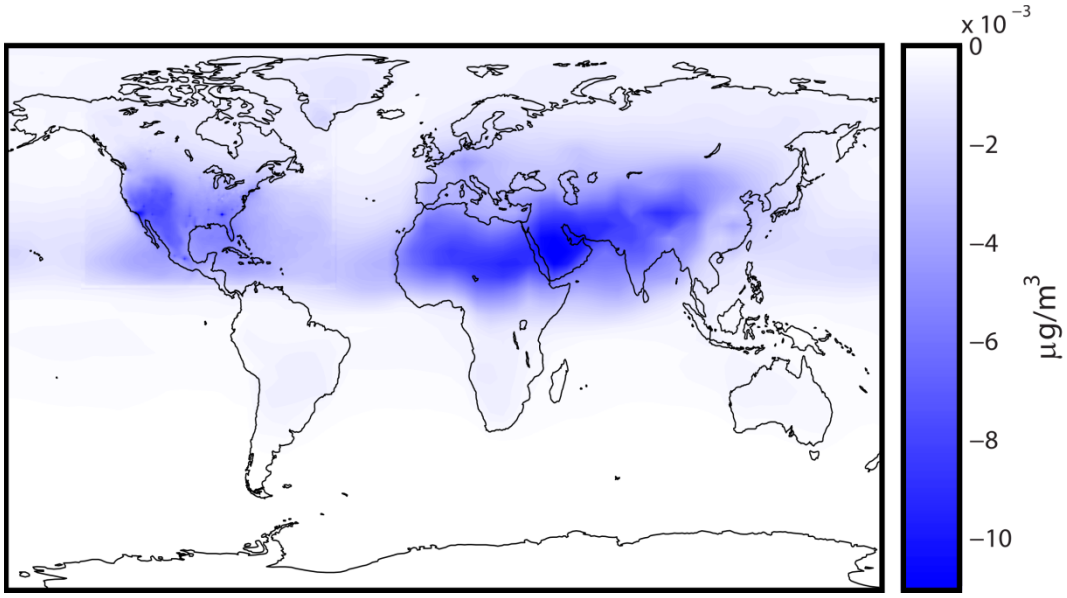

Figure 1. The annual average surface sulfate concentration change due to ULSJ as calculated by GEOS-Chem at 4°×5°, with nested 0.5°×0.667° results superimposed over the contiguous US.

3.2. Health Impacts

Using the EPA-derived CRF and global GEOS-Chem results, ULSJ causes a reduction of approximately 2300 premature mortalities per year (95% CI: 890-4200), of which about 120 are in the US (95% CI: 46-210) when changes in total ground-level $PM_{2.5}$ concentrations are considered. When US-only implementation is considered, approximately 77 premature mortalities are avoided within the US based on nested GEOS-Chem results. When only LTO emissions impacts are considered, CMAQ simulation results show nearly 80 avoided premature mortalities within the US when global implementation is considered. LTO simulation results by nested GEOS-Chem for the US due to global and US-only implementation both predict approximately 40 avoided premature mortalities.

Using results from nested GEOS-Chem in the contiguous US increases the mortalities avoided by ULSJ by 17%. Contiguous US CMAQ calculations indicate 85% more avoided premature

mortalities in the US than nested GEOS-Chem, or 92% greater than global GEOS-Chem. Applying the older WHO CRF as a sensitivity, ULSJ results in approximately 1500 avoided premature mortalities globally per year, of which approximately 140 are in the US. The global mortality estimate is reduced given the lower CRF applied in countries with higher ambient $PM_{2.5}$ concentrations, such as China and India.

Avoided premature mortalities estimates for selected other countries using the EPA-derived CRF are: India, 870; China, 220; Pakistan, 95; Germany, 83; Russia, 73; Egypt, 39; UK, 25; France, 21; and Saudi Arabia, 11. Countries where aviation-attributable baseline $PM_{2.5}$ is dominated by nitrates benefit from ULSJ relatively less than sulfate-rich countries. For example, baseline aviation-attributable $PM_{2.5}$ exposure in China is 73% nitrate (excluding ammonium mass) and ULSJ results in a 1% reduction in aviation-attributable $PM_{2.5}$ exposure. On the other hand, baseline exposure in Saudi Arabia is 80% sulfate and ULSJ results in a 47% reduction. Globally, aviation-attributable $PM_{2.5}$ exposure is reduced by 6% by ULSJ.

We also compare estimated avoided mortalities due to aviation to mortalities due to $PM_{2.5}$ from all sources (anthropogenic and biogenic). Ostro[25] estimates approximately 800,000 mortalities per year are due to exposure to particulate matter. Thus, aviation avoided mortalities based on the EPA and WHO CRFs correspond to 0.3% and 0.2% reduction in total global PM related deaths, respectively.

3.3. Climate Impacts

Figure 2 shows the (warming) radiative forcing due to the reduction in aircraft SO_x emissions and resultant reduction in sulfate direct climate forcing. The average ULSJ-attributable warming due to this mechanism is +3.3 mW/m^2 (95% CI: 1.4-6.0) globally, or +6.1 mW/m^2 (95% CI: 2.6-11.2) for the northern hemisphere.

Applying a one-year pulse of emissions in the APMT-Impacts Climate Module, the time-integrated forcing out to +800 years of ULSJ is +3.1 mW/m^2.yrs due to lifecycle CO_2 changes and +3.3 mW/m^2.yrs due to SO_4 reduction. The equivalent central estimates for temperature response are +2.3 mK.yrs and +2.5 mK.yrs. This indicates that discounting future climate

impacts will increasingly weight the importance of the sulfate direct climate-forcing component of the climate disbenefit of ULSJ.

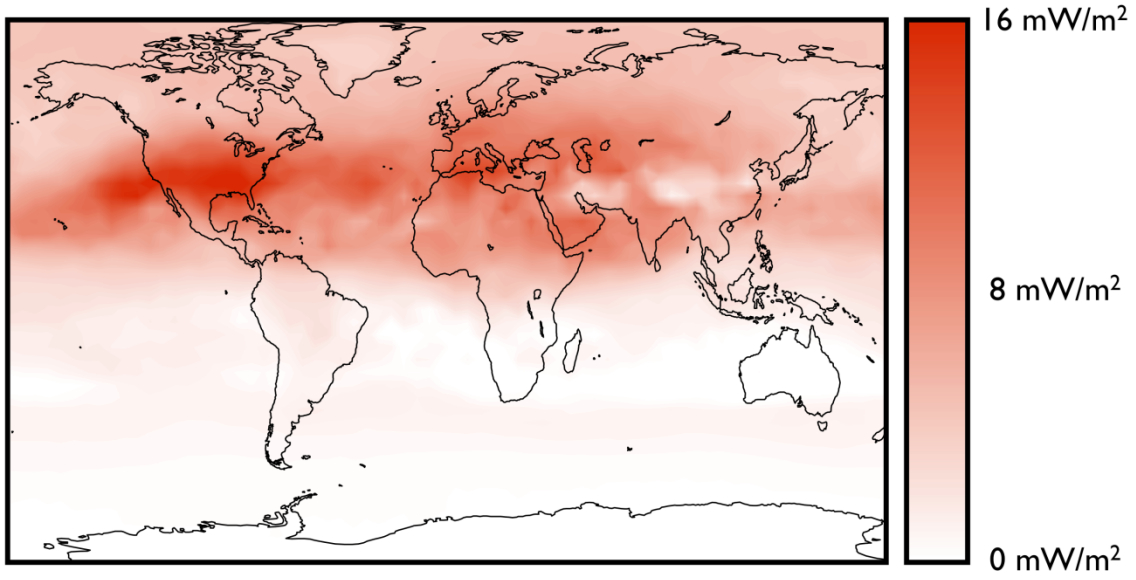

Figure 2. Change in sulfate direct climate forcing due to 97.5% removal of aviation fuel-S (i.e. a warming due to a decrease in cooling).

3.4. Additional Production Costs

Analyzing US Energy Information Administration price history data (from 2001-2011) for the introduction of ultra-low sulfur highway diesel fuel – which has similar properties to Jet-A/A1 – we estimate that desulfurizing fuel costs 3.7-6.6 ¢/gal. (1¢ = US2006 $0.01 and 1 gal. = 3.785 L). This can be compared to estimates by QinetiQ – an additional production cost of 4.5-6.7 ¢/gal.[27]

As an alternative approach, we estimate capital and feedstock costs directly using a representative refinery (see TA). Natural gas is estimated to cost of 1-3 ¢/gal. of Jet A/A-1 produced with a corresponding capital cost (with depreciation over 30 years) of 0.6 ¢/gal. This gives a total of 1.6-3.6 ¢/gal. Combining this range with the price history data listed above, we determine a nominal value of 3.7 ¢/gal., with lower and upper bounds of 1.6 and 6.6 ¢/gal., respectively.

Scaling this to total civil aviation fuel burn, ULSJ will cost $2.5bn (95% CI: 1.3-3.8) in US2006$ globally, or $0.89bn (95% CI: 0.5-1.4) for the US portion of fuel burn.

3.5. Benefit-Cost Analysis

The central non-discounted public health benefit of ULSJ is estimated at $2.0bn/year, but when the same discount rate as applied to climate costs is applied to health benefits, the central monetized health benefit estimate is $[1.8, 1.8, 1.6]bn/yr, while the central monetized climate damage estimate is $[2.1, 1.5, 0.7]bn/year for a [2, 3, 7]% discount rate choice. Corresponding lower and upper bounds for health benefits are $[0.21, 0.20, 0.18] and $[7.6, 7.3, 6.6] bn/yr, respectively, and for climate disbenefits are $[0.13, 0.10, 0.06]bn/year and $[6.3, 4.3, 2.1]bn/year, respectively. There is a [46, 57, 77]% chance that public health benefits exceed climate disbenefits.

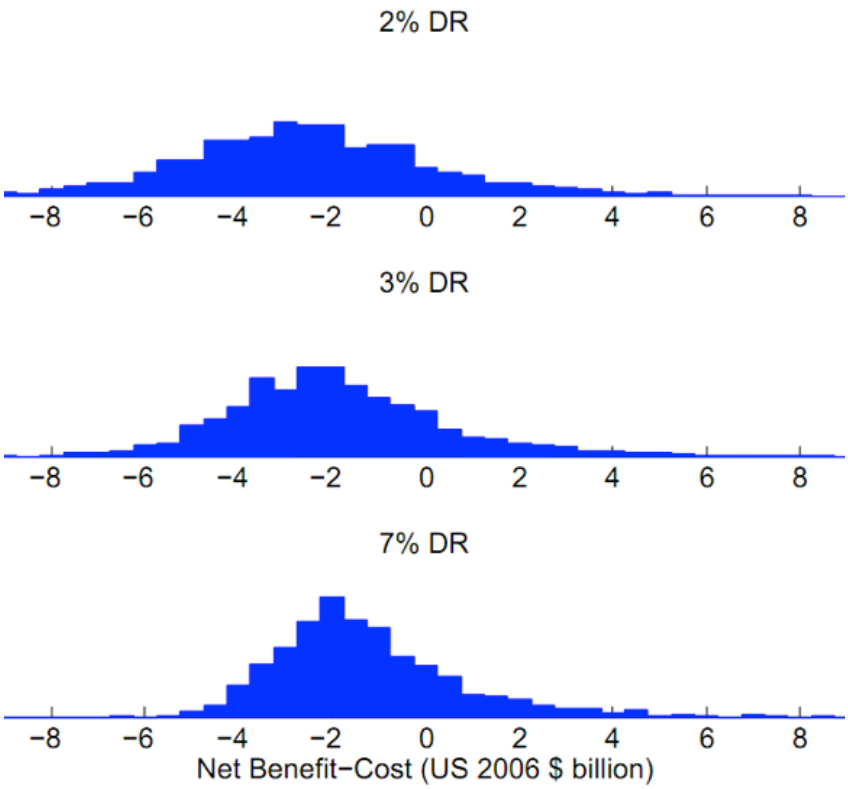

Figure 3. The probability distribution for yearly net cost (-) or net benefit (+) of ULSJ under global implementation for discount rates of 2%, 3% and 7%. Country-specific VSLs are used.

Figure 3 depicts the probability distribution of the overall net difference between costs and benefits of ULSJ (i.e. benefits minus costs and disbenefits). There is a [85, 83, 80]% chance that the policy has a net negative benefit when including implementation costs and climate disbenefits, but the net benefit does not statistically differ from zero (i.e. the confidence interval captures a cost-neutral outcome).

If all avoided premature mortalities are valued using the aforementioned US VSL range – instead of country-specific VSLs – then there is an 84% chance that ULSJ is net beneficial (taking a discount rate of 3%) with an equal likelihood that the net benefit is higher or lower than $11bn/year.

For the US, public health benefits also exceed climate disbenefits and there is a greater than even chance of a net policy cost when including implementation costs. The ULSJ policy net benefit-cost does not statistically differ from zero in the US. For US impacts due to global implementation, the central monetized health benefit estimate is $[0.62, 0.60, 0.54]bn/yr, while the central monetized climate damage estimate is $[0.29, 0.20, 0.10]bn/year for a [2, 3, 7]% discount rate choice. Corresponding lower and upper bounds for health benefits are $[0.06, 0.06, 0.06] and $[2.4, 2.4, 2.1] bn/yr, respectively, and for climate disbenefits are $[0.01, 0.01, 0.01]bn/year and $[1.0, 0.68, 0.34]bn/year, respectively. When US-only implementation is considered, the central monetized health benefit estimate is $[0.40, 0.38, 0.35]bn/yr, while the central monetized climate damage estimate is $[0.10, 0.07, 0.04]bn/year for a [2, 3, 7]% discount rate choice. Corresponding lower and upper bounds for health benefits are $[0.04, 0.04, 0.04] and $[1.6, 1.5, 1.4] bn/yr, respectively, and for climate disbenefits are $[0.0, 0.0, 0.0]bn/year and $[0.36, 0.24, 0.12]bn/year, respectively. Total aggregated benefit-cost results as well as additional distribution figures are presented in the TA.

The greatest quantified contributors to uncertainty in rank order by total effect index (see TA) are the US VSL, $PM_{2.5}$ mortality CRF, the cost of HDS , modeled aviation-attributable $PM_{2.5}$, global income elasticity, and the climate damage function in APMT-Impacts. A significant issue is that if only LTO emissions and benefits associated with the reduction in LTO SO_x emissions are accounted for – as is conventional when considering aviation's impact on air quality – our results show that ULSJ has a statistically significant net cost (see TA). This implies that the

ability of CTMs to correctly capture vertical transport from cruise altitudes and scavenging is of central importance.

4. Discussion

Jet A/A-1 is unusual as a transportation fuel in not being subject to a current or planned ultra-low sulfur standard in developed countries. Within the context of the FAA's aspirational goal of reducing aviation's significant health impacts in 2018 by 50% relative to 2005, and considering the time constraints of technology changes combined with anticipated growth, ULSJ may be a suitable option. In the US, the final rule mandating ultra-low sulfur diesel fuel was made in 2001, with 80% of the fuel being imported/produced required to meet a 15 ppm specification in 2006, and 100% in 2010. This implies that progress towards ULSJ implementation may be possible by 2018 in a US context if a similar timeline is assumed. However, the implications of ULSJ are intrinsically international due to the intercontinental nature of aircraft pollution caused by cruise emissions.[2] Furthermore, as aircraft refuel in different countries (e.g. flights from Europe to North America will be fueled in Europe), consideration of ULSJ at an international level may be justified.

We have shown that the net benefit of ULSJ does not statistically differ from zero, with a greater than 50% chance that the additional feedstock and capital costs coupled with climate disbenefits exceed public health benefits when country-specific VSLs are applied. Approximately 1000-4000 premature mortalities per year will be averted under a ULSJ scenario. There are appreciable uncertainties that indicate the possibility of either positive or negative net benefits. This indicates that ULSJ may be justifiable if there are other (e.g. non-economic) rationales for its introduction.

Although there were many contributors to uncertainty, the greatest quantified contributor was the VSL, which has significant uncertainty within a US context and heightened uncertainty in a global application. We note that if the US VSL were applied to all countries, then ULSJ would be cost-beneficial with discounted global public health benefits centrally estimated as $7.8bn. There is no economic rationale for doing this, given significant differences in national income. However, policy-makers may be more comfortable with approaches that assume an equal value

in mortality risk reduction across all lives (i.e. constant VSL). An alternative strategy would be to avoid valuation of mortality and conduct a cost-effectiveness analysis. When doing so, we find a central estimate of $2 million per premature mortality averted, where the costs include both implementation costs and climate disbenefits for a 3% discount rate when global implementation is considered. US cost effectiveness due to global implementation and US-only implementation is $11 million and $15 million per premature mortality averted, respectively.

Our analysis also reinforced the importance of cruise emissions to public health impacts of aviation. If only LTO emissions were included, the public health benefits are significantly outweighed by the costs of implementation and climate disbenefits. This emphasizes the importance of appropriately capturing vertical transport from cruise altitudes, and our comparisons between modeled and simulated tracers indicate that vertical transport and wet removal rates are captured in the model applied with an uncertainty that is small relative to other modeling uncertainties. Climate-feedbacks and indirect effects of reduced atmospheric sulfate and CO_2 concentrations have not been assessed.

5. References

(1) Lee, D. S.; Pitari, G.; Grewe, V.; Gierens, K.; Penner, J. E.; Petzold, A.; Prather, M. J.; Schumann, U.; Bais, A.; Berntsen, T.; Iachetti, D.; Lim, L. L.; Sausen, R. Transport impacts on atmosphere and climate: Aviation. *Atmos. Environ.* **2010,** 44 (37), 4678-4734.

(2) Barrett, S. R. H.; Britter, R. E.; Waitz, I. A. Global mortality attributable to aircraft cruise emissions. *Environ. Sci. Technol.* **2010,** 44 (19), pp. 7736-7742.

(3) Woody, M.; Baek, B. H.; Adelman, Z.; Omary, M.; Lam, Y. F.; West, J. J.; Arunachalam, S. An assessment of Aviation's contribution to current and future fine particulate matter in the United States. *Atmos. Environ.* **2011,** 45, 3424-3433.

(4) Ratliff, G.; Sequeira, C.; Waitz, I.; Ohsfeldt, M.; Thrasher, T.; Graham, G.; Thompson, T.; Graham, M.; Thompson, T. *Aircraft Impacts on Local and Regional Air Quality in the United States.* PARTNER report (Report No. PARTNER-COE-2009-002).

(5) Brunelle-Yeung, E.; Masek, T.; Rojo, J. J.; Levy, J. I.; Arunachalam, S.; Miller, S. M.; Barrett, S. R. H.; Kuhn, S. R.; Waitz, I. A. Methods for assessing the impact of aviation environmental policies on public health. To appear in *Transport Policy.* **2011.**

(6) The Boeing Company. *Boeing Current Market Outlook 2011-2030*; Boeing, U.S., 2011.

(7) Levy, J. I.; Woody, M.; Baek, B. H.; Shankar, U.; Arunachalam, S. Current and future particulate matter-related mortality risks in the United States from aviation emissions during landing and takeoff. *Risk Anal.* **2011**, in press. DOI: 10.1111/j.1539-6924.2011.01660.x.

(8) Hileman, J. I.; Stratton, R. W.; Donohoo, P. E. Energy content and alternative jet fuel viability. *J. Propul. Power.* **2010,** 26 (6), 1184-1195.

(9) ASTM International, West Conshohocken, PA. *Standard Specification for Aviation Turbine Fuels, Std. ASTM D1655-09*, 2007. DOI:10.1520/D1655-09.

(10) UK Ministry of Defence. *Defence Standard 91-91, Issue 7 (18 February 2011), Turbine Fuel, Kerosine Type, Jet A-1, NATO Code: F-35, Joint Service Designation: AVTUR,* 2011.

(11) United States Environmental Protection Agency. *Control of Air Pollution From New Motor Vehicles; Revisions to Motor Vehicle Diesel Fuel Sulfur Transition Provisions; and Technical Amendments to the Highway Diesel, Nonroad Diesel, and Tier 2 Gasoline Programs: Direct final rule*; EPA, U.S., 2005.

(12) Wilkerson, J. T.; Jacobson, M. Z.; Malwitz, A.; Balasubramanian, S.; Wayson, R.; Fleming, G.; Naiman, A. D.; and Lele, S. K. Analysis of emission data from global commercial aviation: 2004 and 2006. *Atmos. Chem. Phys.* **2010,** 10, 6391-6408,

(13) Stettler, M.E.J.; Eastham, S.; Barrett, S.R.H. Air Quality and Public Health Impacts of UK Airports. Part I: Emissions. *Atmos. Environ.* **2011,** 45 (31), 5415-5424.(14) Bey, I.; Jacob, D. J.; Yantosca, R. M.; Logan, J. A.; Field, B.; Fiore, A. M.; Li, Q.; Liu, H.; Mickley, L. J.; Schultz, M. Global modeling of tropospheric chemistry with assimilated meteorology: Model description and evaluation. *J. Geophys. Res.* **2001**, 106 (23), 23,073-23,096.

(14) US Environmental Protection Agency. National Emissions Inventory Air Pollutant Emissions Trends Data. http://www.epa.gov/ttn/chief/trends/index.html.

(15) Bey, I.; Jacob, D. J.; Yantosca, R. M.; Logan, J. A.; Field, B.; Fiore, A. M.; Li, Q.; Liu, H.; Mickley, L. J.; Schultz, M. Global modeling of tropospheric chemistry with assimilated meteorology: Model description and evaluation. *J. Geophys. Res.* **2001**, 106 (23), 23,073-23,096.

(16) Byun, D.W.; Schere, K.L. Review of the Governing equations, Computational Alogrithms, and Other Components of the Models-3 Community Multiscale Air Quality (CMAQ) Modeling System. *Applied Mechanics Reviews* **2006**, 59 (2), 51-77.

(17) Chipperfield, M.P. New Version of the TOMCAT/SLIMCAT Off-Line Chemical Transport Model: Intercomparison of Stratospheric Tracer Experiments *Q. J. R. Meteorol. Soc.*, 132, 1179-1203, doi:10.1256/qj.05.51, 2006.

(18) Mahashabde, A.; Wolfe, P.; Ashok, A.; Dorbian, C.; He, Q.; Fan, A.; Lukachko, S.; Mozdzanowska, A.; Wollersheim, C.; Barrett, S.R.H.; Locke, M.; Waitz, I.A. Assessing the environmental impacts of aircraft noise and emissions. *Prog. Aerosp. Sci.* **2011,** 47 (1), 0376-0421.

(19) US Environmental Protection Agency. *The Benefits and Costs of the Clean Air Act: 1990 to 2020*; Office of Air and Radiation: Washington, DC, 2011.

(20) Pope, C. A.; Burnett, R. T.; Thun, M. J.; Calle, E. E.; Krewski, D.; Ito, K.; Thurston, G. D. Lung cancer, cardiopulmonary mortality, and long-term exposure to fine particulate air pollution. *JAMA* **2002**, 287 (9), 1132-1141.

(21) Laden, F.; Schwartz, J.; Speizer, F. E.; Dockery, D. W. Reduction in fine particulate air pollution and mortality: Extended follow-up of the Harvard Six Cities study. *Am. J. Respir. Crit. Care Med.* **2006**, 173 (6), 667-672.

(22) United States Environmental Protection Agency. *Expanded Expert Judgment Assessment of the Concentration-Response Relationship Between $PM_{2.5}$ Exposure and Mortality: Final Report*. EPA, U.S., 2006.

(23) Roman, H. A.; Walker, K. D.; Walsh, T. L.; Conner, L.; Richmond, H. M.; Hubbell, B. J.; Kinney, P. L. Expert judgment assessment of the mortality impact of changes in ambient fine particulate matter in the U.S. *Environ. Sci. Technol.* **2008,** 42 (7), 2268-2274.

(24) Cooke, R. M.; Wilson, A. M.; Tuomisto, J. T.; Morales, O.; Tainio, M.; Evans, J.S. A probabilistic characterization of the relationship between fine particulate matter and mortality: Elicitation of european experts. *Environ. Sci. Technol.* **2007,** 41 (18), 6598-6605.

(25) B. Ostro. *Outdoor air pollution: Assessing the environmental burden of disease at national and local levels. Environmental Burden of Disease Series, No. 5* World Health Organization, 2004.

(26) Hammitt, J.K.; Robinson, L.A. The Income Elasticity of the Value per Statistical Life: Transferring Estimates between High and Low Income Populations. *Journal of Benefit-Cost Analysis*. **2011,** 2(1)

(27) QinetiQ *Reduction of sulphur limits in aviation fuel standards (SULPHUR)*; Report QinetiQ/09/01835 Issue 1.1, Farnborough, 2010; http://www.easa.eu.int/rulemaking/docs/research/EASA_SULPHUR_Project_11-01-2010.pdf.

6. Acknowledgements

Daewon Byun passed away on February 9, 2011. Daewon Byun, one of the principal architects of CMAQ, was a scientist who believed in a comprehensive view of meteorology and air quality. He carefully applied mathematical arguments to ensure that the models were mathematically as well as physically appropriate. He will always be remembered as a friend to all his colleagues. He did not have a chance to review or comment on this manuscript.

We are grateful to the FAA Office of Environment and Energy. In particular we thank Mohan Gupta, Warren Gillette, S. Daniel Jacob, Rangasayi Halthore, Christopher Sequeira and Lourdes Maurice. We would like to thank Mark Jacobson, Marc Stettler, Russell Stratton, Jim Hammit and Lisa Robinson for useful discussions.

This work was sponsored by the FAA Office of Environment and Energy. Any views or opinions expressed in this work are those of the authors and not the FAA.

TECHNICAL ANNEXES

A. ULSJ Background

A.1. *ULSD Case Study*

Given the similarities between diesel and jet fuel,[T1] ultra-low sulfur diesel (ULSD) implementation within the United States was used as a comparative case study for ULSJ. ULSD, through EPA rulemaking, was phased-in to production for on and off-road uses. Table T1 shows the timeline for on-road implementation of ULSD, while Table T2 shows the timeline for off-road implementation of ULSD. US implementation of ULSD exhibited a pattern of a gradual increase in fuel sulfur content (FSC) stringency as the fuel passed from refineries to retail outlets. This implementation was seen over a time period of 10 years for both on and off-road uses.

Table T1: On-road implementation timeline of ULSD in the US.[T2,T3]

Requirement	Date	Description
Announcement of Diesel Fuel Sulfur Content Regulation for On-Road Vehicles	May 1997	Reducing sulfur content of diesel fuel for heavy-duty diesel engines is identified as a potential pathway to improve air quality.
Proposed Heavy-Duty Engine and Vehicle Standards and Highway Diesel Fuel Sulfur Control Requirement	May 2000	Proposed requirement to reduce sulfur content of diesel fuel for highway vehicles to no greater than 15 parts per million (ppm) with a start date of June 1, 2006.
Heavy-Duty Engine and Vehicle Standards and Highway Diesel Fuel Sulfur Control Requirements Final Rule	January 2001	Final rule requires that refiners begin producing 15 ppm sulfur content diesel fuel beginning June 1, 2006.
Refiners and Importers: 80% of Diesel Fuel Imported/Produced must be ULSD	June 2006	N/A
Fuel Terminals: Fuel listed as ULSD must meet 15 ppm specification	September 2006	N/A
Retail Outlets: Fuel listed as ULSD must meet 15 ppm specification	October 2006	N/A
Refiners and Importers: 100% of Diesel Fuel Imported/Produced must be ULSD	June 2010	N/A
Fuel Terminals: All highway diesel must be ULSD	October 2010	N/A
Retail Outlets: All highway diesel must be ULSD	December 2010	Based on a ULSD pump survey, 85% of pumps were dispensing ULSD in the 4th quarter of 2006. 100% of highway diesel fuel pumps are now dispensing ULSD as of the 3rd quarter of 2010.

Table T2: Off-road implementation timeline of ULSD in the US.[T2,T3]

Requirement	Date	Description
Proposed Clean Air Non-Road Diesel Rule	April 2003	Reduce diesel fuel sulfur content to a maximum of 500 ppm starting in 2007 for non-road applications (including locomotive and marine applications). Reduce diesel fuel sulfur content to a maximum of 15 ppm by 2010.
Final Clean Air Non-Road Diesel Rule	May 2004	Non-road diesel fuel sulfur content must be reduced from current levels (about 3000 ppm) to 15 ppm by 2010.
Refiners and Importers: Non-Road, Locomotive, and Marine Fuel	June 2007	Fuel must meet 500 ppm standard.
Fuel Terminals: Non-Road, Locomotive, and Marine Fuel	August 2007	Fuel must meet 500 ppm standard.
Retail Outlets: Non-Road, Locomotive, and Marine Fuel	October 2007	Fuel must meet 500 ppm standard.
Refiners and Importers: Non-Road Fuel	June 2010	Fuel must meet 15 ppm standard.
Refiners and Importers: Locomotive and Marine Fuel	June 2010	Fuel must meet 15 ppm standard.
Fuel Terminals: Non-Road Fuel	August 2010	Fuel must meet 15 ppm standard.
Fuel Terminals: Locomotive and Marine Fuel	August 2012	Fuel must meet 15 ppm standard.
Retail Outlets: Non-Road Fuel	October 2012	Fuel must meet 15 ppm standard.
Retail Outlets: Locomotive and Marine Fuel	October 2012	Fuel must meet 15 ppm standard.

A.2. *Other Studies*

A.2.1. QinetiQ Report on Jet Fuel Sulfur Limit Reduction

A report prepared by QinetiQ[T4] addressed ULSJ implementation in Europe. It estimated that due to the additional hydroprocessing required, there will be a 0.01 to 0.015 EUR/liter additional required cost in ULSJ production, which is approximately 4 to 7 cents (2006 US$) per gallon. The report also outlined many of the potential impacts the additional hydroprocessing would have on fuel properties as well as operational effects due to the reduction in fuel sulfur content. Potential climate impacts were described, but were not quantified. SO_2 emissions as a function of FSC were estimated for a representative local airport by scaling against a previous dispersion model study at Heathrow Airport[T5] based on emissions derived from the First Order Approximation methodology.[T6] The report concluded there is unlikely to be any measurable health effect due to FSC reduction when only LTO emissions are considered. Full-flight emissions impacts were not addressed.

A.2.2. Energy Information Administration (EIA) Report on Market Effects Due to ULSD

An EIA report from 2001[T7] analyzed the possible effects of ultra low sulfur diesel (ULSD) implementation on the diesel fuel market within the US. Based on a cost curve analysis, a 6.5 to 8.2 (2006 US$) cent/gal marginal cost increase for ULSD production was estimated to cover additional capital and hydrotreating costs for an assumed future supply and demand. In comparison, the EPA[T8] predicted a full compliance US average cost of 5.2 cents/gal (2006 US$).

A.2.3. Other Transportation Sectors

Marine fuels have also received significant attention in terms of their global air quality impact.[T9] A policy analysis performed by Corbett and Winebrake[T9] estimated a 70 to 85% reduction in marine SO_x emissions due to marine gas oil (MGO) and marine diesel oil (MDO) implementation (lower sulfur alternatives) over the standard marine residual oil (RO). Additional CO_2 emissions were estimated to be less than 1%. In a human health policy analysis, Winebrake et al.[T10] estimated the total health impacts due to a global marine fuel sulfur content limit. Findings showed a 41,200 reduction in premature mortalities for a global fuel sulfur content limit of 5000 ppm as compared to 87,000 premature mortalities with the assumed baseline emissions scenario. Marine fuel use is defined as an off-road diesel fuel and all marine fuel must meet the 15 ppm standard by the end of 2012, as outlined in Table T2, for all US marine applications except for RO used by ocean-going ships.

B. Air Quality Modeling

B.1. *Emissions*

Emissions were derived from output from the FAA's aviation environmental design tool (AEDT). AEDT calculates aircraft fuel burn and emissions on a flight-by-flight basis, covering the majority of civil aviation. A procedure similar to that applied by Barrett et al.[T11] was used to modify AEDT output for use in our analysis, which is outlined in Table T3 where AEDT outputs are bolded. For the baseline (present-day) case FSC = 600 ppm was assumed, while for the ULSJ scenario FSC = 15 ppm was used.

Table T3: Emission indices methodology for air quality simulations.[T11] Bolded Variables are from AEDT.

Species	Baseline Emissions (g)	Description/Notes
CO_2	3159 × **FUEL**	CO_2 aircraft emissions, constant is adjusted to 3150 for ULSJ, FUEL represents the fuel burn value obtained from AEDT
H_2O	1231 × **FUEL**	Aircraft H_2O emissions
NO_x as NO_2	**NO_x**	AEDT default value, NO/NO_2 mole fraction partitioning changes between LTO/non-LTO
CO	**CO**	AEDT default value
HC as CH_4	**HC**	CH_4 equivalent, AEDT default value, speciated
TOG	1.16 × **HC**	Total organic gases aircraft emissions, speciated
BC < 3000ft	**PMNV**	Black carbon emissions below 3000 ft, AEDT default value for Black carbon with small amounts of metals (PMNV)
BC > 3000ft	0.03 × **FUEL**	Black carbon emissions above 3000 ft
OC < 3000ft	**PMFO**	Organic carbon emissions below 3000 ft, AEDT default value for organic PM from fuel (PMFO)
OC > 3000ft	0.03 × **FUEL**	Organic Carbon emissions above 3000 ft
SO_2	(FSC/1000) × [(100 - E)/100] × **FUEL** x (64/32)	SO_2 emissions, based on fuel sulfur content (FSC) in ppm (by wt) and wt-% of fuel sulfur emitted at S^{VI} (E)
S^{VI} as SO_4	(FSC/1000) × **(**E/100) × **FUEL** × (96/32)	Assumes S^{VI} emitted as SO_4

B.2. *Chemical Transport Model (CTM) Descriptions*

Three different models were used to model air quality impacts of ULSJ implementation globally as well as within the contiguous US for a study year of 2006 using the same aircraft emissions as derived above.

B.2.1. Global and Nested GEOS-Chem Model Descriptions

The GEOS-Chem model is a global three-dimensional model of tropospheric chemistry driven by 2006 meteorological observations from the Goddard Earth Observing System (GEOS) of the NASA Global Modeling Assimilation Office[T12]. GEOS-Chem has been used to study the intercontinental transport of aerosols and aerosol precursors[T13,T14,T15,T16,T17,T18] and in a recent air quality mortality assessment for shipping.[T19] A model sharing substantially common code for photochemistry, emissions and deposition was applied for the IPCC Special Report on Aviation and the Global Atmosphere.[T20] A detailed wet deposition scheme is included, which has been constrained by observations.[T21] BC, OC and H_2SO_4-HNO_3-NH_3 aerosols are simulated.[T17]

The GEOS-Chem grid has a horizontal resolution of 4° × 5° and a vertical resolution of 47 layers defined from the surface to 0.01 hPa for GEOS-5 simulations. Secondary organic aerosols were

included[T22] in GEOS-Chem simulations, which were used to provide consistent boundary conditions to CMAQ by spatially and temporally maps and interpolated to CMAQ boundaries. Nested GEOS-Chem uses a 0.5° × 0.666° horizontal resolution grid within the US with GEOS-5 meteorology at its native resolution.

B.2.2. CMAQ Model Description

CMAQ is a high-resolution regional air quality model used by the EPA to support regulatory impact assessment. It is used in this study to model air quality effects of ULSJ in the continental US. ISORROPIA was used to model secondary inorganic aerosols, and the bond IV chemical mechanism was used for gas phase chemistry. The model and its implementation are described in greater detail in the CMAQ 4.6 Operational Guidance Document.[T23]

The background inventory was compiled from the EPA 2005 NEI database consistent with GEOS-Chem. Meteorological data from 2006 was converted with MM5 from GEOS data, the same as that used in the GEOS-Chem simulations. The meteorological input for CMAQ modeling was generated by MM5.[T24] The model is initialized with the GMAO global meteorological data which is the same set of input driving the GEOS-Chem model. As the GMAO data in 2° × 2.5° horizontal resolution downscaling to the 36 km grid spacing MM5 simulation, three dimensional fields are vertically interpolated from the GMAO hybrid coordinates to MM5 sigma coordinates. Thirty-five vertical layers are defined from surface to 100 hPa containing increased layers in the upper atmosphere where aircraft typically fly. MM5 physical options are Grell cumulus scheme, Noah land-surface model, medium-range forecast (MRF) PBL scheme, simple ice for microphysics, and rapid radiative transfer model (RRTM) for radiation parameterization. The grid nudging is applied to maintain the dynamic consistency of MM5 simulation with the GMAO analysis.

The CMAQ domain is a high-resolution Lambert conformal projection of the continental United States and parts of Canada and Mexico. It consists of 112 × 148 square grid cells at 36km to a side, when viewed as a Lambert projection.

B.2.3. p-TOMCAT Model Description

The 3-D chemistry transport model p-TOMCAT detailed by O'Connor et al.[T25] and Cook et al.[T26] is an updated and parallelized version of the earlier TOMCAT model.[T27,T28,T29] It includes a gas-phase methane-oxidation scheme with simplified NMHC treatment (ethane, propane) and calculates the behavior of 54 species with more than 150 chemical reactions (with rates are based on IUPAC2005 and O'Connor et al.[T25]). Photolysis rates are calculated off-line with the Cambridge 2-D model.[T30] The tropospheric sulfur cycle is based on Berglen et al.[T31] The model has 35 hybrid-pressure levels from the surface to 10 hPa, with a vertical resolution of approximately 700m in the upper troposphere and lower stratosphere (UTLS) region. A horizontal grid resolution of 2.8° × 2.8° was used. At the upper boundary O_3, CH_4 and NO_x are prescribed with climatological values from the Cambridge 2D-Model. The p-TOMCAT model does not consider heterogeneous and halogen chemistry in the stratosphere. With the upper boundary located at 10 hPa (~32 km), only a limited representation of stratospheric processes is available.

A recent validation of p-TOMCAT, with airborne observations, together with an inter-comparison of the results with those from other models is published by Brunner et al.[T32,T33] Therein it is shown that the model is capable of reproducing present-day atmospheric conditions and the results are within the range calculated by other atmospheric models. The only aerosol present in the version of p-TOMCAT used in this project is the sulfuric acid aerosol and it is involved in heterogeneous chemistry in the model.

B.3. *Air Quality Simulation Results and Comparison Between CTMs*

B.3.1. Air Quality Modeling Results for Global ULSJ Implementation

GEOS-Chem simulations are performed for both full-flight and LTO emissions scenarios for standard aviation (baseline) and ULSJ aviation (policy). Globally averaged aviation-attributable ground-level $PM_{2.5}$ and SO_4 concentrations are plotted and presented below.

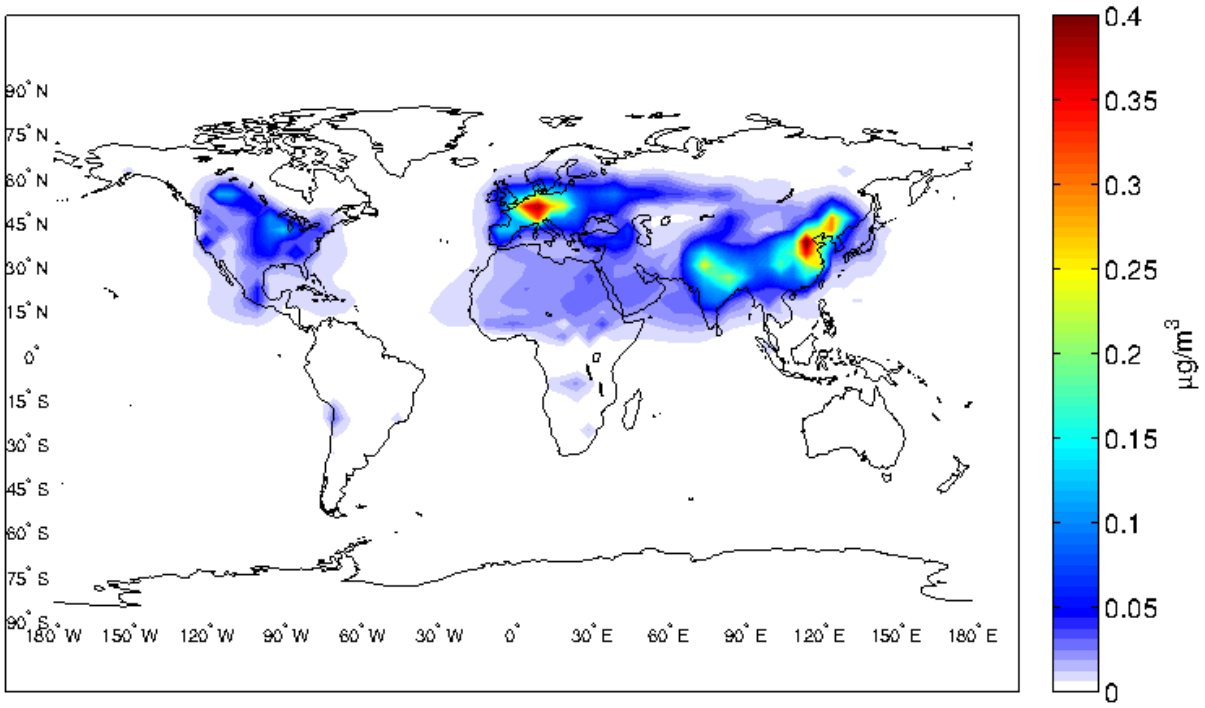

Figure T1: Globally averaged aviation-attributable ground-level $PM_{2.5}$ concentrations for standard jet fuel when full-flight emissions are considered.

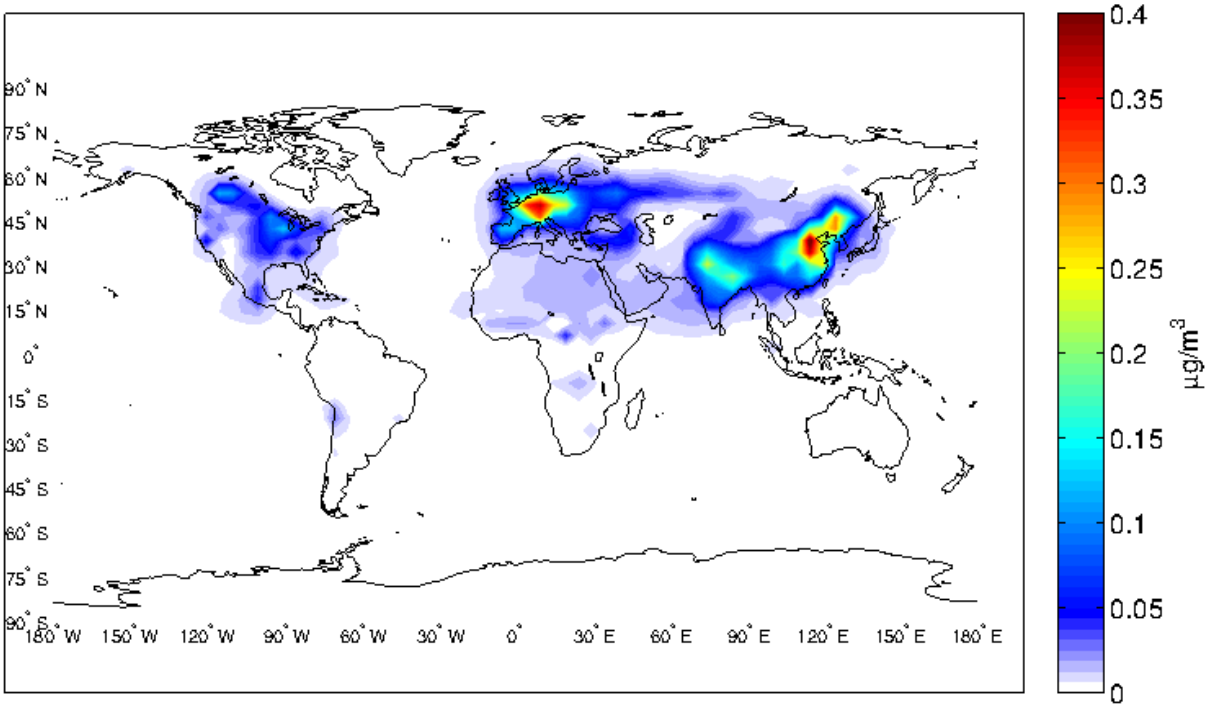

Figure T2: Annually averaged aviation-attributable ground-level $PM_{2.5}$ concentrations for ULSJ when full-flight emissions are considered.

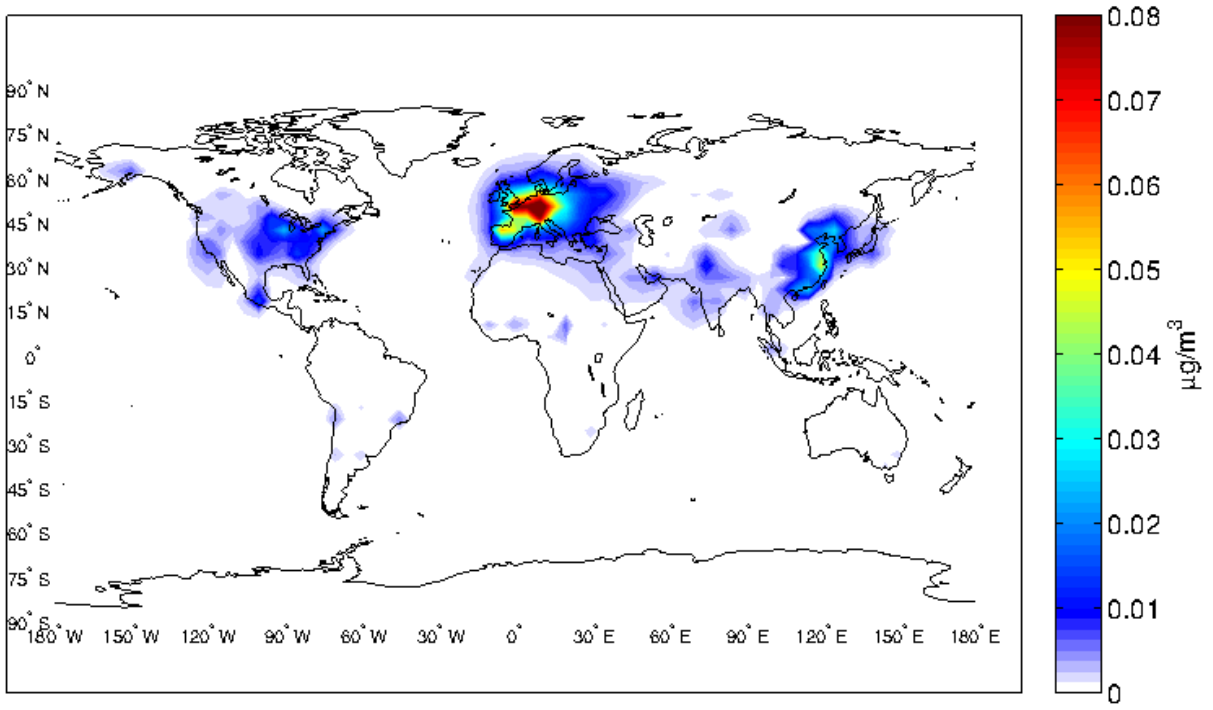

Figure T3: Annually averaged aviation-attributable ground-level $PM_{2.5}$ concentrations for standard jet fuel when LTO emissions are considered.

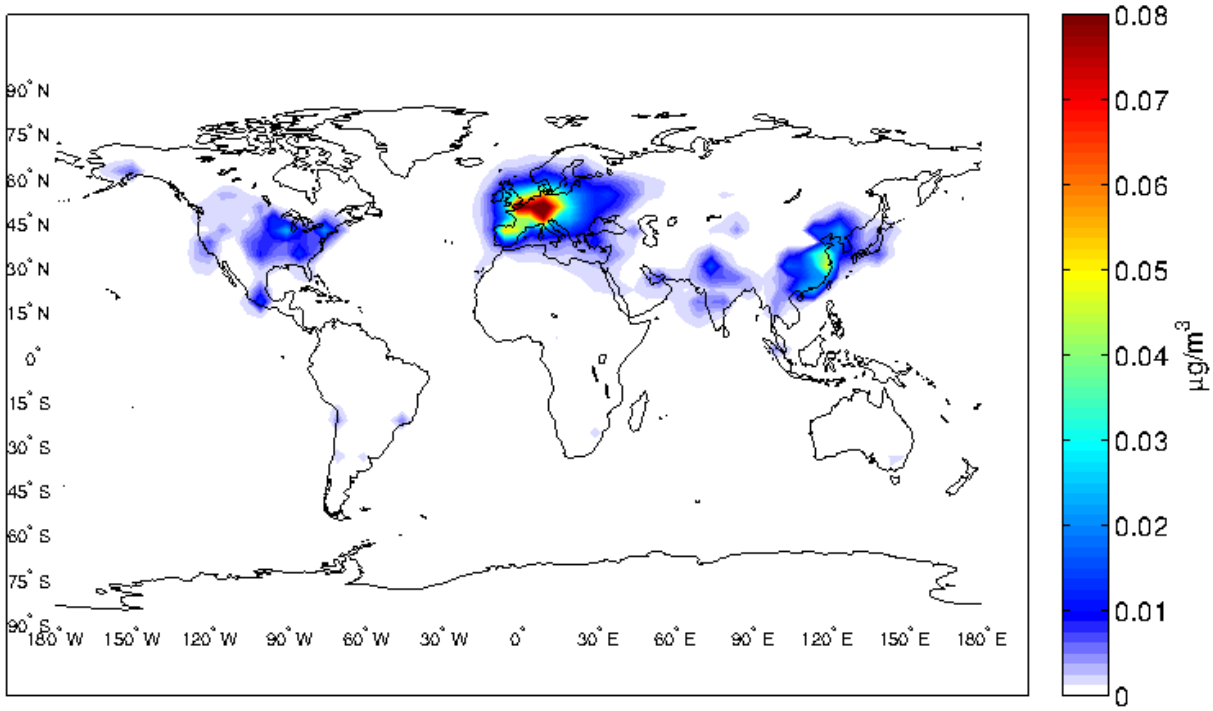

Figure T4: Annually averaged aviation-attributable ground-level $PM_{2.5}$ concentrations for ULSJ when LTO emissions are considered.

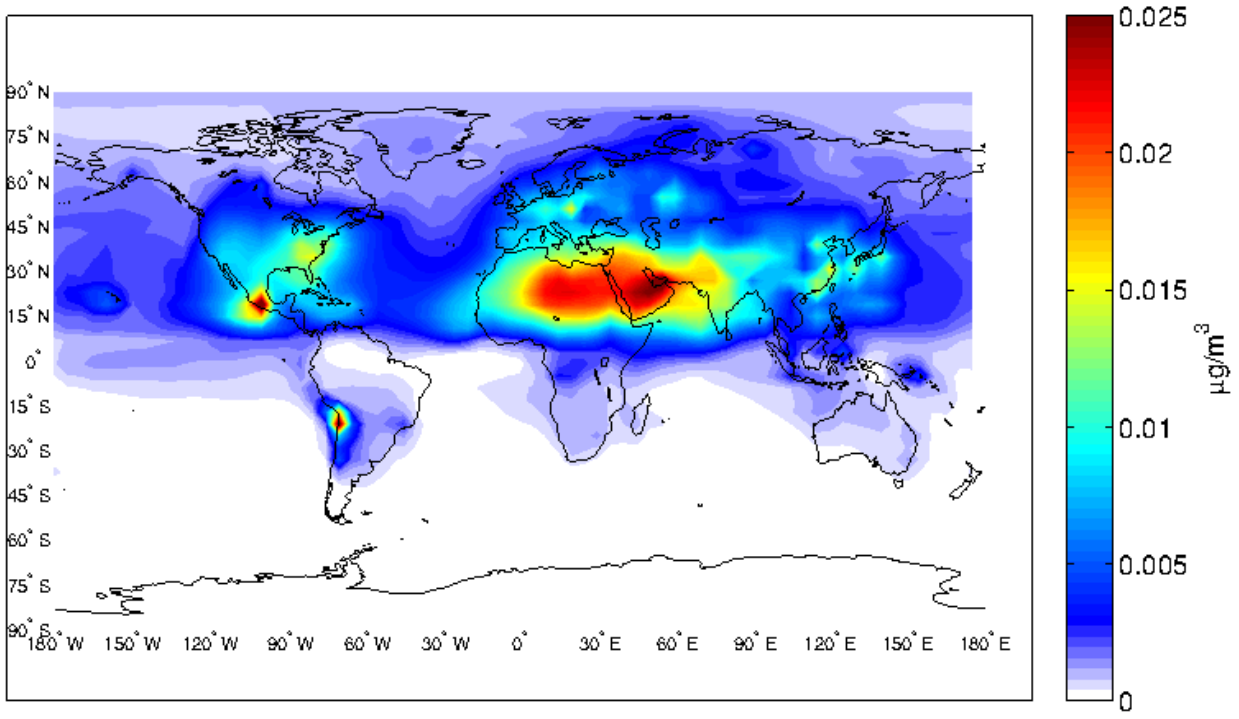

Figure T5: Annually averaged aviation-attributable ground-level SO_4 concentrations for standard jet fuel when full-flight emissions are considered.

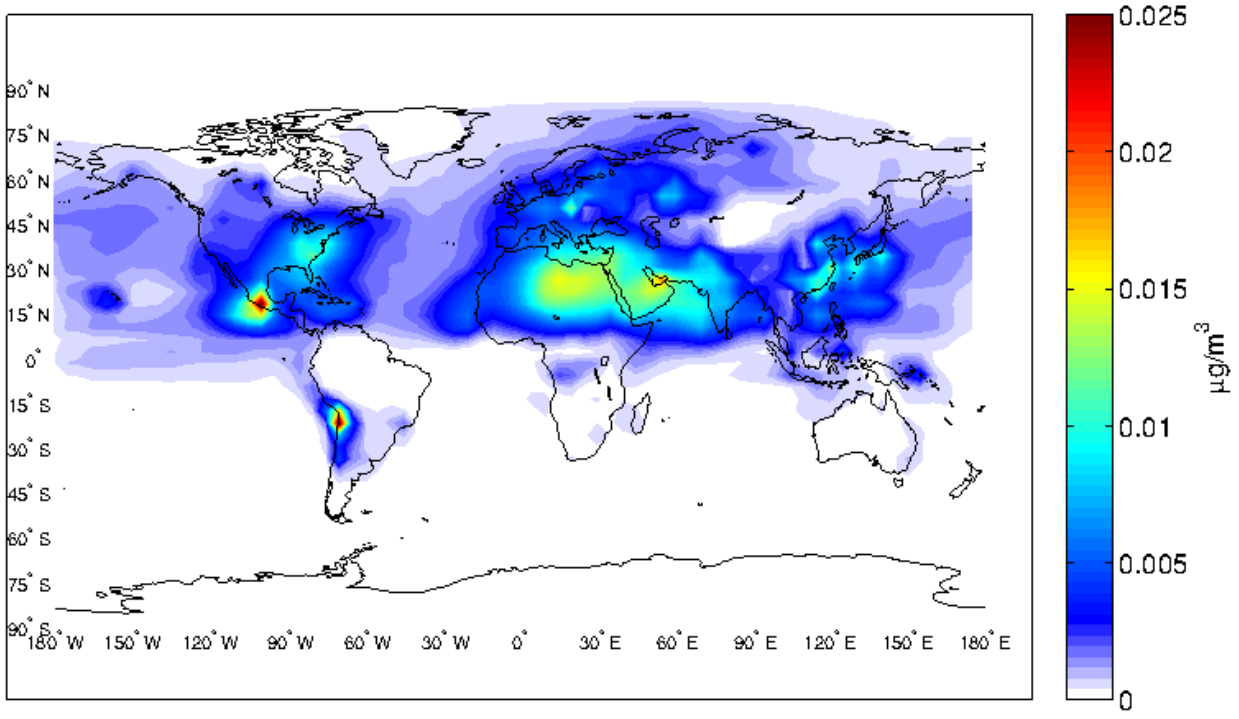

Figure T6: Annually averaged aviation-attributable ground-level SO_4 concentrations for ULSJ when full-flight emissions are considered.

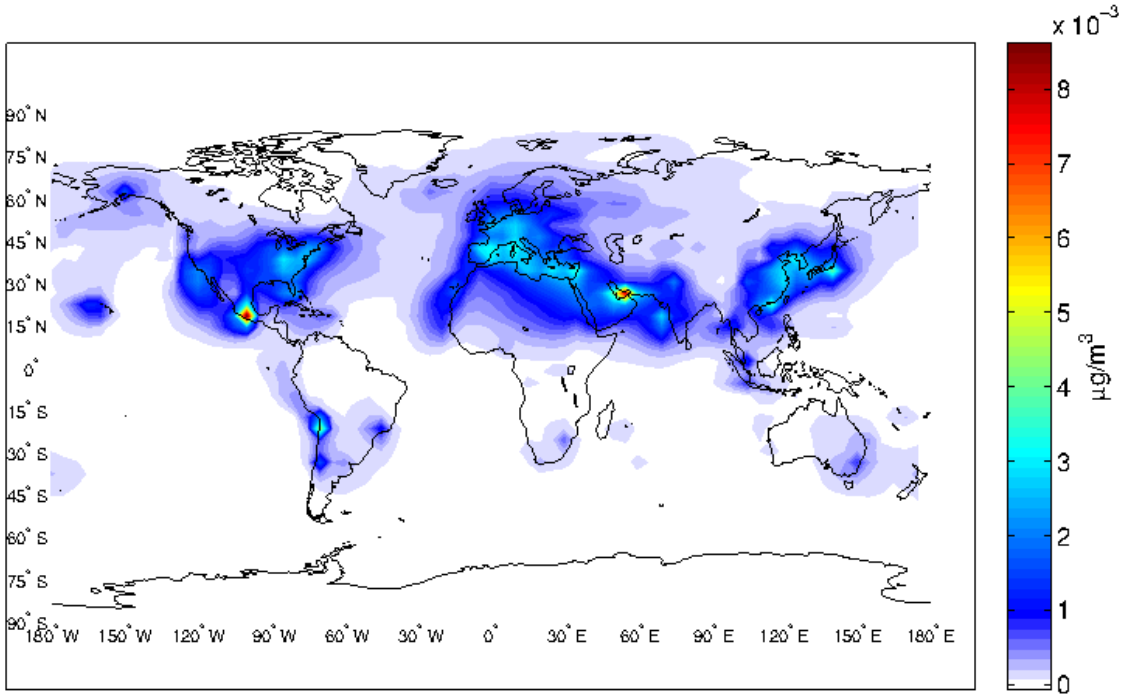

Figure T7: Annually averaged aviation-attributable ground-level SO_4 concentrations for standard jet fuel when LTO emissions are considered.

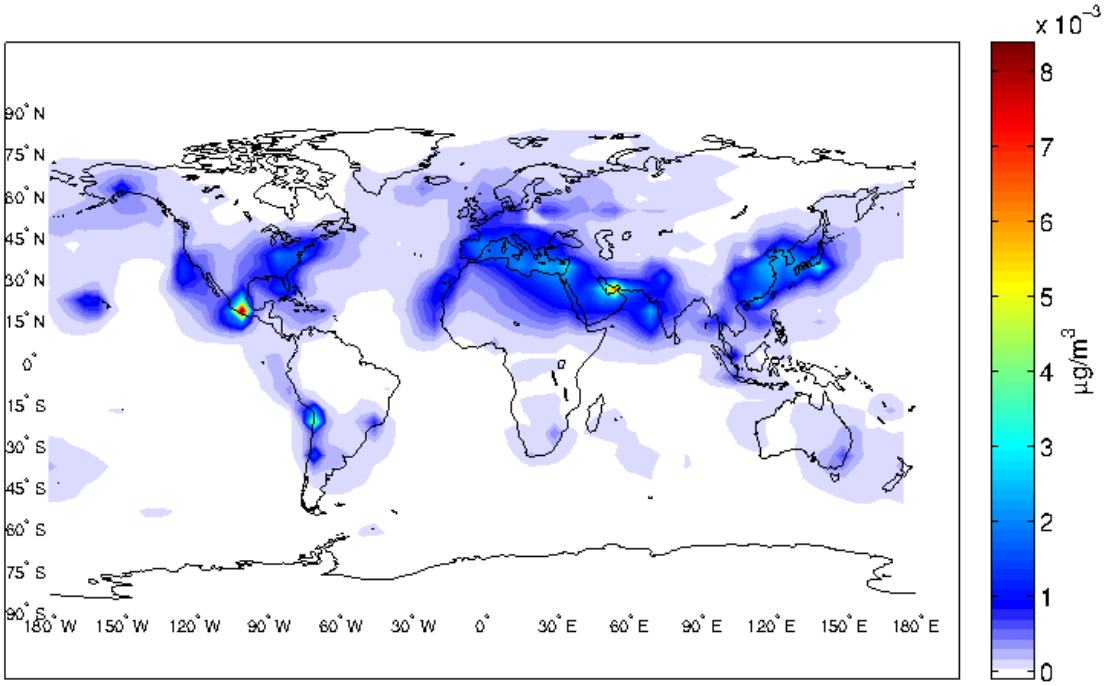

Figure T8: Annually averaged aviation-attributable ground-level SO_4 concentrations for ULSJ when LTO emissions are considered.

B.3.2. Comparison Between GEOS-Chem, Nested GEOS-Chem and CMAQ Models

Figure T9 shows a comparison of annually averaged aviation-attributable ground-level $PM_{2.5}$ concentrations in the US across global and nested models.

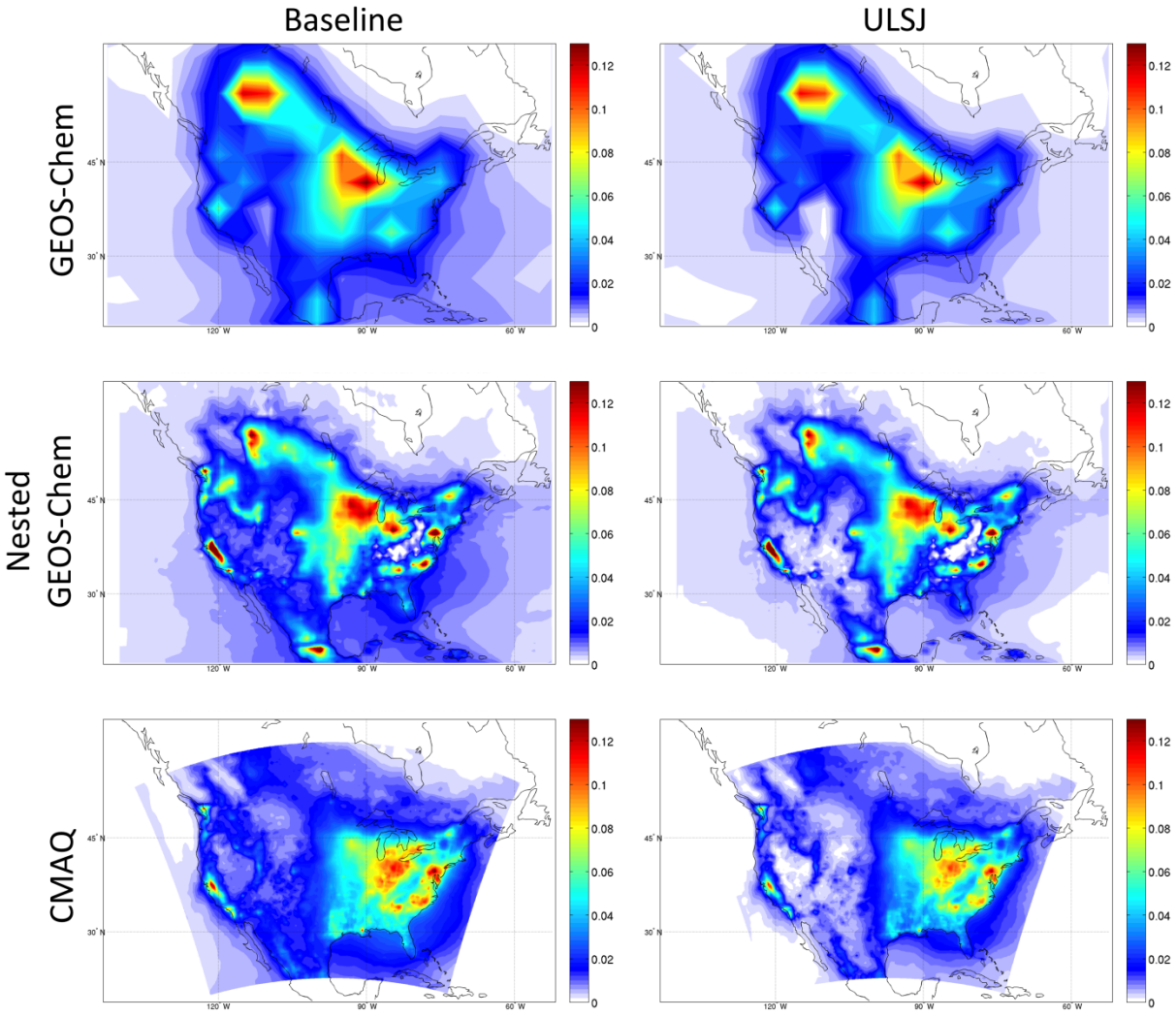

Figure T9: Annually-averaged aviation-attributable ground-level $PM_{2.5}$ concentration ($\mu g/m^3$) comparison for standard (left) and ULS (right) jet fuel emissions.

Figure T10 shows a comparison of annually averaged aviation-attributable ground-level SO_4 concentrations in the US across global and nested models.

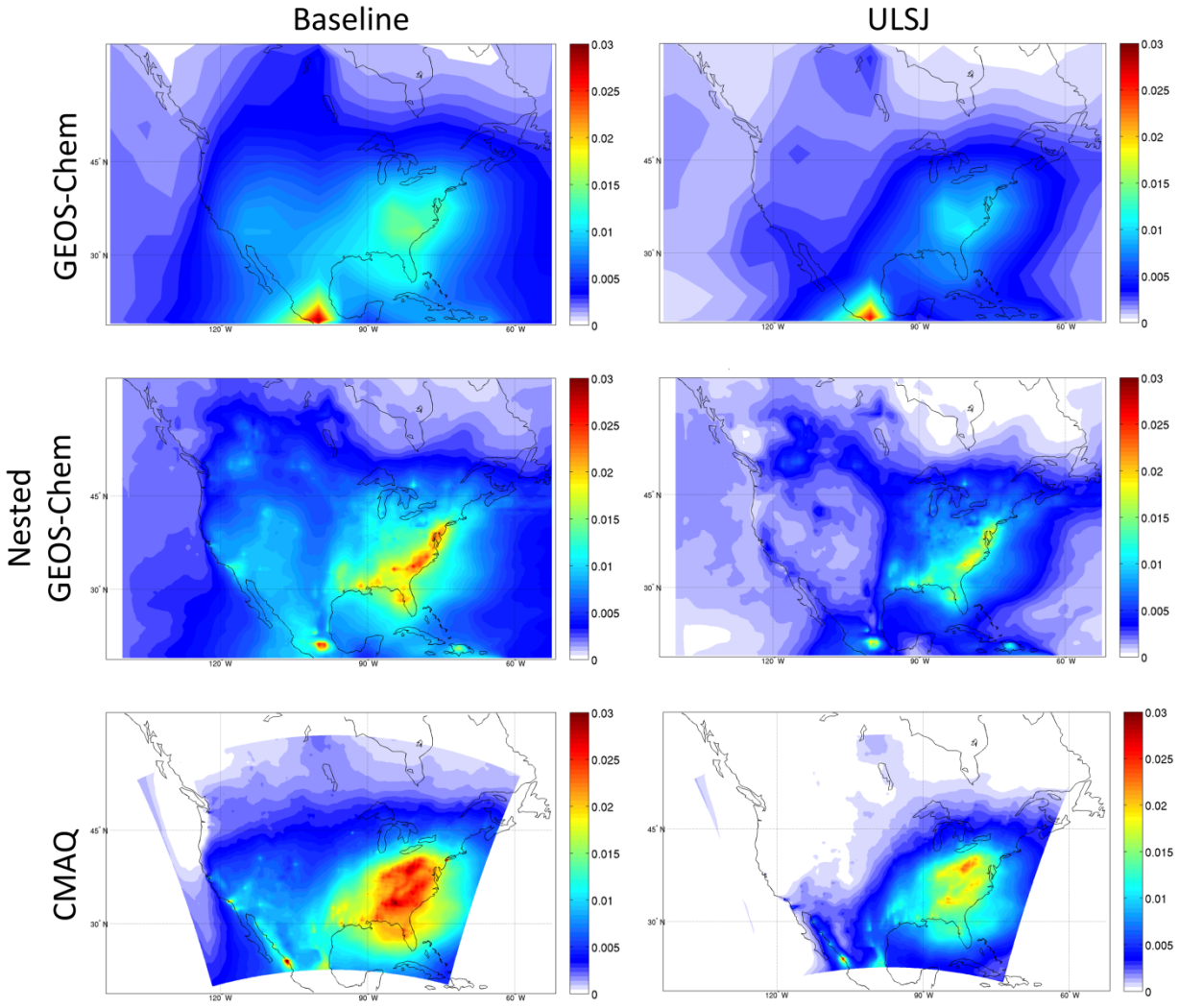

Figure T10: Annually-averaged aviation-attributable ground-level SO_4 concentration ($\mu g/m^3$) comparison for standard (left) and ULS (right) jet fuel emissions.

Ground level $PM_{2.5}$ concentrations, including SO_4, are broadly consistent across models in terms of spatial distribution, but average, minimum, and maximum concentration magnitudes are not reproduced across the models. Mean ground-level aviation-attributable $PM_{2.5}$ concentrations are higher in nested GEOS-Chem (0.083 $\mu g/m^3$) than in GEOS-Chem (0.077 $\mu g/m^3$), and both are higher than CMAQ (0.068 $\mu g/m^3$). Maximum concentration magnitudes show a different behavior, being highest in CMAQ (0.030 $\mu g/m^3$), followed by nested GEOS-Chem (0.026 $\mu g/m^3$), then global GEOS-Chem (0.016 $\mu g/m^3$). Also, the CMAQ simulations do not produce a spike in $PM_{2.5}$ concentration in Western Canada that is seen in the GEOS-Chem simulations.

B.3.3. Comparison Between GEOS-Chem and p-TOMCAT Models

Figure T11 shows a zonal mean comparison of SO_4 concentrations between global GEOS-Chem and p-TOMCAT simulations for baseline and ULSJ implementation when full-flight emissions are considered.

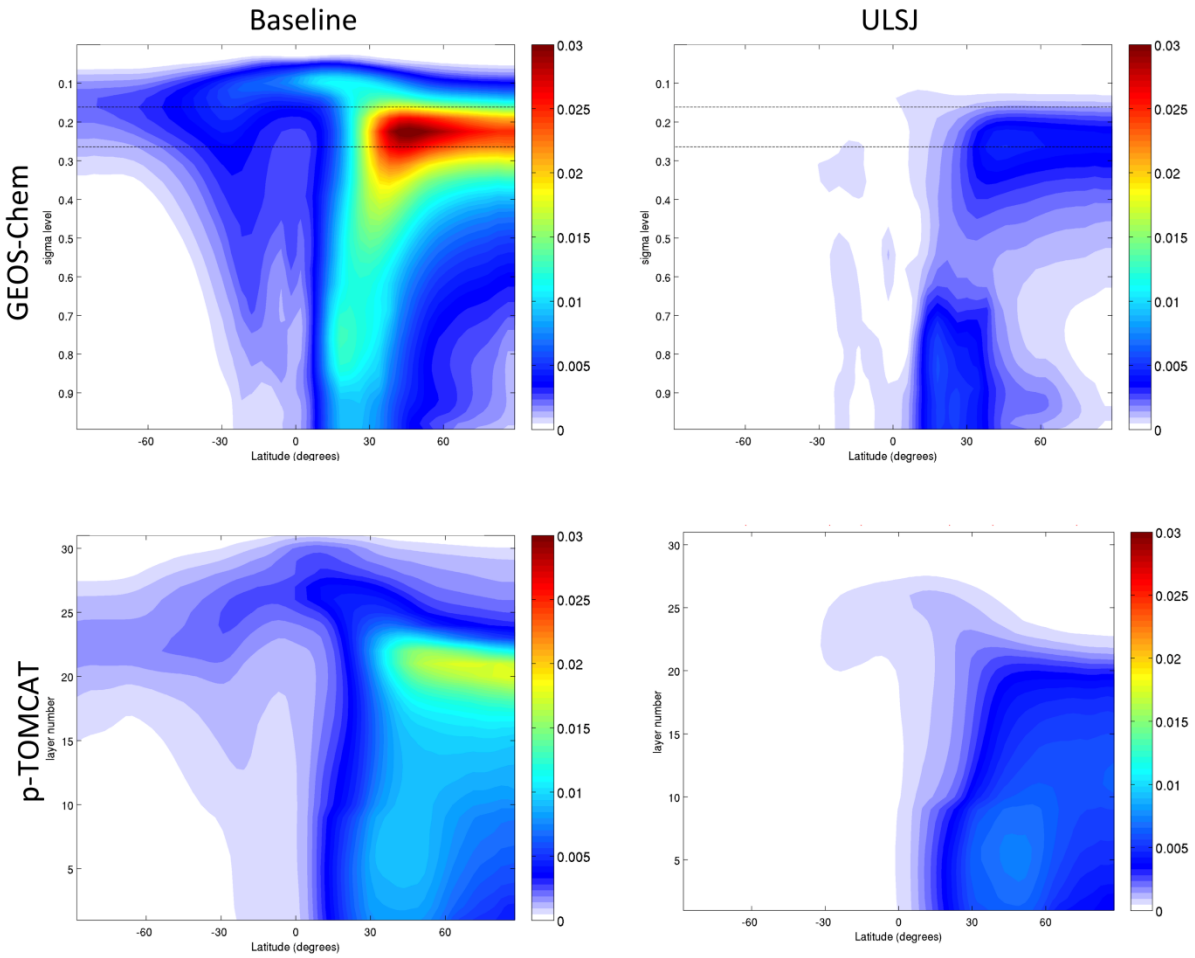

Figure T11: Comparison of GEOS-Chem and TOMCAT annually-averaged baseline and ULSJ aviation-attributable zonal mean concentrations (ppbv) of SO_4 plotted against layer number when full flight emissions are considered.

Figure T12 shows a ground-level concentration comparison of SO_4 concentrations between global GEOS-Chem and p-TOMCAT simulations for baseline and ULSJ implementation when full-flight emissions are considered.

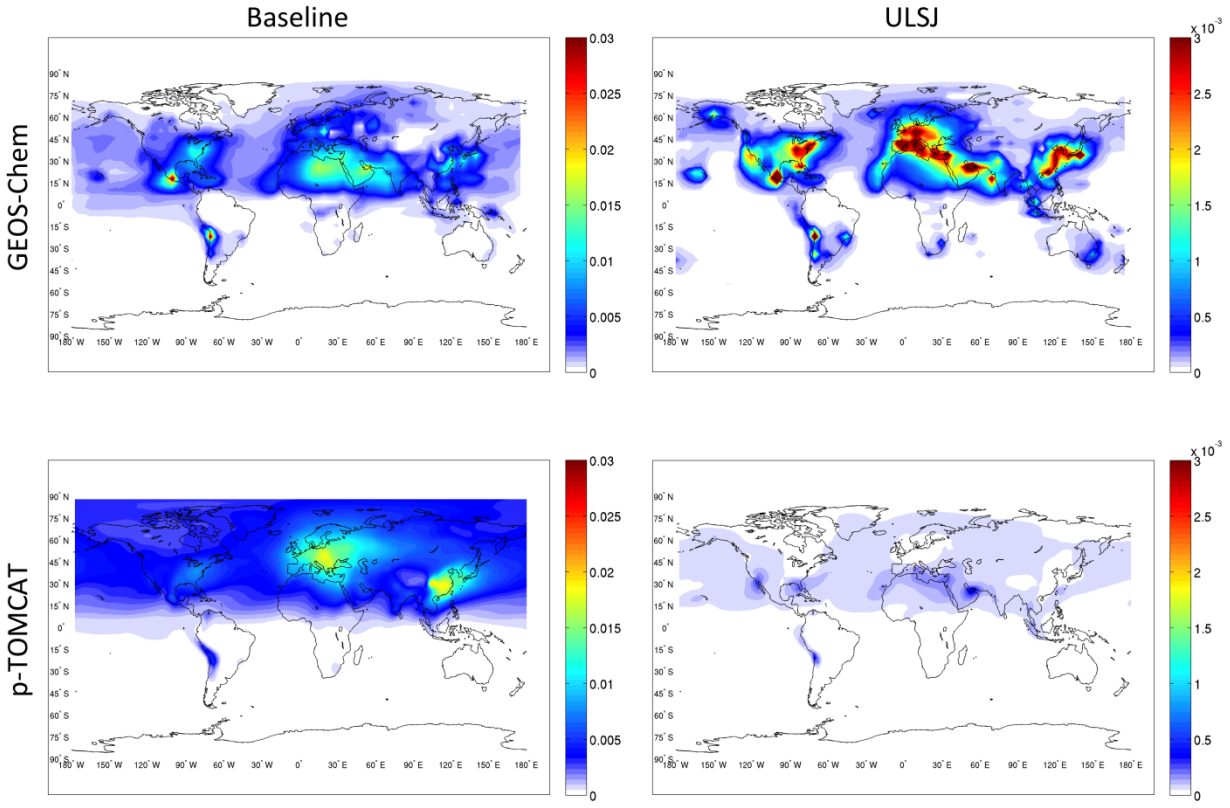

Figure T12: Comparison of GEOS-Chem and TOMCAT ULSJ aviation-attributable annually-averaged ground-level concentrations (μg/m^3) of SO_4 plotted against layer number when full flight emissions are considered.

C. Climate Impacts

Two changes in emissions due to ULSJ implementation are considered in this study: a decrease in aircraft SO_x emissions and an increase in well-to-wake (WTW) greenhouse gas (GHG) emissions. Because sulfate aerosol concentrations are reduced given the decrease in the sulfur content in the jet fuel, we determine the impact on radiative forcing (RF), a metric used to quantify the net effect of a particular species on the global radiation energy balance. Lee et al.[T34] provides values for aviation RF impacts, estimating the sulfate aerosol impact as -4.8 (90% CI: -0.79 to -29.3) mW/m^2 for 2005 aviation, where the negative RF value implies cooling. Sulfate aerosols have a cooling effect on the atmosphere, thus a decrease in the sulfur content of fuel would lead to a net warming effect when comparing ULSJ to standard aviation jet fuel when

only direct effects are considered. The increase in WTW GHG emissions was analyzed in Stratton et al.[T35] The relevant details from that report are provided in section C.2.

Important caveats in the RF calculations that follow are that changes in optical focusing caused by sulfuric acid coating on BC and indirect effects were not accounted for.

C.1. *Sulfate RF Calculation*

RF impacts from sulfate aerosols are calculated based on global GEOS-Chem simulations. Section C.1.1 discusses how RF is calculated from aerosol optical depth (AOD) values from the GEOS-Chem simulations.

C.1.1. Sulfate Aerosol RF Calculation Methodology

Eq. (1) is used to determine the globally averaged direct radiative forcing due to sulfate aerosols, or sulfate direct climate forcing (SDCF), from aerosol optical depth (τ) quantities calculated in GEOS-Chem[T36,T37]:

$$SDCF = -\frac{1}{4}F_T T^2(1-A_c)2(1-\bar{R}_s)^2(\bar{\beta}_{sd}\tau_{sd} + \bar{\beta}_{aq}\tau_{aq}), \quad (1)$$

where $\frac{1}{4}F_T$ is the global mean top-of-the-atmosphere radiative flux, T is the fraction of incident light transmitted by the atmospheric layer above the aerosol layer, A_c is the fractional amount of cloud cover, $\bar{R}_s$ is the area averaged albedo of the underlying surface, $\bar{\beta}_{sd}$ is the backscattering coefficient of a solid particle of interest, $\bar{\beta}_{aq}$ is the backscattering coefficient of an aqueous particle of interest, τ_{sd} is the optical depth of a solid particle of interest, and τ_{aq} is the optical depth of an aqueous particle of interest. This equation assumes the aerosol is a purely scattering particle (i.e. no absorption of solar radiation) and is optically thin (i.e. $\tau << 1$),[T36,T37] which are appropriate assumptions for the sulfate aerosol species present in the atmosphere.[T38] A derivation of Eq. (1) can be found in Seinfeld and Pandis.[T38]

Eq. (1) is a simplified one box model representation of the atmosphere. In general, a radiative transfer model (RTM) is used to determine the net perturbation a particular atmospheric species has on the global radiative balance, comparing cases with and without the aerosol to determine RF.[T37] In this one box representation, a single aerosol layer is assumed through which the net

flux is determined by using globally and temporally averaged parameter values present in Eq. (1). GEOS-Chem has no built in RTM. Because a more rigorous calculation of SDCF, as was done in Wang et al.,[T37] is outside the scope of this paper, it is assumed that this one box model approach is first order accurate. Transition between solid and aqueous states for sulfate aerosols is governed by a hysteresis cycle,[T37] where the relative humidity (RH) history of a particle is related to the hygroscopic growth that occurs. No hysteresis loop behavior is assumed in the GEOS-Chem simulations and sulfate aerosol particles are assumed to always be on the upper hysteresis branch.[T39,T48] Several studies have attempted to quantify the impact of sulfate hysteresis behavior on sulfate aerosol RF.[T37,T48,T40]

$\overline{\beta}$ can be estimated based on a particle's asymmetry factor, *g*, where *g* is an intensity-weighted average of the cosine of the scattering angle[T37,T38,T41]and is also a function of RH.[T40,T42] Wiscombe and Grams[T41] estimate the average value of $\overline{\beta}$ to be the following:

$$\overline{\boldsymbol{\beta}} = \frac{\mathbf{1}}{\mathbf{2}} - \frac{\mathbf{7}}{\mathbf{16}}\boldsymbol{g} \quad (2)$$

where, *g* is a function of the size of the particle, thus $\overline{\beta}$ (overbar denotes time average) is a function of RH given the hygroscopic growth that occurs due to water condensation.

Aerosol optical depth (AOD) values are obtained from GEOS-Chem simulations for the background (not including aviation), baseline aviation (background + aviation with standard jet fuel), and ULSJ aviation (background + aviation with ULSJ fuel) cases. These AOD values, however, are presented for a 400 nm wavelength of incoming solar radiation. Wang et al.[T37] evaluates AODs at 550 nm, "a wavelength that is representative of the mean across the solar spectrum." In general, RFs are calculated by taking a weighted average over the entire solar radiation spectrum as aerosol optical properties are wavelength dependent.[T42] A simplified weighted RF calculation is described in Nemesure et al.[T42] For this analysis, however, AODs at 550 nm are computed and used to determine sulfate aerosol RF. The version of GEOS-Chem used in this analysis cannot compute AODs at a specified wavelength other than at the default wavelength of 400 nm, although a recently developed post-processing module, FlexAOD,[T43] does have this functionality. FlexAOD can also compute asymmetry factors, which can be used

to determine the backscattering coefficient based on Eq. (2). Using FlexAOD, sulfate aerosol AODs are recomputed at 550 nm and used in Eq. (1).

The sulfate species bin within GEOS-Chem and FlexAOD also includes nitrates and ammonium where no distinction is made in optical properties between the different species. Limited research has been performed on the direct RF impacts of nitrates and ammonium alone, but nitrate contributions to overall aerosol mass is small relative to sulfate when background concentrations are considered and impact on direct RF is uncertain.[T44] Within GEOS-Chem, all three of these species are treated identically (i.e. purely scattering), thus Eq. (1) is still applicable. Using this bin to compute RFs also captures the nitrate bounce-back effect and its potential impact on direct climate forcing due to a reduction in atmospheric sulfate concentrations.

RF values for standard aviation minus the background and ULSJ aviation minus the background are calculated for four regions: global, northern hemisphere, Europe, and Asia. Values for all anthropogenic and biogenic sources of sulfate are also calculated. These RF values are area weighted to reflect the differences in grid box size given that GEOS-Chem uses a uniform polar grid (4° × 5°).

C.1.2. RF Uncertainty

The IPCC TAR[T45] provides uncertainty values and ranges (based on Penner et al.[T46]) for all of the coefficients in Eq. (1). The minimum and maximum values provided in the paper are used as bounds for a triangular distribution. No uncertainty estimate was provided for F_T.

Table T4: Coefficients in Eq. (1) and associated values and uncertainties.[T46]

Coefficient	Nominal Value	Uncertainty Range
$\boldsymbol{T^2}$	0.58	0.4 – 0.83
$\boldsymbol{1 - A_c}$	0.39	0.35 – 0.44
$\boldsymbol{(1 - \bar{R}_s)^2}$	0.72	0.65 – 0.8

Wiscombe and Grams[T41] provide a high, low, and mean value for the backscattering coefficient, $\bar{\beta}$. The mean value is previously shown in Eq. (2). The upper and lower bounds can be estimated as the following:

$$\bar{\beta}_{\text{high}} = \frac{1}{2} - \frac{3}{8}g \quad (3)$$

$$\bar{\beta}_{\text{low}} = \frac{1}{2} - \frac{1}{2}g \quad (4)$$

Uncertainty in the optical depth values from GEOS-Chem is not easily obtained due to the inherent complexity that exists in the model. Rather than attempt to determine how uncertainty propagates through the model based on initial uncertainties in the input data, the uncertainty for optical depth was determined by survey. IPCC AR4[T47] provides sulfate aerosol optical depth values across nine different models that used identical input emissions. These nine values are used to define an uncertainty factor for the optical depth values, which is presented in Table T12. This approach also captures uncertainty related to atmospheric processing and removal of SO_x emissions.

C.1.3. RF Results

Table T5 shows the calculated RF values for the SO_x pathway (i.e. Baseline-ULSJ), which corresponds to sulfate aerosol formation from direct aviation SO_x emissions. These values correspond to a global implementation of ULSJ. Total background sulfate RF values are also provided in order to further compare against values from the literature.

Table T5: Aviation sulfate RF by component and region.

Region **(RF in mW/m^2)**	**2.5% Percentile**	**Average**	**Median**	**97.5% Percentile**
Global	-6.0	-3.4	-3.3	-1.4
Northern Hemisphere	-11.2	-6.3	-6.1	-2.6
Europe	-15.9	-9.0	-8.8	-3.7
Asia	-8.2	-4.7	-4.5	-1.9
Background (W/m^2)	-1.44	-0.82	-0.80	-0.35

The total direct radiative forcing for sulfate, nitrate, and ammonium aerosols estimated from this analysis is -0.80 W/m^2. Results from Kiehl et al.[T40] and Wang et al.[T37] are not directly comparable as they only consider direct RF due to sulfate aerosols alone, where the latter only considers anthropogenic aerosols, although direct RF estimations of -0.56 W/m^2 and -0.389 W/m^2, respectively, show that the estimates made in this analysis are on the correct order of magnitude. Directly comparable results are found in Martin et al.,[T48] which also used GEOS-Chem and reported a direct RF of -0.605 W/m^2 for sulfate, nitrate, and ammonium aerosol species when biogenic and anthropogenic emissions are both considered under the assumption that aerosols were on upper hysteresis branch. The results from this analysis show a 36% bias

when compared to Martin et al. Liao et al.[T49] reports a sulfate aerosol RF of -0.49 W/m^2, but the annually and globally weighted average AOD at 550 nm is reported to be 0.024, while the simulations for this analysis produce an AOD of 0.034. Also, the use of RTMs (which were implemented in all of the aforementioned studies) more accurately models the flux between aerosol layers as well as accounting for the attenuation in solar radiation intensity as light penetrates the atmosphere. The SO_x pathway RF of -3.3 mW/m^2 is about 45% lower than the Lee et al.[T34] RF of -4.8 mW/m^2, although this value is captured within the 95 percentile range. The Lee et al.[T34] value is based off of a scaling from fuel burn indices relative to a reference value determined in Sausen et al.[T50]

C.2. *WTW GHG Emissions*

As a part of their analysis of alternative jet fuels, Stratton et al.[T35] performed a life cycle green house gas (GHG) emissions analysis of standard jet fuel and ULSJ using the Greenhouse Gases, Regulated Emissions, and Energy Use in Transportation (GREET) framework developed by Argonne National Laboratories. Their approach uses a weighted average of GHG emissions from all potential crude oil sources (12 different countries/regions) feeding into US refineries, i.e. just the extraction and raw material transportation aspects of the cycle. The baseline case is further defined by the assumptions made concerning the refining efficiency. It is assumed that the refining energy efficiency of conventional jet fuel is 93.5% (i.e. MJ of fuel for a unit quantity of jet fuel/MJ input to refinery). A life cycle analysis of standard jet fuel using 2005 production data yields a total WTW GHG emissions value of 87.5 gCO_2e/MJ. This value includes the extraction and transportation emissions as well as refining and combustion emissions.

For the corresponding baseline case, ULSJ differs from conventional jet fuel in terms of its life cycle analysis in two important ways. First, from a 2001 General Motors study,[T51] a 2% energy penalty is assumed for reducing the sulfur content in diesel fuel from 350 to 5 ppm, i.e. 2% more energy is required during the processing and refining stage of the life cycle given the additional HDS of the diesel fuel that is required. Given the similarities between diesel and jet fuel, this same 2% penalty assumption is extended to the case of ULSJ. This penalty is seen in the refining energy efficiency, which is reduced to 91.5% for ULSJ. Second, there is a 0.4% decrease in combustion CO_2 emitted per unit of fuel energy due to a change in the hydrogen-carbon ratio as a

result of the additional hydroprocessing. Both of these factors are accounted for in the life cycle analysis for ULSJ and yield a WTW GHG emissions total of 89.1 gCO_2e/MJ. Thus, a 2% increase in WTW GHG emissions is seen between the baseline cases for conventional jet fuel and ULSJ.

A high and low value of 90.7 and 87.5 gCO_2e/MJ are assumed as the uncertainty range in this analysis. Given that regional jet fuel data for the US shows an average FSC of 600-700 ppm and the ULSD study that is the basis of this work used a FSC of 350 ppm, it can then be expected that the assumed energy penalty could be as great as 4%. As determined in the baseline emissions scenario, a 2% energy penalty yields an 89.1 gCO_2e/MJ WTW GHG life-cycle emissions value, it then follows that a 4% energy penalty yields an additional 1.6 gCO_2e/MJ, or 90.7 gCO_2e/MJ. The low value is equal to the WTW GHG emissions value of conventional jet fuel where the FSC of the inputted crude oil is assumed to be less than 15 ppm, thus no additional processing would be required. A higher baseline energy penalty could be assumed given the higher FSC of jet fuel on average compared to diesel fuel. There is, however, considerable uncertainty in what energy penalty will be seen in ULSJ production because the chemical make-up of jet fuel (as outlined in Hileman et al.[T52]) in general has simpler hydrocarbon structures than diesel fuel. Thus the energy input required to desulfurize jet fuel from 350 to 5 ppm is potentially less than the energy input required to desulfurize diesel fuel the same amount.

C.3. *APMT-Impacts Climate Module*

As part of the aviation environmental portfolio management tool (APMT) project that focuses on quantifying and valuing the environmental effects of aviation activity, a framework in which climate impacts are assessed in a computationally inexpensive manner was initially developed by Marais et al.[T53] and then further developed by Mahashabde et al.[T54] This section will briefly describe the overall structure of the APMT-Impacts Climate module and explain the relevant parts of the code important to this analysis.

The APMT-Impacts Climate Module (from here on referenced as “APMT-Climate”) is used to value climate impacts on a global scale in this analysis. APMT-Climate takes as inputs fuel burn, CO_2, and NO_x emissions. Climate impacts due to a variety of species and effects, including

sulfate aerosol cooling, are derived or scaled from these inputs. Sulfate aerosols are designated "short-lived" effects, i.e. effects that are scaled directly from fuel burn and whose RF effects are assumed only to last the year in which it is emitted. For this climate analysis, only two climate impacts are considered: reduction in sulfate cooling due to FSC reduction and an increase in CO_2 RF due to the increase in WTW GHG emissions.

The RF due to SO_4 can be calculated using the following relationship:

$$RF_{\mathrm{SO_4}}(t) = \begin{cases} RF_{\mathrm{GEOS-Chem}} \frac{\lambda_{\mathrm{short},j}}{\lambda_{\mathrm{CO_2}}}, t = \text{emission year} \\ 0, \qquad\qquad t > \text{emission year} \end{cases}, \quad (5)$$

where $RF_{\text{GEOS-Chem}}$ is the RF value for sulfate aerosols calculated from the GEOS-Chem simulations as outlined in Section C.1, λ is the climate efficacy value for the short-lived and CO_2 effect, and t is a time variable in integer years. The climate efficacy relates the proportional change between the RF of the given species and the resulting temperature response of the system. Given the uncertainty in these estimates, this analysis assumes all efficacy values to be one, i.e. each effect produces the same proportional response in temperature given a unit RF input to the system.

The increase in CO_2 emissions is reflected in the emissions inputs required by the code, as mentioned previously. Although these are not direct aviation emissions, the method by which the CO_2 RF value is determined is based on total atmospheric CO_2 concentrations, and thus the source of the CO_2 is inconsequential. APMT-Climate deals with CO_2 effects by determining the overall change in concentration given the input emission index based on an impulse-response function and then integrating the product of these values over time. A logarithmic relationship is then used to determine the RF of CO_2 in the atmosphere for the study year relative to pre-industrial CO_2 levels. Further details are provided in Marais et al.[53] and Mahashabde et al.[54]

Once RFs have been computed, surface temperature changes are calculated by using a simplified analytical heat transfer model.[T55] After the induced temperature changes are calculated, these values are then passed to a damage function that computes the impact on global GDP, as is the case with the DICE-2007 model.[T56] Although RF effects for short-lived terms are only considered for the year of emission, the temperature effects can last multiple years resulting from

the transient heat model, thus the total damage is provided as a net present value (NPV) of damages taken in relation to the base year of 2006.

This analysis is limited to a one-year pulse emission scenario for the policy (ULSJ) and baseline (standard jet fuel) cases. As mentioned previously, RF effects for sulfate aerosols last only in the year they are emitted, but CO_2 RF impacts are tracked into the future due to the lifetime of the species. Temperature effects are also tracked into the future for all species given the analytical heat transfer model. A time horizon of 800 years is assumed for this analysis.

D. Health Impacts

D.1. *Health Impacts of $PM_{2.5}$ Exposure*

Many studies have linked $PM_{2.5}$ concentrations to adverse health endpoints in the US and elsewhere. For this analysis, only premature mortality is considered given its dominance over other monetized health endpoints in benefit-cost analyses.[T57] We focus more specifically on premature deaths associated with long-term exposure to $PM_{2.5}$, as derived from cohort studies. Critical issues from the perspective of developing concentration-response functions (CRFs) applicable to a global analysis include whether the function is linear across a wide range of concentrations, whether there are differential CRFs by health outcome (given differing patterns of disease-specific mortality across countries), and more generally, whether estimates can be derived with an adequate degree of certainty given issues such as differential toxicity of various particle constituents.

The association between long-term exposure to $PM_{2.5}$ and premature mortality was most notably characterized in the American Cancer Society (ACS) [T58,T59] and Harvard Six Cities cohort studies,[T60,T61] with the conclusions regarding causality and the magnitude of the association corroborated by an EPA expert elicitation study.[T62] Broadly, there is an array of literature[T63] indicating effects largely on cardiovascular or respiratory disease, with potential causal pathways that may include chronic obstructive pulmonary disease (COPD)[T64,T65] and atherosclerosis.[T66] An impact on lung cancer risk due to PM exposure is thought to exist, but the relationship remains not as well characterized.[T67,T68,T69] Given the evidence base, as described in more detail below, we focus on deaths resulting from cardiopulmonary (CP) diseases and lung cancer (LC).

In terms of the shape of the CRF, multiple cohort studies have indicated that a linear association best fits the data, including in a Six Cities investigation that used Bayesian model averaging approaches to allow for threshold models and other non-linear structures to be probabilistically combined.[T70] The expert elicitation study and regulatory applications have all concurred with this conclusion. However, this has only been determined within the range of concentrations observed in the ACS and Six Cities cohort studies (as well as other studies largely in developed countries), and it is possible that the slope differs at high concentrations typically found in the developing world. As discussed below, applications in the context of global burden of disease modeling have assumed log-linear relationships (largely to avoid implausibly large burden of disease values in developing countries), which results in a lower premature mortality response at higher background $PM_{2.5}$ concentrations.[T88]

Differential toxicity among $PM_{2.5}$ constituents is a subject of ongoing research and is relevant given that the change in ground-level $PM_{2.5}$ due to ULSJ implementation is seen primarily in SO_4 species. The relative impact of SO_4 species on public health becomes important in determining the magnitude of avoided mortalities seen due to a reduction in FSC. While some studies argue that inorganic aerosols are not causally associated with health outcomes.[T71] others have shown positive associations between sulfate and a variety of CP endpoints,[T72,T73,T74] and expert committees have concluded that there is no specific basis at this time to deviate from an assumption of equal toxicity.[T53,T75] Intervention studies have also illustrated health improvements associated with fuel sulfur reductions – for example, Hedley et al.[T76] showed that a reduction in SO_x emissions in Hong Kong due to a sulfur content restriction of 5000 ppm for fuel used in power plants was accompanied by a 2.1% reduction in all-cause mortality, a 3.9% reduction in respiratory disease related mortalities, and a 2.0% reduction in cardiovascular related mortalities. In this analysis, we follow standard approaches and assume that all $PM_{2.5}$ species, including those derived from SO_x emissions, have equal health impacts, but recognize that this is a significant uncertainty not formally incorporated into our Monte Carlo analysis.

D.2. *Concentration Response Functions*

For our primary analysis, evidence from US-based cohort studies is extrapolated to other countries, but several assumptions are required. First, a linear CRF is applied throughout the

range of global concentrations, which could overestimate impacts in countries such as China and India if a log-linear functional form is more appropriate. Second, it is assumed that all avoided mortalities that result from ULSJ implementation will be seen in a reduction in cardiopulmonary disease and lung cancer related deaths. Third, consideration is limited to members of the population with an age greater than 30, consistent with the original cohort studies. The CRF then has the following form:

$$\Delta(\text{Premature Mortalities}) = \sum_{ij}[\beta_k^{CP} f_{k,30+} P_{ij} \Delta x_{ij} B_k^{CP} + \beta_k^{LC} f_{k,30+} P_{ij} \Delta x_{ij} B_k^{LC}], \quad (6)$$

where k denotes the country of interest, which is a function of the grid cell location, i,j (i.e. $k = k(i,j)$), $f_{k,30+}$ is the fraction of the population above 30 years of age in a specific country, B is the disease specific baseline per capita mortality rate in a specific country, CP denotes values in terms of cardiopulmonary disease, LC denotes values in terms of lung cancer, β is the fractional increase in mortality given one $\mu g/m^3$ increase in annual average $PM_{2.5}$ (i.e. risk coefficient) and is a function of the disease of interest, P_{ij} is the total population in grid cell, i,j, and $\Delta\chi_{ij}$ is the change in $PM_{2.5}$ concentration in a grid cell, i,j with units of $\mu g/m^3$. In Eq. (8), the summation symbol and indices, i,j, show that in order to obtain the total avoided mortalities, it is necessary to sum across all grid points defined by the gridded population data, GRUMP,[T77] which has a finer grid resolution (2.5' × 2.5') than global GEOS-Chem (4° × 5°). Each population grid cell is assigned to the closest corresponding GEOS-Chem grid cell (by grid center point) to determine population/concentration products as required by Eq. (8).

The change in the number of premature mortalities is split between both disease groups with two different β values, which are assumed not to change across countries and are based on epidemiological data for the US. Separating the effects of CP and LC allows us to capture differential baseline mortality rates across countries and avoid using all-cause mortality rates that may include outcomes unrelated to air pollution in developing countries. Under the assumption that CP and LC premature mortalities dominate and comprise all premature mortalities seen by a change in ground-level $PM_{2.5}$ concentration, the disease-specific risk coefficients within the US are related to the all-cause (AC) values by

$$\beta_{US}^{AC} B_{US}^{AC} = \beta_{US}^{CP} B_{US}^{CP} + \beta_{US}^{LC} B_{US}^{LC}, \quad (7)$$

where β_{US}^{CP} and β_{US}^{LC} are unknown. Baseline incidence rates for the US are computed using data from the WHO Global Burden of Disease (GBD)[T78] database. β_{US}^{AC} is centered on a 1% increase in premature mortality given a 1 μg/m^3 increase in ground-level $PM_{2.5}$ concentration, based on a Weibull distribution fit to estimates from the ACS and Six Cities studies.[T59,T61] This value is comparable to the average value across the median estimates from experts in the expert elicitation study,[T62] and follows current EPA methodology[T57] (and is therefore described as "the EPA CRF" below).

The number of CP related deaths is much greater than LC related deaths in the US, and the CP risk coefficient is characterized with more certainty. As a result, Eq. (7) can be defined in terms of β_{US}^{CP} and a ratio between the uncertain disease specific relative risks, γ. Eq. (7) then becomes

$$\beta_{US}^{AC} B_{US}^{AC} = \beta_{US}^{CP}[B_{US}^{CP} + \gamma B_{US}^{LC}] \quad (8) \quad \text{where}$$

$$\gamma = \frac{(RR^{LC}-1)}{RR^{LC}} / \frac{(RR^{CP}-1)}{RR^{CP}}, \quad (9)$$

and *RR* is the ratio between the number of health incidences in the baseline pollution case to the number of health incidences when only background pollution is considered. (*RR-1)/RR* is then the percentage change in mortality given a change in ground-level $PM_{2.5}$ concentration. Rearranging Eq. (8) produces the following equation for the risk coefficient.

$$\beta_{US}^{CP} = \frac{\beta_{US}^{AC} B_{US}^{AC}}{[B_{US}^{CP} + \gamma B_{US}^{LC}]} \quad (10)$$

To solve for β_{US}^{CP}, an appropriate value of γ must be determined. Table T6 shows the central estimates for these *RR*, adjusted to percent increase per $\mu g/m^3$ increase in $PM_{2.5}$.

Table T6: Percentage increase in avoided mortalities given a 1 μg/m^3 increase in ground-level $PM_{2.5}$ concentration, values from Pope et al.[T59] and Laden et al.[T61]

	Pope	Laden
All Cause	0.6	1.4
Cardiopulmonary	0.8	2.2
Lung Cancer	1.2	2.1

Based on the values in Table T6, if each *RR* value is allowed to vary within the specified range above, γ can range from 0.5 (1.2/2.2) to 2.6 (2.1/0.8) where a uniform distribution is assumed for each *RR*. Eqs. (9) and (12) yield the following result:

$$\Delta(\text{Premature Mortalities}) = \sum_{ij}[f_{k,30+}\, P_{ij} \Delta\chi_{ij} \beta_{US}^{CP}(B_k^{CP} + \gamma B_k^{LC})] \quad (11)$$

As a sensitivity analysis, we considered the WHO methodology described by Ostro,[T79] which was applied by Barrett et al.[T80] to determine the number of mortalities that result from full-flight operations by aircraft. This function has the following form:

$$RR_k = \left(\frac{\chi_A + 1}{\chi_B + 1}\right)^{\beta} \quad (12)$$

$$\text{Premature Mortalities} = \sum_k \frac{RR_k - 1}{RR_k} B_k P_k \quad (13)$$

where χ_A and χ_B are the concentrations for the policy and baseline cases, which for this study would be ULSJ aviation and standard aviation, respectively, β is a disease specific power coefficient, B_k is the baseline incidence rate for a specific disease, P_k is the exposed population, and *k* corresponds to a given country and total mortalities are determined by summing across all countries. Thus, this methodology uses background concentrations compared across policy cases in order to determine a relative risk per country (RR_k), which is then related to a percent increase in premature mortality given some change in $PM_{2.5}$ concentration. This method results in a lower marginal risk at higher concentrations.

Baseline incidence rates are a function of grid cell location (i.e. the country that coincides with that grid cell) and are determined using the WHO GBD database ,[T78] which provides cause specific mortality information bracketed by age group for each country. Given that the ACS and Harvard Six Cities cohort studies focused on populations 30 and 25 years and older, respectively, country specific mortality data is required specifically for the 30 years and older (30+) age bracket. WHO GBD data, however, are provided only for the 15+ bracket. As a first approximation, it is assumed that no CP and LC deaths occur in the 15-30 age bracket, and that the mortality data provided for the 15+ bracket can be exactly applied to the 30+ bracket. Relative uncertainties for all cause mortality rates are also provided for each country. Applying

these uncertainties to cause-specific deaths underestimates the uncertainty for CP and LC related deaths, but no cause-specific relative uncertainties are provided. 30+ population data for each country are obtained using the US Census IDB.[T81] Given that similar data is used to determine the WHO GBD database values as are used to perform the population projections in the US Census IDB, the relative uncertainties from the GBD database are also applied to the population projections.

D.3. *Health Impacts Results*

Avoided mortalities by country due to ULSJ implementation are presented in Table T7 for both EPA and WHO CRFs. The WHO values are deterministic.

Table T7: Avoided mortalities by country due to ULSJ implementation.

	EPA-derived CRF from Eq. (13), Full-Flight Emissions			**EPA-derived CRF from Eq. (13), LTO Emissions**			**WHO CRF from Eq. (7)**	
							Full-Flight	**LTO**
Country	**2.5% Percentile**	**Mean**	**97.5% Percentile**	**2.5% Percentile**	**Mean**	**97.5% Percentile**		
Afghanistan	5.2	16	31	0.0	0.0	0.0	14	-0.1
Albania	0.4	1	1.9	0.1	0.3	0.4	0.6	0.1
Algeria	2.9	7.3	13	0.4	1.2	1.9	12	1.6
Angola	1.0	2.7	5.5	-0.20	-0.10	0.0	1.20	0.0
Antigua and Barbuda	0.0	0.0	0.0	0.0	0.0	0.0	0.0	0.0
Argentina	0.7	1.7	3.1	0.1	0.3	0.5	2.8	0.4
Armenia	1.6	4.1	7.9	0.0	0.0	0.0	2.6	0.0
Australia	0.4	0.9	1.6	0.1	0.2	0.3	1.4	0.3
Austria	2.3	5.8	11	0.1	0.4	0.6	1.8	0.2
Azerbaijan	1.8	4.5	8.3	0.0	0.1	0.2	3.7	0.1
Bahrain	0.1	0.2	0.4	0.0	0.0	0.0	0.2	0.0
Bangladesh	32	81	150	0.7	1.8	3.2	39	0.8
Belarus	5.2	13	24	-0.5	-0.3	-0.1	4.8	-0.1
Belgium	4.1	11	20	0.1	0.3	0.6	3.1	0.1
Belize	0.0	0.0	0.1	0.0	0.0	0.0	0.1	0.0
Benin	0.4	1	2	0.1	0.3	0.5	1	0.2
Bhutan	0.4	1.3	2.6	0.0	0.0	0.1	0.6	0.0
Bolivia	0.1	0.3	0.5	0.0	0.0	0.0	0.4	0.0
Bosnia-Herzegovina	0.6	1.5	2.7	0.1	0.3	0.6	0.7	0.2
Botswana	0.0	0.1	0.1	0.0	0.0	0.0	0.1	0.0
Brazil	3.2	8.2	15	0.6	1.6	2.9	15	2.4
Brunei Darussalam	0.0	0.0	0.0	0.0	0.0	0.0	0.0	0.0
Bulgaria	1.4	3.5	6.3	0.1	0.3	0.5	1.6	0.1
Burkina Faso	1.8	5	9.6	0.2	0.4	0.8	7.9	0.4
Burundi	0.1	0.4	0.8	0.0	0.0	0.0	0.5	0.0
Cambodia	0.4	1.2	2.4	0.0	0.1	0.2	1.7	0.1

	EPA-derived CRF from Eq. (13), Full-Flight Emissions			EPA-derived CRF from Eq. (13), LTO Emissions			WHO CRF from Eq. (7)	
							Full-Flight	LTO
Country	**2.5% Percentile**	**Mean**	**97.5% Percentile**	**2.5% Percentile**	**Mean**	**97.5% Percentile**		
Cameroon	2	5.4	11	0.4	0.9	2	5.1	0.9
Canada	2.3	6	11	0.3	0.7	1.2	5.9	0.8
Cape Verde	0.0	0.0	0.1	0.0	0.0	0.0	0.2	0.0
Central African Republic	-2.6	-1.3	-0.5	0.6	1.5	3.2	-0.3	0.6
Chad	2.2	5.8	12	0.8	2	4.5	6.9	1.7
Chile	0.1	0.2	0.4	0.0	0.1	0.1	0.3	0.1
China	85	220	390	-270	-150	-59	72	-13
Colombia	0.6	1.5	2.7	0.0	0.0	0.0	4.1	0.1
Commonwealth of Dominica	0.0	0.0	0.0	0.0	0.0	0.0	0.0	0.0
Comoros	0.0	0.0	0.0	0.0	0.0	0.0	0.0	0.0
Congo	0.0	0.1	0.3	0.0	0.0	0.0	0.1	0.0
Congo Democratic Republic	1.2	3.3	6.3	-0.7	-0.4	-0.1	2.6	-0.2
Costa Rica	0.1	0.2	0.3	0.0	0.0	0.0	0.7	0.0
Croatia	1	2.5	4.6	0.3	0.7	1.3	1.2	0.3
Cyprus	0.1	0.3	0.5	0.0	0.0	0.1	0.3	0.0
Czech Republic	4.3	11	20	-1.3	-0.7	-0.3	2.9	-0.2
Denmark	1.2	3.1	5.8	0.1	0.3	0.5	1.5	0.1
Djibouti	0.1	0.2	0.4	0.0	0.0	0.0	0.5	0.0
Dominican Republic	0.8	1.9	3.4	0.0	0.1	0.1	5.7	0.2
East Timor	0.0	0.0	0.0	0.0	0.0	0.0	0.0	0.0
Ecuador	0.0	0.1	0.2	0.0	0.0	0.0	0.4	0.1
Egypt	15	39	70	1.1	3	5.2	46	3.4
El Salvador	0.2	0.5	0.9	0.0	0.0	0.0	1.2	0.0
Equatorial Guinea	0.0	0.0	0.1	0.0	0.0	0.0	0.1	0.0
Eritrea	0.3	0.9	1.7	0.0	0.0	0.1	1.3	0.0
Estonia	0.3	0.8	1.5	-0.2	-0.1	0.0	0.5	-0.1
Ethiopia	6.5	18	36	0.3	0.8	1.8	30	1
Federated State of Micronesia	0.0	0.0	0.0	0.0	0.0	0.0	0.0	0.0
Fiji	0.0	0.0	0.0	0.0	0.0	0.0	0.0	0.0
Finland	0.4	1.1	2	0.1	0.2	0.3	1	0.1
France	8.3	22	39	1.1	2.9	5.1	11	1.8
FYROM/Macedonia	0.3	0.9	1.6	0.1	0.2	0.3	0.5	0.1
Gabon	0.0	0.1	0.1	0.0	0.0	0.0	0.1	0.0
Gambia	0.1	0.4	0.8	0.0	0.2	0.2	0.6	0.2
Georgia	1.1	2.8	5.1	0.0	0.0	0.0	1.9	0.0
Germany	32	83	150	1.8	4.7	8.4	25	1.4
Ghana	0.7	2	4	0.2	0.5	1	2.3	0.4
Greece	1.2	3.1	5.7	0.2	0.5	0.9	2.8	0.5
Grenada	0.0	0.0	0.0	0.0	0.0	0.0	0.0	0.0
Guatemala	0.3	0.8	1.5	0.0	0.0	0.0	2	0.1
Guinea	0.6	1.7	3.2	0.2	0.5	1.1	1.6	0.3
Guinea-Bissau	0.1	0.3	0.7	0.0	0.1	0.1	0.5	0.1
Guyana	0.0	0.0	0.1	0.0	0.0	0.0	0.1	0.0
Honduras	0.2	0.6	1.1	0.0	0.0	0.0	1.6	0.0
Hungary	2.7	7	13	0.2	0.6	1.1	2.2	0.2

	EPA-derived CRF from Eq. (13), Full-Flight Emissions			EPA-derived CRF from Eq. (13), LTO Emissions			WHO CRF from Eq. (7)	
							Full-Flight	LTO
Country	**2.5% Percentile**	**Mean**	**97.5% Percentile**	**2.5% Percentile**	**Mean**	**97.5% Percentile**		
Iceland	0.0	0.0	0.0	0.0	0.0	0.0	0.0	0.0
India	340	870	1600	-93	-55	-20	390	-15
Indonesia	4.8	12	22	0.5	1.3	2.3	20	2.6
Iran	12	29	54	0.1	0.3	0.5	28	0.4
Iraq	5.8	15	28	0.2	0.6	1.1	15	0.6
Ireland	0.2	0.6	1.1	0.1	0.2	0.3	0.7	0.2
Israel	0.8	2	3.7	0.1	0.2	0.3	2.5	0.2
Italy	9.8	25	46	3.2	8.4	15	15	4.9
Ivory Coast	0.7	1.8	3.6	0.0	0.1	0.2	2.6	0.1
Jamaica	0.3	0.7	1.3	0.0	0.0	0.0	2.1	0.1
Japan	5.7	15	27	1.3	3.4	6.3	14	3.6
Jordan	0.6	1.5	2.8	0.0	0.1	0.2	1.9	0.1
Kazakhstan	2.9	7.5	14	0.3	0.7	1.2	6.9	0.6
Kenya	0.5	1.5	2.9	0.0	0.0	0.1	4.2	0.1
Kiribati	0.0	0.0	0.0	0.0	0.0	0.0	0.0	0.0
Korea	3.3	8.5	16	0.5	1.3	2.3	2.1	0.3
Kuwait	0.2	0.5	1	0.0	0.0	0.0	0.5	0.0
Kyrgyz Republic	0.9	2.3	4.2	0.1	0.2	0.5	2.3	0.2
Lao People's Democratic Republic	0.3	0.9	1.7	-0.1	-0.1	0.0	0.6	0.0
Latvia	0.6	1.5	2.8	-0.3	-0.2	-0.1	0.9	-0.1
Lebanon	0.7	2	3.6	0.1	0.2	0.3	2.1	0.2
Lesotho	0.0	0.1	0.1	0.0	0.0	0.0	0.1	0.0
Liberia	0.1	0.2	0.5	0.0	0.0	0.0	0.6	0.0
Libyan Arab Jamahiriya	0.5	1.4	2.6	0.1	0.2	0.3	2.1	0.3
Lithuania	1.5	3.9	7.1	0.0	0.0	0.1	1.4	0.0
Luxembourg	0.1	0.3	0.6	0.0	0.0	0.0	0.1	0.0
Madagascar	0.1	0.2	0.4	0.0	0.0	0.0	0.7	0.0
Malawi	0.1	0.3	0.6	0.0	0.0	0.0	0.6	0.0
Malaysia	0.4	1.1	2.1	0.0	0.1	0.2	1.5	0.1
Maldives	0.0	0.0	0.1	0.0	0.0	0.0	0.1	0.0
Mali	2.1	5.7	11	-0.3	-0.2	-0.1	9.9	-0.2
Malta	0.1	0.2	0.3	0.0	0.0	0.1	0.2	0.0
Mauritania	0.4	1	2.2	0.0	0.0	0.0	2.5	0.0
Mauritius	0.0	0.0	0.0	0.0	0.0	0.0	0.1	0.0
Mexico	6.5	17	30	0.5	1.3	2.3	26	2.1
Mongolia	0.1	0.3	0.6	0.0	0.0	0.0	0.5	0.0
Morocco (includes Western Sahara)	3.9	10	18	0.3	0.7	1.3	19	1.4
Mozambique	0.1	0.4	0.7	0.0	0.0	0.0	0.8	0.0
Namibia	0.0	0.0	0.1	0.0	0.0	0.0	0.1	0.0
Nepal	7.3	18	34	-1.9	-1.1	-0.4	8.3	-0.3
Netherlands	3	7.7	14	0.3	0.8	1.5	2.8	0.4
New Zealand	0.0	0.0	0.0	0.0	0.0	0.0	0.1	0.0
Nicaragua	0.2	0.4	0.8	0.0	0.0	0.0	1.5	0.0
Niger	2.7	8	15	0.2	0.5	1.1	15	1.1
Nigeria	11	30	60	0.9	2.2	4.9	37	2.9

	EPA-derived CRF from Eq. (13), Full-Flight Emissions			EPA-derived CRF from Eq. (13), LTO Emissions			WHO CRF from Eq. (7)	
							Full-Flight	LTO
Country	**2.5% Percentile**	**Mean**	**97.5% Percentile**	**2.5% Percentile**	**Mean**	**97.5% Percentile**		
Norway	0.3	0.7	1.3	0.0	0.1	0.2	0.9	0.2
Oman	0.3	0.8	1.6	0.0	0.0	0.1	1	0.1
Pakistan	37	95	170	-18	-9.7	-3.8	51	-3.1
Panama	0.0	0.1	0.2	0.0	0.0	0.0	0.5	0.0
Papua New Guinea	0.0	0.0	0.1	0.0	0.0	0.0	0.2	0.0
Paraguay	0.1	0.2	0.4	0.0	0.0	0.0	0.3	0.0
Peru	0.2	0.5	0.9	0.0	0.0	0.1	1.1	0.1
Philippines	1.7	4.5	8.3	0.1	0.2	0.3	13	0.5
Poland	11	27	50	-1.6	-0.9	-0.3	7.5	-0.5
Portugal	0.7	1.7	3.1	0.2	0.5	0.9	2.6	0.7
Republic of Moldova	0.9	2.3	4.2	-0.5	-0.3	-0.1	1	-0.1
Romania	3.7	9.3	17	-4.8	-2.8	-1	3	-0.8
Russia	28	73	140	-18	-11	-3.6	37	-2.7
Rwanda	0.1	0.4	0.7	0.0	0.0	0.0	0.4	0.0
Saint Kitts and Nevis	0.0	0.0	0.0	0.0	0.0	0.0	0.0	0.0
Saint Lucia	0.0	0.0	0.0	0.0	0.0	0.0	0.0	0.0
Saint Vincent	0.0	0.0	0.0	0.0	0.0	0.0	0.1	0.0
Sao Tome and Principe	0.0	0.0	0.0	0.0	0.0	0.0	0.0	0.0
Saudi Arabia	4	11	22	0.4	1	1.9	13	1.1
Senegal	1.3	3.6	7.2	0.3	0.8	1.8	5.3	1.3
Serbia and Montenegro	3.1	7.9	14	0.5	1.2	2.2	3.6	0.6
Seychelles	0.0	0.0	0.0	0.0	0.0	0.0	0.0	0.0
Sierra Leone	0.5	1.6	3.3	0.2	0.4	1.1	1.7	0.3
Singapore	0.1	0.3	0.6	0.0	0.1	0.1	0.3	0.1
Slovakia	2.3	5.8	11	0.1	0.3	0.5	1.3	0.1
Slovenia	0.4	1.1	2	0.1	0.3	0.6	0.5	0.1
Solomon Islands	0.0	0.0	0.0	0.0	0.0	0.0	0.0	0.0
South Africa	0.7	1.8	3.4	0.1	0.2	0.3	2.2	0.2
Spain	5.8	15	27	1.5	4.1	7.1	14	3.7
Sri Lanka	1.5	3.8	7.1	0.0	0.1	0.2	9.2	0.3
Sudan	5.8	16	31	0.2	0.7	1.2	22	0.8
Suriname	0.0	0.0	0.0	0.0	0.0	0.0	0.1	0.0
Swaziland	0.0	0.0	0.0	0.0	0.0	0.0	0.0	0.0
Sweden	1.1	2.8	5.1	0.0	0.0	0.0	2.2	0.1
Switzerland	1.2	3	5.5	0.3	0.8	1.3	1.1	0.2
Syrian Arab Republic	1.6	4.1	7.4	0.1	0.3	0.5	3.9	0.3
Tajikistan	0.9	2.4	4.6	0.1	0.2	0.4	2.2	0.2
Thailand	2.6	6.8	12	0.1	0.2	0.3	7.1	0.4
Togo	0.3	0.7	1.4	0.1	0.3	0.5	0.7	0.2
Tonga	0.0	0.0	0.0	0.0	0.0	0.0	0.0	0.0
Trinidad and Tobago	0.0	0.1	0.2	0.0	0.0	0.0	0.5	0.0
Tunisia	1.3	3.4	6.1	0.3	0.7	1.2	5	0.9
Turkey	8.3	21	39	0.8	2.3	3.8	16	1.5
Turkmenistan	1.4	3.5	6.4	0.1	0.3	0.5	4.1	0.3
Uganda	0.7	1.8	3.4	0.0	0.1	0.1	2.9	0.1
Ukraine	23	57	100	-22	-13	-4.9	21	-4.1
United Kingdom	9.7	25	45	2.8	7.2	13	14	4.2

	EPA-derived CRF from Eq. (13), Full-Flight Emissions			EPA-derived CRF from Eq. (13), LTO Emissions			WHO CRF from Eq. (7)	
							Full-Flight	LTO
Country	**2.5% Percentile**	**Mean**	**97.5% Percentile**	**2.5% Percentile**	**Mean**	**97.5% Percentile**		
United Rep. of Tanzania	0.6	1.7	3	0.0	0.0	0.0	4	0.1
United States of America	46	120	210	12	31	56	140	34
Uruguay	0.0	0.1	0.2	0.0	0.0	0.0	0.3	0.0
Uzbekistan	3.9	9.9	18	0.6	1.5	2.6	8.9	1.2
Vanuatu	0.0	0.0	0.0	0.0	0.0	0.0	0.0	0.0
Venezuela	0.6	1.5	2.7	0.0	0.0	0.1	4.3	0.1
Viet Nam	4	10	19	-0.8	-0.5	-0.2	9.4	0.2
Western Samoa	0.0	0.0	0.0	0.0	0.0	0.0	0.0	0.0
Yemen	3.3	9.6	19	0.1	0.2	0.5	14	0.4
Zambia	0.2	0.5	1	0.0	0.0	0.0	0.4	0.0
Total	**890**	**2300**	**4200**	**-390**	**-130**	**100**	**1500**	**58**

Note: positive values indicate avoided mortalities (i.e. saved lives) while negative numbers indicate an increased mortalities (i.e. lives lost) after ULSJ implementation.

Avoided mortality numbers from the US nested GEOS-Chem and CMAQ are provided in Table T8. Note that based on the EPA CRF formulation, for the US specifically, the avoided mortalities are independent of γ, i.e. the ratio between the disease specific relative risks.

Table T8: Regional simulations avoided mortalities results for US from global implementation of ULSJ.

		Full-Flight Emissions			LTO Emissions	
	2.5% Percentile	**Mean**	**97.5% Percentile**	**2.5% Percentile**	**Mean**	**97.5% Percentile**
Nested GEOS-Chem	56	140	260	18	44	81
CMAQ	93	230	430	33	83	150

When compared to the global GEOS-Chem simulation avoided mortality numbers, the nested GEOS-Chem values are 17% higher than the global GEOS-Chem results, while the CMAQ results are 92% higher on average when full-flight emissions are considered.

Table T7 shows that when using the EPA CRF formulation, considering only LTO emissions results in a global net increase in mortalities (net health disbenefit), while using the WHO formulation results in a global net decrease in mortalities (net health benefit) when compared to the baseline scenario. Based on the previously defined CRFs, any increase in ground-level $PM_{2.5}$

concentrations will result in an increase in mortalities (i.e. negative values). The differences in global avoided mortalities between the two CRFs can be explained by the non-linearity of the WHO function. For instance, China's (the US's) change in concentration due to ULSJ implementation for LTO emissions is +0.002 $\mu g/m^3$ (-0.001 $\mu g/m^3$) while the background concentration is 45.5 $\mu g/m^3$ (6.2 $\mu g/m^3$), where the values are population weighted. A gradient can be defined for each CRF, where the WHO gradient is defined as (*RR-1)/RR*, and the EPA gradient is defined as the product of the risk coefficient and the change in ground-level $PM_{2.5}$ concentration. Applying the data that was used to derive the population weighted values, the WHO CRF gradient is 12 times lower than the gradient assumed by the EPA CRF in China and 8 times lower than the gradient assumed by the WHO CRF in the US. As a result, the WHO CRF predicts -13 avoided mortalities compared to the -150 avoided mortalities predicted by the EPA CRF (whereas in the US, it is 34 versus 31 avoided mortalities, WHO and EPA, respectively). Thus, countries such as China, including India where background $PM_{2.5}$ concentrations are also high, cause an overall increase in mortalities when health impacts are scaled linearly to ground-level concentration changes for LTO impacts (-130 on average, not discounted).

D.4. *Valuing Avoided Premature Mortalities*

The EPA suggests the use of the value of a statistical life (VSL) as a means to value avoided premature mortalities when conducting benefit-cost analyses (CBA).[T82] Many studies have explored VSL values in the United States and other relatively high income countries,[T83,T84,T85] but uncertainty remains in determining how to apply VSLs from higher income countries to lower income countries in order to provide an appropriate estimate in these countries where no VSL estimates have been made.

VSL is constructed from a person's willingness to pay (WTP) for an arbitrarily small but finite reduction in risk, corresponding with the aggregate population WTP due to an expected fatality. Wage-risk studies estimate WTP by comparing an individual's perceived risk within a certain type of employment versus the amount of compensation the individual receives, i.e. wage. Beyond higher income countries, few credible VSL estimates exist. Miller[T83] provided estimates for 49 countries, including several low income countries. For this analysis, it is necessary to extrapolate a VSL from one country and apply it to another country in which no estimate has

been made. From Hammitt and Robinson,[T85] who conducted a study on applying US VSL specifically to sub-Saharan Africa, the following relationship can be used to extend a VSL from one country to another.

$$\mathrm{VSL}_B = \mathrm{VSL}_A \cdot \left(\frac{I_B}{I_A}\right)^{\mathrm{IE}}, \quad (14)$$

where *A* and *B* denote the base country and country of interest, respectively, VSL are the VSLs for the respective countries, *I* is a measure of income for each country, and IE is the income elasticity associated with VSL.

This method requires the selection of a base VSL. For the purposes of this study, the US is used as the base country with a VSL of $7.4 million in 2006 dollars as suggested by the EPA.[T82] This value is derived from 26 US VSL studies where values have been adjusted for inflation. A Weibull distribution was then fitted to the data with a scale parameter of 7.75 and a shape parameter of 1.51.[T82] Hammitt and Robinson[T85] recommend using gross national income (GNI) per capita as an income measure for each country. The major source of uncertainty lies in the value of IE used. IE is a reflection of the proportion of an individual's income that is used towards risk reduction. Within higher income countries, it has been shown that IE's less than one are appropriate,[T85] meaning that an increase in income level does not cause a proportional increase in VSL. When performing cross-country comparisons where there is a large discrepancy in income level, however, IEs greater than one are plausible given that as the average income of a person is reduced, a reduction in the proportion of income used towards risk reduction follows. What this value for IE should be, however, remains highly uncertain. Hammitt and Robinson[T85] suggest applying a range of IEs from 1 to 2, where a uniform distribution is assumed in this analysis.

Hammitt and Robinson[T85] also suggest comparing calculated VSL values to the expected future earnings and consumption so as not to undervalue VSLs in low income countries since VSLs should be at least equal to the net present value of future earnings lost due to premature mortality. Hammitt and Robinson[T85] make an estimate of expected future earnings by taking the NPV of unadjusted GNI per capita for half the expected lifetime for a person in the country of interest assuming a 3% discount rate, where

$$\text{NPV} = \sum_{t=1}^{T} \frac{C_t}{(1+r)^t}, \quad (15)$$

and *t* defines the current time period (yearly basis), *T* defines the end time period, C_t is the (income) flow for that period, and *r* is the discount rate (0.03). For this analysis, the cash flow for the period is defined as the GNI per capita for the base year of 2006 for each country. Where appropriate (i.e. when VSL falls below the NPV of future earnings), this value is substituted for the VSL.

Valuing mortality risk reductions across countries, however, has ethical implications in that it may be interpreted as a life being more highly valued in higher income countries than in lower income countries. VSLs are rather a reflection of an individual's willingness to reduce his or her own risk in premature mortality subject to the economic constraints present in that country.[T85] Policymakers may object on moral grounds to a variable VSL approach. As such, the Department of Transportation (DOT) sets guidelines so that all individuals in the US are valued equally,[T86] and attempts to use differential values across individuals in the US were met with significant resistance. This idea can also be extended across countries, i.e. assume a constant VSL valuation for all avoided mortalities as a result of ULSJ implementation where this may be viewed as a policy choice rather than a concept strongly supported by economic theory. Because no "global" VSL exists, a valuation using a constant US VSL is provided.

The benefit of ULSJ implementation is valued by multiplying the number of avoided mortalities for a given country by that country's corresponding VSL and summing while also taking into account discounted health benefits in the future. The standard mortality lag structure as recommended by the EPA is used in this analysis. It assumes that 30% of avoided mortalities are seen in the year of implementation, 50% in years 2-5, and the remaining 20% spread out over years 6-20. Non-discounted costs are also presented in Table T9 as a comparison.

D.5. *Results of VSLs Across Countries*

Table T9 presents the VSLs determined for each country as described previously as well as total valuation from health impacts when no lag structure is considered (non-discounted health impacts). All values are in 2006 US dollars, and the GNI data, which is purchasing power parity adjusted, was obtained from the World Bank database.[T87]

Table T9: VSL and non-discounted valuation of avoided premature mortalities due to ULSJ implementation by country in US 2006 $ Million.

	GNI/capita		VSL		ULSJ Valuation
	2006 US$		2006 US$		2006 US$
Country		2.5% Percentile	Mean	97.5% Percentile	Mean
Afghanistan	990	21,000	45,000	200,000	700,000
Albania	7,010	250,000	530,000	1,700,000	530,000
Algeria	7,160	240,000	540,000	1,700,000	3,900,000
Angola	3,780	60,000	220,000	870,000	590,000
Antigua and Barbuda	17,060	500,000	1,700,000	4,800,000	15,000
Argentina	11,710	340,000	1,000,000	3,100,000	1,700,000
Armenia	4,950	130,000	320,000	1,200,000	1,300,000
Australia	33,010	930,000	4,400,000	11,000,000	4,000,000
Austria	35,810	950,000	5,000,000	13,000,000	28,000,000
Azerbaijan	5,390	120,000	350,000	1,300,000	1,600,000
Bahrain	29,410	710,000	3,700,000	9,700,000	900,000
Bangladesh	1,240	26,000	58,000	250,000	4,700,000
Belarus	9,760	190,000	770,000	2,500,000	10,000,000
Belgium	34,450	740,000	4,700,000	12,000,000	49,000,000
Belize	5,870	110,000	390,000	1,400,000	14,000
Benin	1,330	20,000	60,000	270,000	61,000
Bhutan	3,740	61,000	220,000	860,000	270,000
Bolivia	4,300	68,000	260,000	1,000,000	63,000
Bosnia-Herzegovina	7,350	130,000	530,000	1,800,000	780,000
Botswana	11,740	150,000	990,000	3,100,000	50,000
Brazil	8,810	140,000	670,000	2,200,000	5,400,000
Brunei Darussalam	50,170	800,000	8,200,000	21,000,000	53,000
Bulgaria	10,790	160,000	880,000	2,800,000	3,100,000
Burkina Faso	1,090	11,000	45,000	220,000	220,000
Burundi	350	3,800	12,000	65,000	4,800
Cambodia	1,570	18,000	71,000	330,000	84,000
Cameroon	2,010	19,000	95,000	430,000	520,000
Canada	36,410	500,000	5,100,000	13,000,000	30,000,000
Cape Verde	2,880	34,000	150,000	640,000	7,500
Central African Republic	690	5,400	26,000	140,000	-34,000
Chad	1,080	7,900	44,000	220,000	250,000
Chile	11,380	130,000	950,000	3,000,000	220,000
China	4,790	51,000	290,000	1,100,000	63,000,000
Colombia	7,640	79,000	550,000	1,900,000	810,000
Commonwealth of Dominica	7,490	75,000	530,000	1,800,000	4,200
Comoros	1,150	9,700	47,000	240,000	350
Congo	2,480	17,000	120,000	540,000	16,000
Congo Democratic Republic	270	1,800	8,400	49,000	27,000
Costa Rica	9,630	86,000	750,000	2,400,000	140,000
Croatia	16,310	140,000	1,600,000	4,600,000	4,000,000
Cyprus	25,060	260,000	2,900,000	7,900,000	850,000
Czech Republic	21,230	200,000	2,300,000	6,300,000	25,000,000
Denmark	36,700	490,000	5,100,000	13,000,000	16,000,000
Djibouti	2,180	13,000	100,000	470,000	20,000
Dominican Republic	6,620	48,000	450,000	1,600,000	850,000
East Timor	1,990	12,000	93,000	430,000	900

	GNI/capita		VSL		ULSJ Valuation
	2006 US$		2006 US$		2006 US$
Country		2.5% Percentile	Mean	97.5% Percentile	Mean
Ecuador	6,810	45,000	470,000	1,600,000	54,000
Egypt	4,700	30,000	280,000	1,100,000	11,000,000
El Salvador	5,920	36,000	390,000	1,400,000	190,000
Equatorial Guinea	13,550	99,000	1,200,000	3,700,000	33,000
Eritrea	630	3,100	22,000	120,000	19,000
Estonia	17,930	160,000	1,800,000	5,100,000	1,500,000
Ethiopia	700	3,000	25,000	140,000	450,000
Federated State of Micronesia	3,240	16,000	170,000	730,000	470
Fiji	4,310	20,000	250,000	1,000,000	1,400
Finland	33,410	410,000	4,400,000	11,000,000	4,700,000
France	31,950	390,000	4,200,000	11,000,000	89,000,000
FYROM/Macedonia	8,520	45,000	630,000	2,100,000	560,000
Gabon	11,050	72,000	910,000	2,900,000	62,000
Gambia	1,100	3,700	44,000	220,000	18,000
Georgia	4,130	17,000	240,000	960,000	660,000
Germany	34,410	430,000	4,600,000	12,000,000	390,000,000
Ghana	1,270	3,800	52,000	260,000	100,000
Greece	26,410	280,000	3,100,000	8,400,000	9,800,000
Grenada	7,650	37,000	550,000	1,900,000	6,600
Guatemala	4,270	14,000	250,000	990,000	200,000
Guinea	870	1,900	33,000	170,000	53,000
Guinea-Bissau	990	1,800	38,000	200,000	13,000
Guyana	2,770	6,600	140,000	620,000	4,700
Honduras	3,350	8,700	180,000	760,000	100,000
Hungary	17,300	150,000	1,700,000	4,900,000	12,000,000
Iceland	33,570	410,000	4,500,000	12,000,000	34,000
India	2,540	5,100	130,000	560,000	110,000,000
Indonesia	3,040	7,200	160,000	680,000	1,900,000
Iran	9,880	59,000	780,000	2,500,000	23,000,000
Iraq	2,850	6,400	150,000	640,000	2,200,000
Ireland	36,670	490,000	5,100,000	13,000,000	3,000,000
Israel	24,840	260,000	2,900,000	7,800,000	5,800,000
Italy	30,170	350,000	3,800,000	10,000,000	96,000,000
Ivory Coast	1,520	2,000	65,000	320,000	120,000
Jamaica	7,040	32,000	490,000	1,700,000	350,000
Japan	32,770	400,000	4,300,000	11,000,000	64,000,000
Jordan	4,850	17,000	300,000	1,100,000	450,000
Kazakhstan	8,690	47,000	650,000	2,200,000	4,900,000
Kenya	1,430	1,700	61,000	300,000	89,000
Kiribati	3,630	10,000	200,000	830,000	100
Korea	24,320	250,000	2,800,000	7,500,000	24,000,000
Kuwait	51,130	820,000	8,400,000	22,000,000	4,400,000
Kyrgyz Republic	1,790	2,700	81,000	380,000	180,000
Lao People's Democratic Republic	1,710	2,500	76,000	360,000	66,000
Latvia	14,540	110,000	1,300,000	4,000,000	2,000,000
Lebanon	9,870	59,000	780,000	2,500,000	1,500,000
Lesotho	1,660	2,300	73,000	350,000	3,800
Liberia	250	210	7,200	45,000	1,800

	GNI/capita		VSL		ULSJ Valuation
	2006 US$		2006 US$		2006 US$
Country		2.5% Percentile	Mean	97.5% Percentile	Mean
Libyan Arab Jamahiriya	14,910	120,000	1,400,000	4,100,000	1,900,000
Lithuania	15,610	130,000	1,500,000	4,300,000	5,700,000
Luxembourg	60,210	1,100,000	11,000,000	28,000,000	3,700,000
Madagascar	920	770	35,000	180,000	7,200
Malawi	650	400	23,000	130,000	7,400
Malaysia	12,240	83,000	1,000,000	3,200,000	1,200,000
Maldives	4,650	16,000	280,000	1,100,000	7,700
Mali	980	860	38,000	200,000	210,000
Malta	21,470	210,000	2,300,000	6,400,000	350,000
Mauritania	1,740	2,500	78,000	370,000	81,000
Mauritius	10,900	70,000	890,000	2,800,000	14,000
Mexico	13,520	99,000	1,200,000	3,700,000	20,000,000
Mongolia	2,850	6,400	150,000	640,000	48,000
Morocco (includes Western Sahara)	3,790	11,000	210,000	870,000	2,100,000
Mozambique	670	420	24,000	130,000	8,900
Namibia	5,810	22,000	380,000	1,400,000	17,000
Nepal	1,010	910	39,000	200,000	710,000
Netherlands	39,070	550,000	5,600,000	14,000,000	43,000,000
New Zealand	25,130	260,000	2,900,000	7,900,000	76,000
Nicaragua	2,400	4,600	120,000	530,000	51,000
Niger	640	390	22,000	130,000	180,000
Nigeria	1,790	2,700	81,000	380,000	2,400,000
Norway	53,330	880,000	9,000,000	23,000,000	6,300,000
Oman	20,480	190,000	2,200,000	6,000,000	1,800,000
Pakistan	2,390	4,500	120,000	520,000	11,000,000
Panama	9,380	54,000	720,000	2,400,000	90,000
Papua New Guinea	1,690	2,400	75,000	360,000	2,900
Paraguay	4,080	13,000	230,000	940,000	46,000
Peru	6,360	26,000	420,000	1,500,000	200,000
Philippines	3,090	7,400	160,000	700,000	730,000
Poland	14,640	110,000	1,300,000	4,000,000	37,000,000
Portugal	22,180	220,000	2,400,000	6,700,000	4,100,000
Republic of Moldova	2,860	6,400	150,000	640,000	330,000
Romania	10,870	70,000	890,000	2,800,000	8,200,000
Russia	14,560	110,000	1,300,000	4,000,000	97,000,000
Rwanda	940	800	36,000	190,000	13,000
Saint Kitts and Nevis	13,270	96,000	1,200,000	3,600,000	6,700
Saint Lucia	8,830	49,000	660,000	2,200,000	6,900
Saint Vincent	7,690	37,000	550,000	1,900,000	7,000
Sao Tome and Principe	1,560	2,100	68,000	330,000	440
Saudi Arabia	22,590	220,000	2,500,000	6,800,000	28,000,000
Senegal	1,650	2,300	73,000	350,000	260,000
Serbia and Montenegro	9,935	60,000	780,000	2,500,000	6,100,000
Seychelles	18,160	160,000	1,800,000	5,200,000	4,600
Sierra Leone	670	420	24,000	130,000	38,000
Singapore	46,950	720,000	7,400,000	19,000,000	2,400,000
Slovakia	17,700	160,000	1,800,000	5,000,000	10,000,000
Slovenia	25,140	260,000	2,900,000	7,900,000	3,100,000
Solomon Islands	2,230	4,000	110,000	480,000	260

	GNI/capita		VSL		ULSJ Valuation
	2006 US$		2006 US$		2006 US$
Country		2.5% Percentile	Mean	97.5% Percentile	Mean
South Africa	9,090	51,000	690,000	2,300,000	1,200,000
Spain	29,810	350,000	3,800,000	9,900,000	55,000,000
Sri Lanka	3,850	11,000	220,000	890,000	820,000
Sudan	1,660	2,300	73,000	350,000	1,100,000
Suriname	6,360	26,000	420,000	1,500,000	6,800
Swaziland	4,580	15,000	270,000	1,100,000	6,700
Sweden	36,140	470,000	5,000,000	13,000,000	14,000,000
Switzerland	42,510	620,000	6,400,000	16,000,000	19,000,000
Syrian Arab Republic	4,070	12,000	230,000	940,000	940,000
Tajikistan	1,550	2,000	67,000	330,000	160,000
Thailand	6,970	31,000	480,000	1,700,000	3,200,000
Togo	790	580	29,000	160,000	21,000
Tonga	4,310	14,000	250,000	1,000,000	130
Trinidad and Tobago	22,180	220,000	2,400,000	6,700,000	310,000
Tunisia	6,650	29,000	450,000	1,600,000	1,500,000
Turkey	12,250	84,000	1,000,000	3,200,000	22,000,000
Turkmenistan	4,970	17,000	300,000	1,200,000	1,100,000
Uganda	970	850	37,000	200,000	65,000
Ukraine	6,130	25,000	400,000	1,500,000	23,000,000
United Kingdom	35,110	450,000	4,800,000	12,000,000	120,000,000
United Rep. of Tanzania	1,140	1,100	46,000	230,000	75,000
United States of America	45,640	690,000	7,100,000	18,000,000	830,000,000
Uruguay	10,170	62,000	810,000	2,600,000	91,000
Uzbekistan	2,170	3,800	100,000	470,000	1,000,000
Vanuatu	3,630	10,000	200,000	830,000	230
Venezuela	11,010	71,000	900,000	2,900,000	1,300,000
Viet Nam	2,310	4,200	110,000	500,000	1,100,000
Western Samoa	3,990	12,000	230,000	920,000	310
Yemen	2,120	3,600	100,000	460,000	940,000
Zambia	1,070	1,000	42,000	220,000	22,000
Total					2,500,000,000

Note that not all countries and regions are considered in Table T7 and Table T9. This is due to either a lack of mortality data within the WHO GBD database or a lack of economic data from the World Bank database. To maintain consistency within the analysis, values from other sources were not used. The following countries or territories have been omitted: American Samoa, Andorra, Anguilla, Aruba, Bahamas, Barbados, Bermuda, British Virgin Islands, Cayman Islands, Cook Islands, Cuba, Faeroe Islands, Falkland Islands, French Guiana, French Polynesia, Gibraltar, Greenland, Guadeloupe, Guam, Guernsey, Haiti, Hong Kong, Isle of Man, Jersey, North Korea, Lichtenstein, Macao, Marshall Islands, Martinique, Mayotte, Monaco, Montserrat, Myanmar, Nauru, Netherland Antilles, New Caledonia, Niue, Norfolk Island, Northern Mariana

Island, Occupied Palestinian Territory, Palau, Pitcairn, Puerto Rico, Qatar, Reunion, Saint Helena, Saint Pierre and Miquelon, San Marino, Somalia, Svalbard, Taiwan, Tokelau, Turks and Caicos Islands, Tuvalu, United Arab Emirates, United States Virgin Islands, Wallis and Futuna, and Zimbabwe.

E. Implementation Cost Analysis

Two separate cost analyses were performed. The first used historical price data from ULS diesel to estimate ULSJ costs while the second relied on a cost-curve estimate using petroleum refining data.

E.1. *Price History Analysis*

The only cost aspect considered in the price history analysis is the expected increase in price due to the additional processing required to desulfurize jet fuel. For this analysis, it is assumed that any price increase for ULS production is a function of increased capital and refining costs and not a function of any other market factors that may be relevant. This price analysis is based on price history data of ULS diesel as it has recently been implemented for on-road use in 2006 and is currently being phased into off-road use (ships, locomotives, etc.) as detailed previously in Section A.

The US Energy Information Administration (EIA)[T88] provides price history data for three diesel fuel types: high sulfur (HS) (500+ ppm), low sulfur (LS) (15-500 ppm), and ultra low sulfur (ULS) (<15 ppm). The price differential between ULS/LS and LS/HS are plotted against the amount of ULS/LS and HS diesel fuel supplied, and is shown in Figure T13. Note that throughout this section, references to HS, LS, and ULS refer to diesel fuel.

The black and red lines show the price differentials and correspond to the right-hand axis, while the purple, green, blue, and orange lines show the product supplied and correspond to the left-hand axis. There appears to be a spike in the price differential beginning in 2005 and ending in early 2008. This spike coincides with a change in supply of ULS and LS fuel, which are assumed to be direct substitutes given that a decrease in LS supply is accompanied by an increase in ULS supply, while the total amount of ULS and LS supplied remains approximately constant over the entire time period. This price spike also coincides with the initial phase-in of ULS diesel in 2006

shown in the timeline of standards for on-road implementation provided in Table T1. The cause of this price spike is unclear. It could be a result of market fluctuations given the shift in supply away from LS to ULS. This shift in supply, however, may be exaggerated in Figure T13 given that ULS diesel in Jan. 2005 may already have been produced in non-negligible quantities. No ULS diesel was reported due to the fact that it was not required to be labeled as ULS diesel by regulations at this point.

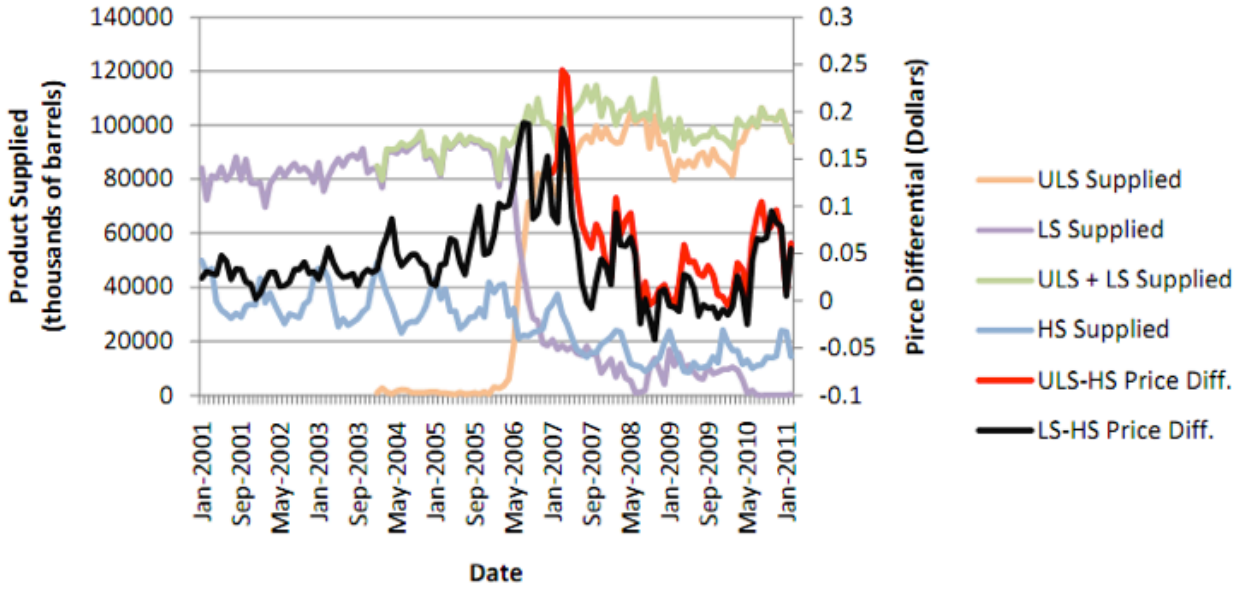

Figure T13: The product supplied of ULS, LS, and HS diesel fuel plotted simultaneously with the price differential for ULS-HS and LS-HS for Jan 2001 to February 2011.

All price history data is condensed into a single representative price differential. For this analysis, the observed price differential in ULS and HS diesel fuel (after adjusting the nominal prices by inflation to the real prices for a base year of 2006) is weighted against the amount of ULS and HS diesel supplied for a given month in order to capture the interaction between price and quantity within the fuel market. HS diesel fuel is defined by a FSC of greater than 500 ppm, and because jet fuel FSC is between 600 and 700 ppm, the ULS/HS price differentials are used rather than the ULS/LS price differentials. One limitation of this method is weighting against negligible amounts of HS fuel (which would drive price differentials downward) due to a phasing out of HS diesel fuel for non-road applications beginning in January 2007. Figure T13 shows a decline in HS diesel production starting around this time, but its production is currently non-negligible and thus not an issue in this analysis.

Three different weighted estimates are determined by considering three distinct time periods. The first time period considered is the "steady state" period in which the price spike stabilizes relative to the noise already present in the data. This period is set from January 2008 to the present. The second time period includes all ULS price data, which is only reported from January 2007 and onward although ULS production numbers are provided starting in January 2004. Not all relevant price data is available (i.e. price data for ULS since introduction of ULS production), for the entire price spike period. For this reason, a third period is analyzed from January 2005 to the present where the LS/HS price differential is used as a substitute for the ULS/HS price differential from 2005-2007 when ULS price data was unavailable. Regardless, all price differentials for this third price scenario are still weighted against ULS and HS production quantities. For the three scenarios described above, the following weighted averages have been calculated: 3.7 cents for the steady state period (low price differential), 5.6 cents for all ULS price data, and 6.5 cents for all price data (high price differential).

E.2. *Cost Buildup Approach*

An alternative approach to estimating production costs is used to corroborate the price differentials determined above. The analysis includes the capital costs for the hydrotreater unit, the steam methane reformer (SMR) unit, and the natural gas (NG) feedstock costs for a representative refinery. Straight-line depreciation is used to bring these various costs together to a per-gallon of ULSJ basis.

E.2.1. Natural Gas Feed Requirement

In hydrodesulfurization (HDS), or more generally hydroprocessing, hydrogen gas (H_2) is used to remove sulfur from the jet fuel stream. NG is used to create H_2 by steam reformation in a SMR unit. The additional NG requirement for HDS is determined from the GREET model[T89] as follows.

From information in GREET, the absolute difference in direct NG use (energy of NG per energy of ULSJ) can be derived from the process efficiencies of ULSJ and conventional jet fuel production along with the process shares of refining. Refining efficiency for a specific petroleum product is defined as the following:

$$\eta = \frac{E_F}{E_F + E_I}, \quad (16)$$

where E_F is the specific energy of the fuel and E_I is energy input to the refinery per unit mass of jet fuel produced. We are interested in the total change in input specific energy between standard jet fuel and ULSJ, or

$$\Delta = E_{I,U} - E_{I,J}. \quad (17)$$

U indicates values for ULSJ, and *J* indicates values for standard jet fuel. Inverting Eq. (16) and taking the difference between the standard jet fuel and ULSJ cases produces the following relationship:

$$\frac{1}{\eta_U} - \frac{1}{\eta_J} = \frac{E_{F,U} + E_{I,U}}{E_{F,U}} - \frac{E_{F,J} + E_{I,J}}{E_{F,J}} \quad (18)$$

If the specific energy of standard jet fuel and ULSJ are assumed to be approximately equal (within 0.3% as outlined in Section H.1), then Eq. (18) reduces to

$$\frac{1}{\eta_U} - \frac{1}{\eta_J} = \frac{E_{I,U} - E_{I,J}}{E_F} = \frac{\Delta}{E_F}. \quad (19)$$

To determine the change in energy associated with additional NG consumption per mass of jet fuel, it is necessary to multiply Eq. (19) by the appropriate process energy share.

$$\Delta NG = \left(\frac{1}{\eta_U} - \frac{1}{\eta_J}\right) \cdot E_F \cdot f_{NG}, \quad (20)$$

where f_{NG} is the total process energy share associated with NG use within the refinery. To determine the additional amount of NG required, Eq. (20) must be multiplied by the density of jet fuel, where energy density is equal to the product of specific energy and density of the jet fuel as reflected in Eq. (21). This expression is then divided by the energy density of NG to acquire the additional volume of NG required (at standard conditions) per unit volume of jet fuel.

$$\Delta NG_{volume} = \left(\frac{1}{\eta_U} - \frac{1}{\eta_J}\right) \cdot D_F \cdot f_{NG} \cdot \frac{1}{D_{NG}}, \quad (21)$$

where D_F is the energy density of jet fuel, and D_{NG} is the energy density of natural gas.

The process energy shares from Stratton et al.[T35] (see Table T10 below) are used for this analysis. This ensures consistency with the analysis of WTW GHG emissions. The process fuels listed in Table T10 provide H_2 for HDS and also power the hydroprocessing itself. Since natural gas and refinery gas account for 80.9% of the total energy, the costs associated with electricity, coke, and residual oil are neglected in this analysis. Refinery gas is defined by the OECD as "non-condensable gas obtained during distillation of crude oil or treatment of oil products (e.g. cracking) in refineries. It consists mainly of hydrogen, methane, ethane and olefins. It includes gases which are returned from the petrochemical industry."

Table T10: Process energy shares for the production of jet fuel[T35]

Type of process fuel	Process energy share (%)
Electricity	3.5
Natural Gas	41.3
Refinery Gas	39.6
Coke	14.3
Residual Oil	1.3
Total	100

The energy density of NG is 983 BTU/ft^3, or 3.66×10^4 kJ/m^3 (lower heating value (LHV), GREET v1.8A). The energy density of ULSJ is 34.3 MJ/L.[T18] From Stratton et al.,[T35] the assumed jet fuel refinery efficiency is 93.5% and ULSJ refinery efficiency is assumed to be 91.5% due to the energy penalty described with the WTW GHG emissions calculation.

Using Eq. (21) and the above stated values, the amount of refinery and natural gas required for the additional hydroprocessing required to desulfurize jet fuel is 2.37 standard cubic feet (scf) per gallon, or 0.018 standard cubic meters (scm) per liter.

E.2.2. Refinery Gas and Natural Gas Feedstock Costs

Figure T14 presents the price history of NG with the feed requirement information to yield the NG cost to create ULSJ from conventional jet fuel. Because refinery gas and natural gas are used for the same purposes in the refinery, these products are assumed to have the same economic value to the refiner, This assumption is needed because there is no external market for refinery gas.

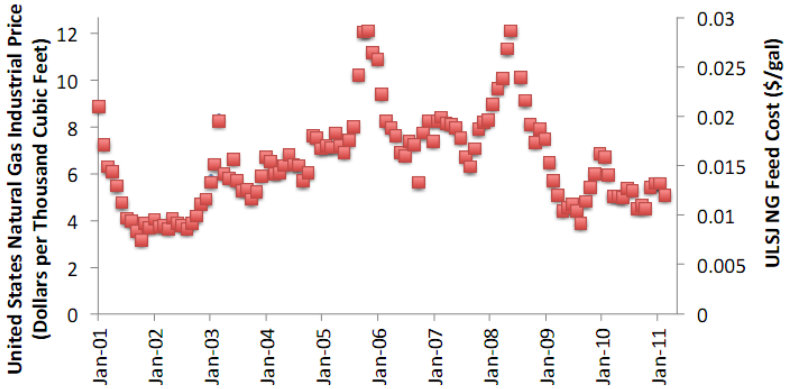

Figure T14: NG Price history[T88] and NG feed cost to create ULSJ from conventional jet fuel based on 2.37 scf/gal (0.018 scm/L) of NG per gallon of ULSJ.

E.2.3. Capital Costs

Additional capital equipment is needed to make jet fuel, but most of the units are common to both ULSJ and conventional jet fuel; as such, the focus of the capital cost analysis is on hydrotreater and SMR units. These units would both be needed to create ULSJ instead of conventional jet fuel. The hydrotreating unit would need to be supplied H_2 gas from a SMR unit. For this analysis, we assume that all of the refinery and natural gas (2.37 scf per gallon of ULSJ) is used towards H_2 production. Cost curves presented in Gary and Handwerk 2007[T90] are used to derive the additional capital costs for increasing the hydrotreater and SMR unit capacities for ULSJ production (pgs. 201 and 276, respectively).

The catalytic desulfurization and hydrogenation unit cost curve is used to estimate the capital expense for a range of hydrotreatment units that range in capacity from 5,000 to 50,000 barrels per day (bpd), or 800,000 to 8,000,000 liters per day. The SMR unit is sized by multiplying the hydrotreating unit capacity by 42 gal/barrel (159 L/barrel) and 2.37 scf per gallon (0.018 scm per liter) (i.e., the additional unit capacity required to desulfurize fuel below 15 ppm). Each mole of NG is assumed to result in 3.85 moles of H_2 gas through steam methane reforming and water gas shift reactions; therefore the product of hydrotreating capacity and the required NG/gallon is multiplied by 3.85 to obtain the total additional amount of H_2 required to treat a gallon of ULSJ fuel. The upper cost curve from the figure on pg. 276 is applied.

The cost curves for the hydrotreater and SMR units are combined to yield the combined capital costs for varied hydroprocessing capacities as shown in Figure T15 (blue line). For example, the combined cost of hydrotreater and SMR units for a capacity of 22,000 bpd is $58 million. This value is then examined using a straight-line depreciation. The US mandates a 10-year depreciation time horizon for tax purposes,[T91] but capital costs in this analysis are depreciated over 30 years[T90] to reflect the useful lifetime of an average refinery to yield a per gallon capital cost (red line).

For 22,000 bpd of capacity, the additional per-gallon cost for capital equipment is $0.017 per gallon when a 10 year depreciation time horizon is considered, but $0.006 per gallon when depreciated over 30 years.

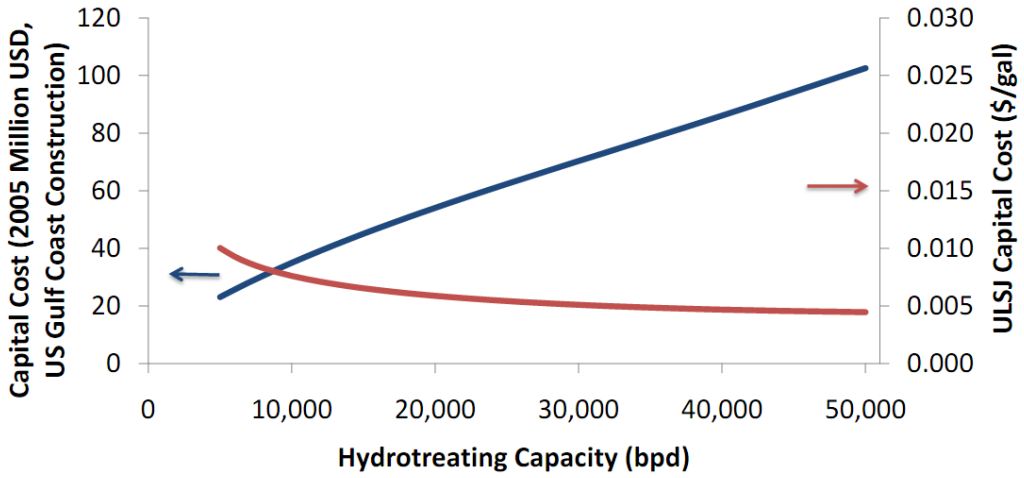

Figure T15: Capital costs for hydrotreating and SMR units as a function of HDS capacity depreciated over 30 years.

The value of 22,000 bpd in the previous paragraph corresponds to the average ULS capacity of US refineries. According to EIA, there were 141 refineries operating in the US in 2009 and US refineries produced 3.1 million bpd of ULS diesel that year. The actual capacity at any given refinery will vary from this value, but as shown in Figure T15 the per gallon capital cost for this average capacity and larger sizes is between 0.004 and 0.006 $/gal. A more rigorous cost buildup approach is to estimate the additional per gallon cost of ULSJ using cash flows that includes capital cost factors such as loan payments, depreciation over 10 years, escalation from 2005 costs (the year in which this analysis is based), a change in location factor seeing as capital costs

would rise outside of the US Gulf Coast, a compounding of increased capital costs due to loan payments and depreciation/capital recovery, inclusion of fixed operating expenses (additional staff, insurance, maintenance, etc.), additional supporting utilities, and discounted cash flows for the "true value of money" for an economic investment. This approach will result in a higher cent/gal cost than estimated above.

E.3. *Cost Distribution*

From the price history analysis, minimum and maximum price differentials of 3.7 and 6.6 cents/gallon are calculated. From the cost-buildup approach, minimum and maximum price differentials of 1.6 and 3.6 cents/gallon are calculated. While the cost-buildup approach is useful in validating the price history analysis, it provides a minimum price differential as it only considers the additional methane required for H_2 production for hydroprocessing and additional refinery processes that may use the methane as a fuel. Other costs that the refineries see as a result of ULSJ implementation that may be hidden within the price history analysis are not captured. Thus, 1.6 cents/gallon is taken as the minimum price differential, while the 6.6 cents/gallon is taken as the maximum price differential. 3.7 cents/gallon is chosen as the nominal price differential given it is the expected price differential when production reaches a steady state as defined in Section E.1. A triangular distribution is assumed.

F. Benefit-Cost Analysis

F.1. *Monte Carlo Analysis Framework*

Monte Carlo techniques are used to quantify the uncertainty present within the benefit-cost analysis (CBA). From Allaire and Willcox,[T92] within a general model, *f(x)*, with an arbitrary number of input parameters, the expected outcome can be determined from a Monte Carlo simulation with the form

$$\frac{1}{N}\sum_{m=1}^{N} f(\boldsymbol{x}^m) \rightarrow \mathbb{E}[f(\boldsymbol{x})] \text{ as } N \rightarrow \infty, \quad (22)$$

where $\boldsymbol{x}$ denotes a vector of input parameters. Eq. (18) states that as the number of Monte Carlo simulations, *N*, goes to infinity, then the mean value of all simulations will approach the expected outcome of the model system. For each simulation, the input parameters are randomly

selected based on distributions assigned to each variable. The outputs presented in each of the results section have all been produced using Eq. (18) unless otherwise noted. Given computational time constraints, *N* is chosen to be 2000. Due to the complexity of GEOS-Chem, it is not practical to perform 2000 air quality simulations. Rather, a 60% uncertainty is assumed for ground-level concentrations and these results are scaled for each Monte Carlo (MC) simulation based on a triangular uncertainty distribution.

F.2. *Assumptions for Global and US Implementation Analysis*

For each of the MC simulations, the following assumptions are made for the global implementation of ULSJ analysis:

- Changes in energy density and specific energy are not considered within this analysis.
- APMT-Climate input parameters are used as described in Table T11 and the distributions and associated values are provided in Table T12.
- Three discount rates are applied to climate costs deterministically: 2, 3, and 7%.
- The EPA CRF methodology is used to calculate the number of avoided mortalities due to ULSJ implementation in this analysis where a mortality lag structure is implemented assuming the same discount rates as applied to climate costs.
- Full-flight health impacts are considered.
- Gross National Income (GNI) per capita adjusted for purchasing power parity (PPP) is used as the income measure to determine VSLs across countries.
- Price differentials are assumed to be applicable on a global level although they are based on US price history data.

The primary assumptions for the US implementation analysis are very similar to those used in the global implementation analysis. The only additional or differing points are the following:

- The calculations provided in the US implementation analysis are the costs seen by the US due to a global implementation of ULSJ.

- Climate costs are scaled by a regional GDP factor to obtain climate costs for just the US (7-23% of total damages[T93]).

- Avoided mortality benefits are those seen by the US due to global implementation.

- Implementation costs are a result of US fuel burn, only (6.74×10^{10} kg for aviation year 2006), i.e. the amount of fuel burn seen in the US region as defined by the nested GEOS-Chem grid.

A US-only implementation analysis is also performed. The overall structure of the analysis is the same as the global implementation analysis, except for the following distinctions:

- Climate costs are calculated based on US fuel burn, only. Given that the DICE-2007 damage function calculates impact on global GDP, the 7-23% fraction for US damages is again applied.

- Avoided mortality benefits are those seen by the US due to US-only implementation, where US-only implementation is approximated by a nested GEOS-Chem simulation with baseline boundary conditions and ULSJ for all flights within the domain

- Implementation costs are a result of US fuel burn.

F.3. *Assumed Uncertainty Distributions*

Table T11 provides a brief description of each input parameter used in the MC analysis. As described in the cost build-up section, the additional price associated with increased hydroprocessing and hydrogen gas capacity determines the amount of additional lifecycle CO2 emissions. The amount of additional hydroprocessing is also directly related to the expected change in fuel energy density and specific energy, as described in the operations section below. Table T12 shows the values and assumed distributions for each of the described input parameters in Table T11.

Table T11: Brief description of each input parameter

Parameter	Units	Description
RF Cirrus	mW/m^2	RF due to cirrus clouds. APMT-Climate parameter.
RF Soot	mW/m^2	RF due to soot formation. APMT-Climate parameter.
RF H2O	mW/m^2	RF due to water vapor. APMT-Climate parameter.
RF Contrails	mW/m^2	RF due to contrail formation. APMT-Climate parameter.
RF2xCO2	W/m^2	RF for a double of CO_2 concentrations from pre-industrial times. This is used for RF normalization and CO_2 RF calculation. APMT-Climate parameter.
Reference Temp. Change	K	Estimated change in temperature since pre-industrial times. Damage function parameter.
Ocean Specific Heat Capacity	J/kgK	Ocean specific heat capacity. Used in RF temperature response model.
Climate Sensitivity	K	Temperature response induced by an RF from CO_2 doubling.
Damage Function Coefficient	None	DICE-2007 damage coefficient.
US Regional Climate Damages Scale	None	Percent of global climate damages seen in the US.
WTW GHG Emissions*	gCO_2e/MJ	Expected additional WTW GHG emissions for ULSJ.
Cloud Cover, Sulfate RF	None	See Sulfate RF section.
Radiation Transmittance, Sulfate RF	None	See Sulfate RF section.
Average Ground Albedo, Sulfate RF	None	See Sulfate RF section.
Backscattering Coefficient	None	Percent change of backscattering coefficient.
Aerosol Optical Depth	None	Percent change of aerosol optical depth.
PM2.5 Concentration	None	Percent change of $PM_{2.5}$ concentrations from GEOS-Chem outputs.
All Cause US β	None	Percent change in premature mortality given a $\mu g/m^3$ change in $PM_{2.5}$ concentration.
CP US β	None	Percent change in CP mortality given a $\mu g/m^3$ change in $PM_{2.5}$ concentration.
LC US β	None	Percent change in LC mortality given a $\mu g/m^3$ change in $PM_{2.5}$ concentration.
All Cause US Baseline Incidence	Deaths per capita	All cause baseline incidence rate for the US.
CP US Baseline Incidence	Deaths per capita	CP baseline incidence rate for the US.
LC US Baseline Incidence	Deaths per capita	LC baseline incidence rate for the US.
CP All Countries Baseline Incidence	Deaths per capita	CP baseline incidence rate for all countries.
LC All Countries Baseline Incidence	Deaths per capita	LC baseline incidence rate for all countries.
30+ Population Fraction	None	Fraction of populations in each country greater than 30 years of age.
US VSL	US $2006	US VSL based on EPA practices.
Global IE	None	Global income elasticity as applied to VSL.
ULSJ Price Differential*	Cents	Additional price due to ULSJ production.
Discount Rate	Percent	Discount rate applied to future climate costs.

*These two parameters are not independent and are defined simultaneously.

Table T12: Monte Carlo Input Values and Distributions (Triangular: [Low, High, Nominal])

Parameter	Nominal Range	Units	Distribution
RF Cirrus[S34]	[0.011,0.087,0.033]	mW/m^2	Triangular
RF Soot[S34]	[0.0056,0.0207,0.034]	mW/m^2	Triangular
RF H2O[S34]	[0.0039,0.0203,0.028]	mW/m^2	Triangular
RF Contrails[S34]	[0.054,0.0256,0.0118]	mW/m^2	Triangular
RF2xCO2	[3.5,4.2,3.7]	W/m^2	Triangular
Reference Temp. Change	[0.4,0.8,0.6]	K	Triangular
Ocean Specific Heat Capacity[S94]	[2.52e8,6.31e8,4.41e8]	J/kgK	Triangular
Climate Sensitivity	[2,4.5,3]	K	Triangular
Damage Function Coefficient	[0.015388,0.041388,0.028388]	None	Triangular
US Regional Climate Damages Scale	[0.07, 0.23]	None	Uniform
WTW GHG Emissions	[87.5,90.5,89]	gCO_2e/MJ	Triangular
Cloud Cover, Sulfate RF	[0.35, 0.44, 0.39]	None	Triangular
Radiation Transmittance, Sulfate RF	[0.4, 0.83, 0.58]	None	Triangular
Average Ground Albedo, Sulfate RF	[0.65, 0.8, 0.72]	None	Triangular
Backscattering Coefficient	[0.78, 1.22, 1]	None	Triangular
Aerosol Optical Depth	[0.3, 1.75, 1]	None	Triangular
PM2.5 Concentration	[0.4, 1.6, 1]	None	Triangular
All Cause US Beta	[0.00355, 0.0181, 0.0106]	None	Triangular
CP US Beta	[0.09, 0.028]	None	Uniform
LC US Beta	[0.014, 0.027]	None	Uniform
All Cause US Baseline Incidence	[0.0139, 0.0145, 0.0142]	Deaths per capita	Triangular
CP US Baseline Incidence	[0.046, 0.048, 0.047]	Deaths per capita	Triangular
LC US Baseline Incidence	[0.0094, 0.0098, 0.0096]	Deaths per capita	Triangular
CP All Countries Baseline Incidence	231 country inputs varied from nominal value based on relative uncertainty found in literature.	Deaths per capita	Triangular
LC All Countries Baseline Incidence	231 country inputs varied from nominal value based on relative uncertainty found in literature.	Deaths per capita	Triangular
30+ Population Fraction	231 country inputs varied from nominal value based on relative uncertainty found in literature.	None	Triangular
US VSL	a = 7.75, b = 1.51	US $2006	Weibull
Global IE	[1, 2]	None	Uniform
ULSJ Price Differential	[1.6, 6.5, 3.7]	Cents	Triangular
Discount Rate	[2, 7, 3]	Percent	Discrete

F.4. *Global Implementation Analysis Results*

Table T13 presents the primary results from the CBA for global implementation of ULSJ. Note that values in parentheses are non-cost beneficial values.

Table T13: Global Implementation CBA Results, given in 2006 US $ Billion

Component	Mean	Median	95% Interval	% Cost Beneficial
Climate				
2%	**(2.35)**	**(2.07)**	**(0.13) – (6.32)**	
3%	**(1.64)**	**(1.46)**	**(0.10) – (4.26)**	
7%	**(0.82)**	**(0.73)**	**(0.06) – (2.08)**	
Air Quality				
2%	**2.34**	**1.83**	**0.21 – 7.55**	
3%	**2.27**	**1.77**	**0.20 – 7.32**	
7%	**2.05**	**1.60**	**0.18 – 6.59**	
Implementation	**(2.52)**	**(2.49)**	**(1.31) – (3.80)**	
Total				
2%	**(2.53)**	**(2.63)**	**(7.70) – 3.37**	15
3%	**(1.89)**	**(2.11)**	**(5.98) – 3.59**	17
7%	**(1.29)**	**(1.62)**	**(4.15) – 3.48**	20

Figure T16 shows the benefit-cost distribution produced by the MC simulations for each of the three scenarios described in Table T13. Positive values represent net cost beneficial scenarios while negative values represent net non-cost beneficial scenarios. From Table T8, there are an estimated 2300 avoided premature mortalities resulting from global ULSJ implementation. When only LTO emissions are considered on a global scale, the central estimated cost is $**(3.7)** billion with a 95% CI of $**(1.5) - (7.1) billion** when assuming a 3% discount rate, thus total costs are statistically significantly different from 0.

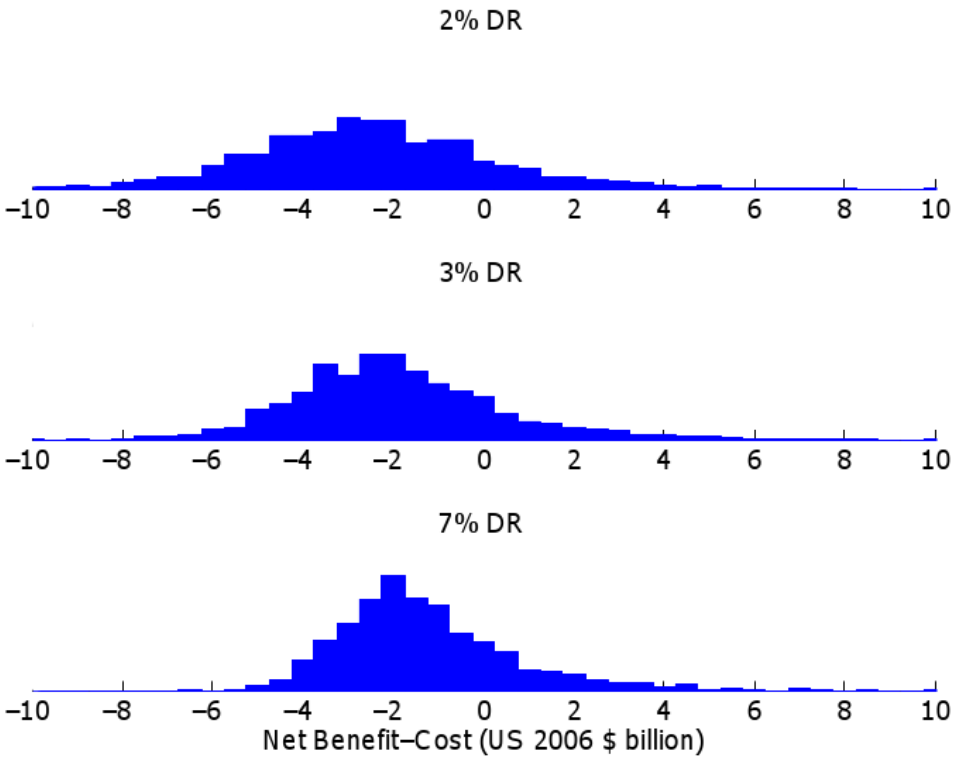

Figure T16: Benefit-cost distribution for global implementation analysis for three different discount rates (DR).

Table T14 shows statistics when climate impacts are weighed against air quality impacts only. Note that climate and air quality statistics are the same as in Table T11.

Table T14: Global Implementation Results from CBA, No Implementation Cost Included

Component	Mean	Median	95% Interval	% Cost Beneficial
Climate				
2%	**(2.35)**	**(2.07)**	**(0.13) – (6.32)**	
3%	**(1.64)**	**(1.46)**	**(0.10) – (4.26)**	
7%	**(0.82)**	**(0.73)**	**(0.06) – (2.08)**	
Air Quality				
2%	**2.34**	**1.83**	**0.21 – 7.55**	
3%	**2.27**	**1.77**	**0.20 – 7.32**	
7%	**2.05**	**1.60**	**0.18 – 6.59**	
Total				
2%	**0.00**	**(0.18)**	**(4.68) – 5.65**	46
3%	**0.63**	**0.31**	**(3.06) – 5.84**	57
7%	**1.23**	**0.85**	**(1.16) – 5.78**	77

Alternatively, implementation costs are weighted against air quality impacts only due to the uncertainty in global climate impacts. This is shown in Table T15.

Table T15: Global Implementation Results from CBA, No Climate Cost Included

Component	Mean	Median	95% Interval	% Cost Beneficial
Air Quality				
2%	**2.34**	**1.83**	**0.21 – 7.55**	
3%	**2.27**	**1.77**	**0.20 – 7.32**	
7%	**2.05**	**1.60**	**0.18 – 6.59**	
Implementation	**(2.52)**	**(2.49)**	**(1.31) – (3.80)**	
Total				
2%	**(0.18)**	**(0.61)**	**(2.94) – 5.20**	37
3%	**(0.25)**	**(0.66)**	**(2.95) – 4.98**	35
7%	**(0.47)**	**(0.84)**	**(3.00) – 4.26**	31

F.5. *US Implementation Analysis*

Table T16 presents the primary results from the CBA for US implementation of ULSJ. Note that values in parentheses are not cost beneficial values.

Table T17 provides health impacts and valuations for the US from global implementation for the other two models i.e. nested GEOS-Chem (nGC) and CMAQ. Valuations are discounted for the lag in health impacts and a nominal VSL of 2006 US $7.4 million is assumed. All values in

Table T17 are nominal values.

Table T16: US Implementation CBA Results, given in 2006 US $Billion

Component	Mean	Median	95% Interval	% Cost Beneficial
Climate				
2%	**(0.35)**	**(0.29)**	**(0.01) – (1.02)**	
3%	**(0.24)**	**(0.20)**	**(0.01) – (0.68)**	
7%	**(0.12)**	**(0.10)**	**(0.01) – (0.34)**	
Air Quality				
2%	**0.77**	**0.62**	**0.06 – 2.44**	
3%	**0.75**	**0.60**	**0.06 – 2.37**	
7%	**0.68**	**0.54**	**0.06 – 2.13**	

Implementation Total	**(0.90)**	**(0.89)**	**(0.47) – (1.36)**	
2%	**(0.48)**	**(0.56)**	**(1.71) – 1.32**	22
3%	**(0.40)**	**(0.50)**	**(1.46) – 1.32**	23
7%	**(0.35)**	**(0.45)**	**(1.26) – 1.20**	23

Table T17: US Impacts Due to Global Implementation Health Impacts and Valuation

	Avoided Mortalities	**Valuation 2006 US $Million**
Nested GEOS-Chem	140	940
Nested GEOS-Chem, LTO	44	300
CMAQ	230	1,500
CMAQ, LTO	83	560

Figure T17 shows the benefit-cost distribution produced by the MC analysis for each of the three scenarios described in Table T16. Positive values represent cost beneficial scenarios while negative values represent not cost beneficial scenarios (i.e. plotted as benefit minus cost).

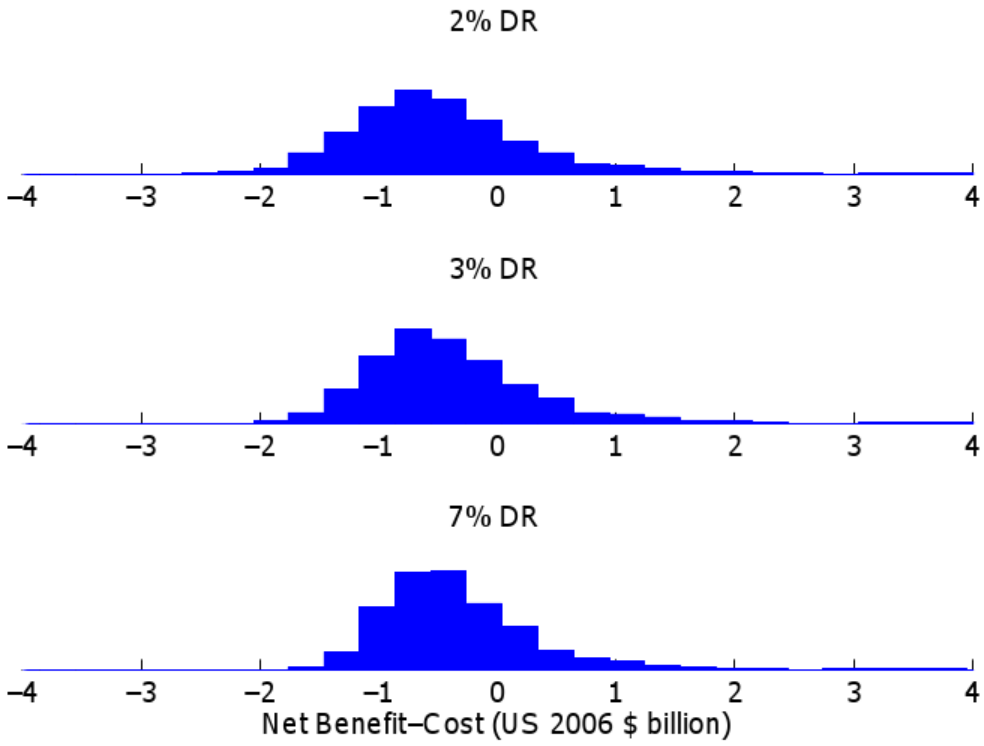

Figure T17: Benefit-cost distribution for US implementation analysis.

F.6. *US-Only Implementation Analysis*

Table T18 presents the primary results from the CBA for US-only implementation of ULSJ. Note that values in parentheses are non-cost beneficial values.

Table T18: US-Only Implementation CBA Results, given in 2006 US $ Billion

Component	Mean	Median	95% Interval	% Cost Beneficial
Climate				
2%	**(0.12)**	**(0.10)**	**(0.00) – (0.36)**	
3%	**(0.09)**	**(0.07)**	**(0.00) – (0.24)**	
7%	**(0.04)**	**(0.04)**	**(0.00) – (0.12)**	
Air Quality				
2%	**0.50**	**0.40**	**0.04 – 1.57**	
3%	**0.48**	**0.38**	**0.04 – 1.52**	
7%	**0.43**	**0.35**	**0.04 – 1.37**	
Implementation	**(0.90)**	**(0.89)**	**(0.47) – (1.36)**	
Total				
2%	**(0.53)**	**(0.58)**	**(1.33) – 0.65**	13
3%	**(0.51)**	**(0.56)**	**(1.27) – 0.64**	12

7%	**(0.51)**	**(0.56)**	**(1.20) – 0.52**	11

Figure T18 shows the benefit-cost distribution produced by the MC simulations for each of the three scenarios described in

Table T18. Positive values represent net cost beneficial scenarios while negative values represent net non-cost beneficial scenarios.

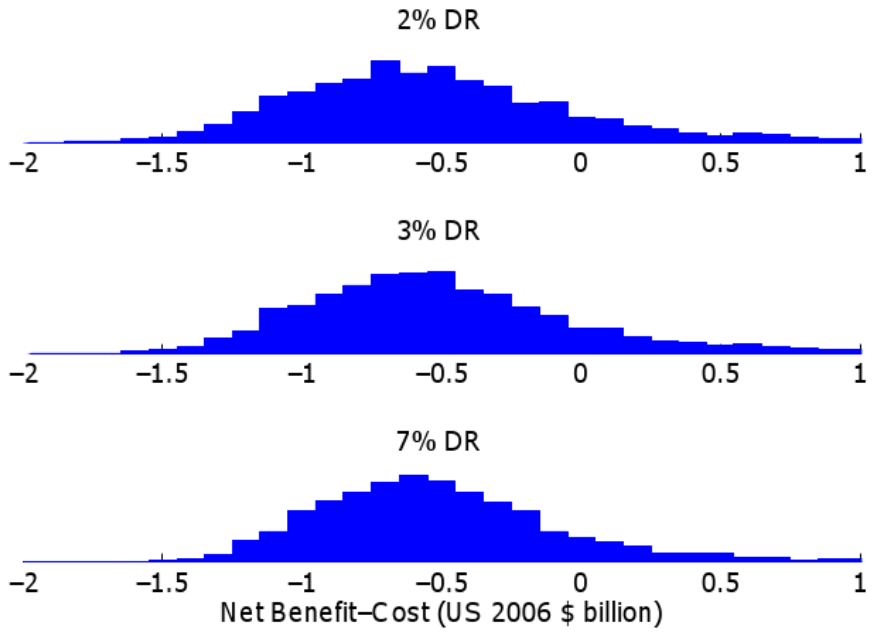

Figure T18: Benefit-cost distribution for US-only implementation analysis.

F.7. *Constant VSL Analysis*

As mentioned previously, the US VSL can be applied to all avoided mortalities to reflect a policy choice that values all premature mortalities equally. The results from this analysis are presented in Table T19 and Figure T19.

Table T19: Constant US VSL Implementation CBA Results, given in 2006 US $ Billion

Component	**Mean**	**Median**	**95% Interval**	**% Cost Beneficial**
Climate				
2%	**(2.35)**	**(2.07)**	**(0.13) – (6.32)**	
3%	**(1.64)**	**(1.46)**	**(0.10) – (4.26)**	
7%	**(0.82)**	**(0.73)**	**(0.06) – (2.08)**	
Air Quality				

2%	**15.28**	**12.20**	**1.27 – 47.93**	
3%	**14.82**	**11.83**	**1.23 – 46.49**	
7%	**13.35**	**10.65**	**1.11 – 41.87**	
Implementation	**(2.52)**	**(2.49)**	**(1.31) – (3.80)**	
Total				
2%	**10.41**	**7.41**	**(4.94) – 43.02**	82
3%	**10.65**	**7.81**	**(3.73) – 42.55**	84
7%	**10.00**	**7.33**	**(2.64) – 38.94**	86

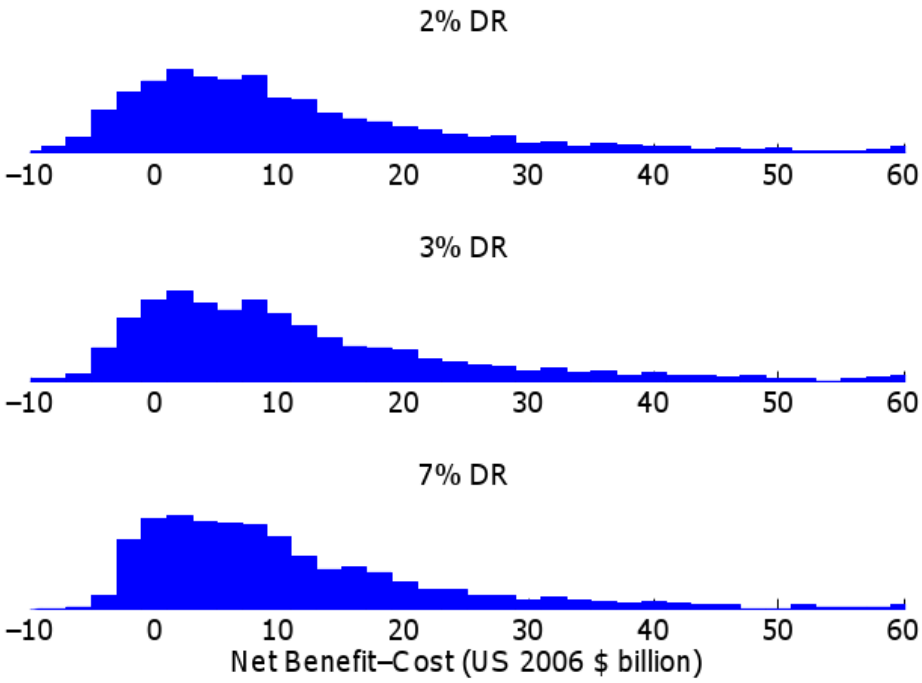

Figure T19: Benefit-cost distribution for a constant US VSL analysis.

F.8. *Cost Effectiveness Analysis*

As an alternative to a benefit-cost analysis, implementation costs and climate disbenefits are presented on a per premature mortality basis within a cost effectiveness framework. Results are presented in Table T20 and are expressed in 2006 US $ million and are presented for the global implementation, US implementation, and US-only implementation scenarios.

Table T20:Cost effectiveness analysis results, given in 2006 US $ Million

Discount Rate	Mean	Median	95% Interval
Global Implementation			
2%	**2.57**	**2.18**	**0.72 – 6.75**
3%	**2.26**	**1.97**	**0.73 – 5.66**
7%	**2.02**	**1.78**	**0.73 – 4.72**

Global Implementation-US			
2%	**13.0**	**13.4**	**4.29 – 32.2**
3%	**12.3**	**10.8**	**4.40 – 30.0**
7%	**12.2**	**10.8**	**4.43 – 28.9**
US-Only Implementation			
2%	**16.7**	**14.8**	**5.86 – 40.3**
3%	**16.6**	**14.6**	**5.95 – 38.9**
7%	**17.6**	**15.5**	**6.43 – 4.12**

G. Uncertainty Quantification Methods

Two sensitivity analysis methods are used to frame the uncertainty of the results of the benefit-cost analysis. While a Monte Carlo framework allows for uncertainty quantification and total variance present in the output metrics, it does not give insight into the relative effects of each input parameter and its influence on both the expected outcome and the associated variance. Each parameter's effect on the output as well as its contribution to variance can be determined using the two methods described below.

G.1. *Nominal Range Sensitivity Analysis*

A nominal range sensitivity analysis (NRSA) as detailed in Jun[T95] is used. A NRSA is a local, first order sensitivity analysis that is used for a deterministic model and shows changes in the final output given these deterministic inputs. Each input is varied from a nominally low to high value as it is inputted into the deterministic model while all other parameters not being tested are held at their modal values. This type of analysis does not capture any interaction sensitivities and is most effective for linear systems. The high, low, and nominal values are defined in Table T12, except for the US VSL, which for the purposes of this analysis, is assumed to have a high, low, and nominal value of $12 million, $1million, and $7.4 million, respectively. Also, nominal values for the uniform distributions are assumed to be the value midway between the defined endpoints.

G.2. *Global Sensitivity Analysis*

While the results of an NRSA may be useful to understand first order and absolute effects of input parameter values on the output value, it provides no information concerning how much uncertainty each parameter contributes to the total output uncertainty. A global sensitivity analysis (GSA) serves to quantify the contribution to variance. GSA is detailed in Allaire and

Willcox,[T92] but the method used for this analysis is implemented as specified by Salteli.[T96] A description outlining this approach is provided here.

Three matrices are defined with random variables: $\boldsymbol{A}$, $\boldsymbol{B}$, and $\boldsymbol{C}$. $\boldsymbol{A}$ is an N x k matrix that contains a set of randomly generated variables, where N is the number of MC simulations and k is the number of input parameters. $\boldsymbol{B}$ is an N x k matrix that contains a different set of randomly generated variables from those in $\boldsymbol{A}$. $\boldsymbol{C}$ is an N x k matrix that is formed by all columns of $\boldsymbol{B}$ except for the i^{th} column, which is replaced by the i^{th} column of $\boldsymbol{A}$. Based on these constructed matrices, Monte Carlo simulations are performed where each column of each matrix is one simulation defined by randomly defined input parameters and each unique matrix defines one complete Monte Carlo run. Thus, because there are $k + 2$ unique matrices formed, a total of $N(k + 2)$ runs are required. From these simulations, we can define the following variables:

$$Var(\boldsymbol{Y}) = Var[\boldsymbol{Y}(\boldsymbol{A}); \boldsymbol{Y}(\boldsymbol{B})], \quad (23)$$

meaning the expected variance of the output is defined by both set of randomly generated variables and $\boldsymbol{Y}$ is the vector of expected outcomes generated by the simulations.

$$S_i = \frac{1}{N}\sum_{i=1}^{k}[\boldsymbol{Y}(\boldsymbol{A}) \cdot \boldsymbol{Y}(\boldsymbol{C}_i) - \boldsymbol{Y}(\boldsymbol{A}) \cdot \boldsymbol{Y}(\boldsymbol{B})]/Var(\boldsymbol{Y}), \quad (24)$$

where the multiplication shown above is scalar component-wise multiplication, and S_i is known as the main effect sensitivity index, which gives the percentage of output variance explained by that input parameter alone, but does not include interaction effects between parameters.[T92]

$$S_{Ti} = 1 - \frac{1}{N}\sum_{i=1}^{k}[\boldsymbol{Y}(\boldsymbol{B}) \cdot \boldsymbol{Y}(\boldsymbol{C}_i) - \boldsymbol{Y}(\boldsymbol{A}) \cdot \boldsymbol{Y}(\boldsymbol{B})]/Var(\boldsymbol{Y}), \quad (25)$$

where S_{Ti} is the total effect sensitivity index, which does account for input interactions.[T92] The results from a GSA can indicate which input parameters require further research and understanding to reduce overall uncertainty in a model or associated analysis. To improve convergence times and reduce the value of N, Salteli[T96] suggests the use of Sobol quasi-random numbers instead of completely random variables. Sobol sets are used in this analysis. N is set to 5000 in determining main effect indices. Total effect indices require an N upwards of 30,000.

G.3. *NRSA Results*

This section presents the results of the NRSA for both global and US implementation, where the primary results are shown in Figure T20 and Figure T21, respectively. Again, US implementation here refers to the US net benefit-cost due to a global implementation of ULSJ.

Note: Blue and green bars represent the change in net benefit-cost attributed to a low or high parameter value, respectively. Only the change in net benefit-cost relative to a base deterministic model output is shown.

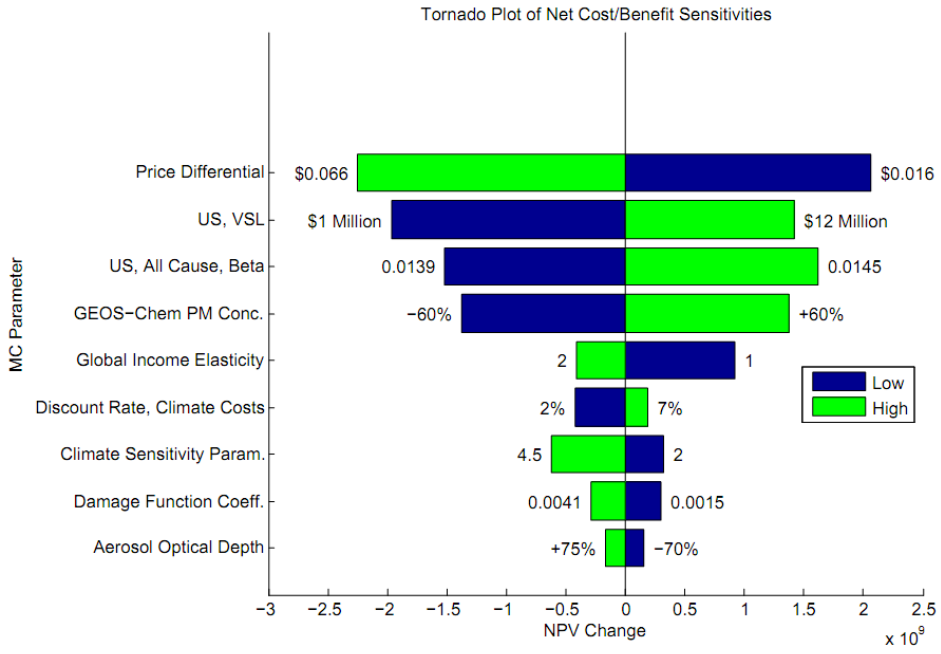

Figure T20: NRSA results for global implementation of ULSJ.

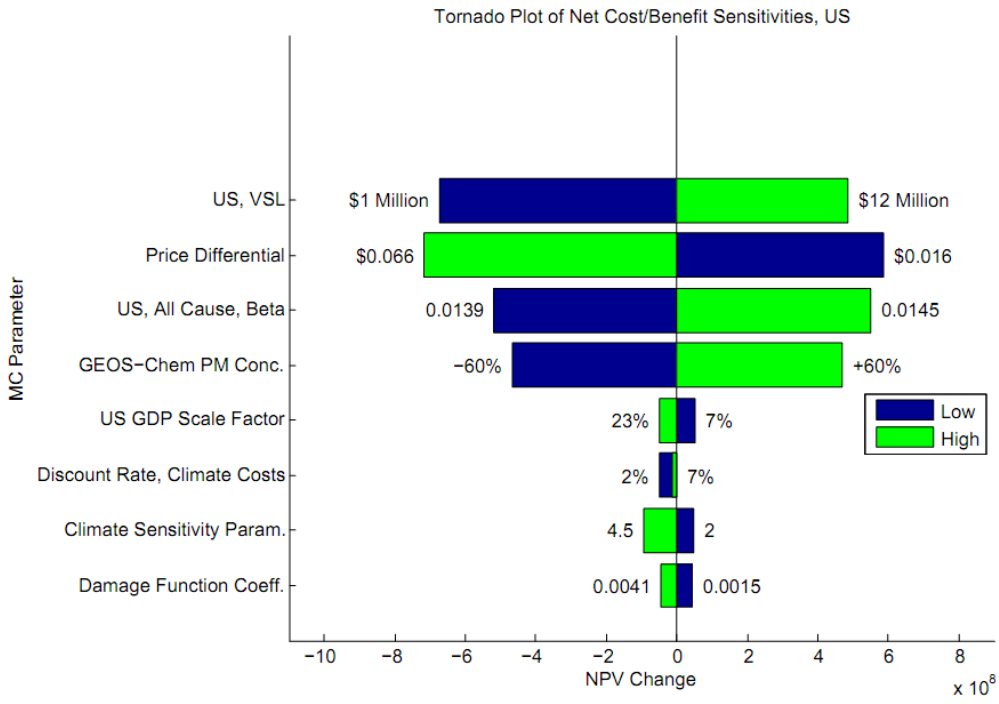

Figure T21: NRSA results for US implementation of ULSJ.

In the global and US analysis, the total net benefit-cost output is most significantly impacted by the US VSL, the price differential, the assumed percent change in premature mortality given a 1μg/m^3 change in $PM_{2.5}$ concentration, and the uncertainty assumed for the ground level PM concentration change found in GEOS-Chem. Other important input parameters are the assumed global income elasticity and components specific to the climate impacts such as the climate sensitivity parameter, damage function coefficient, and the various components of the sulfate RF calculation method. The other APMT-Climate inputs do not appear as significant parameters. The global income elasticity, CP percent increase in premature mortality, and LC percent increase in premature mortality values have no effect on the US analysis because no values applied in the CBA are derived from those parameters as they are in the global analysis. Likewise, the GDP fraction associated with US-only climate costs has no impact on the global analysis. Uncertainty analysis of APMT-Climate has been performed previously and can be found in Jun.[T95]

This sensitivity analysis is useful in that it provides a method in which to gauge the response of the system for a perturbation in an individual parameter. The values shown in the tornado plots above can be used to estimate the benefit-cost response to an increase in US VSL or change in

ground $PM_{2.5}$ concentration relative to the nominal value. For instance, if the US VSL is actually $12 million rather than $7.4 million, then one would expect a $1.5 billion increase in net benefit for the global implementation case, which is shown as a positive $1.5 billion shift in NPV of the net benefit-cost value. This type of analysis, however, is potentially misleading. This analysis provides relatively little insight into each components contribution to uncertainty, i.e. which parameters have the largest impact on the distribution seen from the MC analysis. It is misleading in the sense that the US VSL and the price differential are shown to have the largest impact on the value of the output metric, but the range in values applied in the analysis is significant compared to the other inputs. While this NRSA approach is useful as it provides some insight into what the most influential factors in this CBA within a deterministic framework are, to further understand the major sources of uncertainty in this analysis, we perform a global sensitivity analysis (GSA).

G.3.1. Discount Rate

Within the US NRSA, both endpoints for discount rate produce a decrease in net benefit-cost. This is possible due to the interaction of discounting health benefits and climate disbenefits. Net benefit-cost is plotted against discount rate for deterministic outcomes to better understand this relationship.

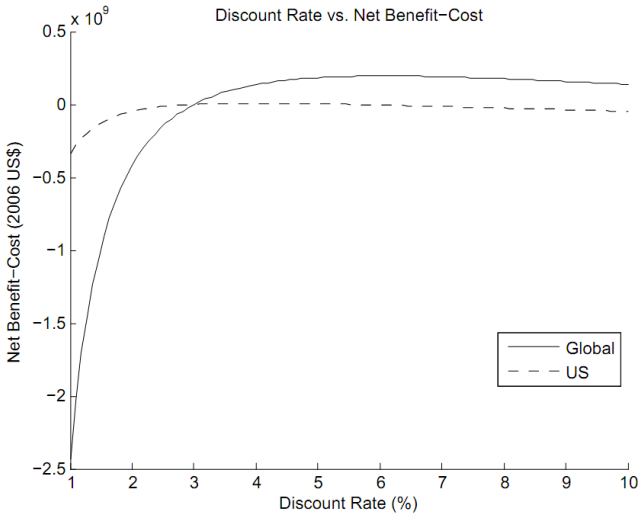

Figure T22: Net benefit-cost plotted against discount rate of the deterministic model used in the NRSA.

Figure T22 shows that in the global and US analyses, the net benefit-cost increases through the nominal rate of 3% (as defined, net benefit-cost at 3% will be 0) and then plateaus as the discount rate increases to 10%. The plateau can be explained by the decrease in value in future costs/benefits, thus the net benefit-cost of the system approaches the benefit-cost in the year of implementation. Also, the US analysis (dashed line) never produces a net benefit, as shown in Figure T21. The shape of the response can be explained by the decreasing climate disbenefits coupled with decreasing health benefits as the discount rate increases. At lower discount rates, climate costs more rapidly decrease compared to the decrease in health impacts. After a local minimum is reached at approximately 6% in the global analysis and 3% in the US analysis, the decrease in climate costs no longer outweighs the decrease in health benefits and a slight downturn is observed. The net result of each analysis then approaches a steady state value as the discount rate continues to increase.

G.4. *GSA Results*

A GSA was performed in order to determine the contribution of each input parameter to the total output variance. Main and total effect indices are reported. Main effect indices report the specific input parameters direct impact on the output variance while the total effect indices also account for input parameter interaction. The results for the most significant factors for the global implementation are shown in Figure T23 and Figure T24. The results for the most significant factors for the US implementation are shown in Figure T25 and Figure T26.

Only input parameters with main effect indices of greater than 2% are plotted. Both the US and Global implementation results yield similar results, although the climate factors were less significant in the US analysis than in the global analysis. It is clear that the US VSL input parameter has the largest impact on output variance with a main effect sensitivity index of approximately 55% and 60% for the global and US analysis, respectively, while all other significant effects are approximately 10% or below. This is not surprising given that the US VSL forms the basis for all potential benefits derived from ULSJ implementation as well as being a highly uncertain value in itself due to the assumed Weibull distribution as defined by the EPA. This analysis also shows that the same parameters shown to be significant in the NRSA are also shown to be significant in the GSA, but relative impacts on the output variance are much

different than in the differences seen on the absolute value of the output. Total effect sensitivity indices are not significantly higher than the main effect sensitivity indices, indicating that second order interaction effects between the input parameters are present but not significant.

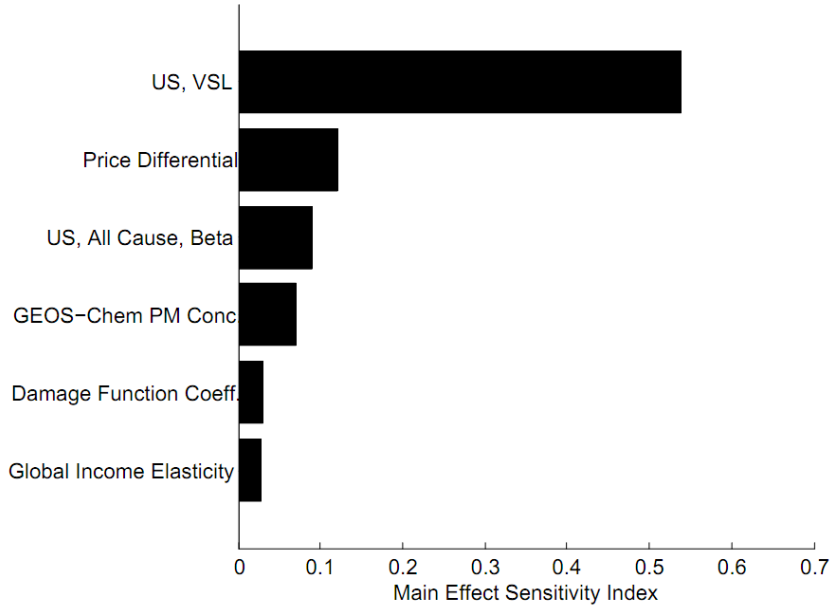

Figure T23: Global Implementation GSA main effect sensitivity index results.

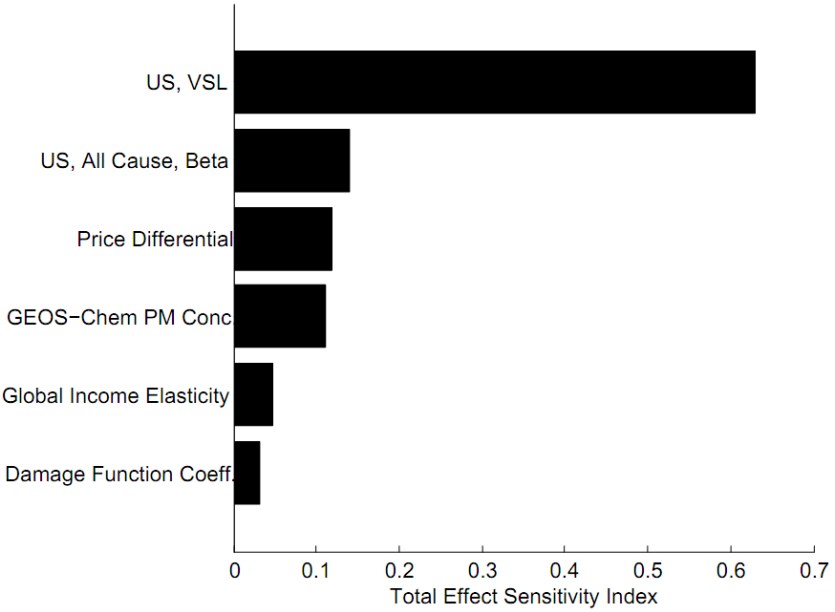

Figure T24: Global Implementation GSA total effect sensitivity index results.

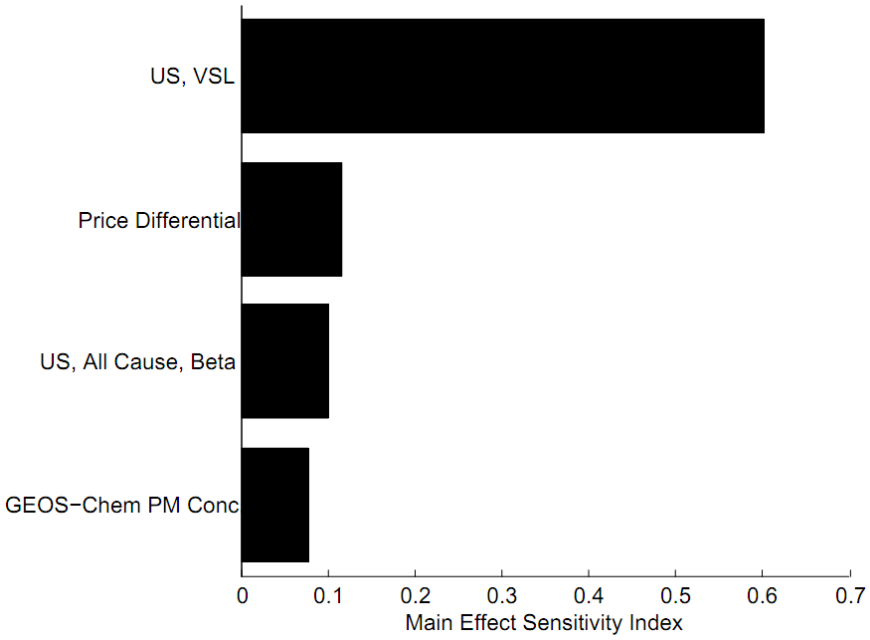

Figure T25: US Implementation GSA main effect sensitivity index results.

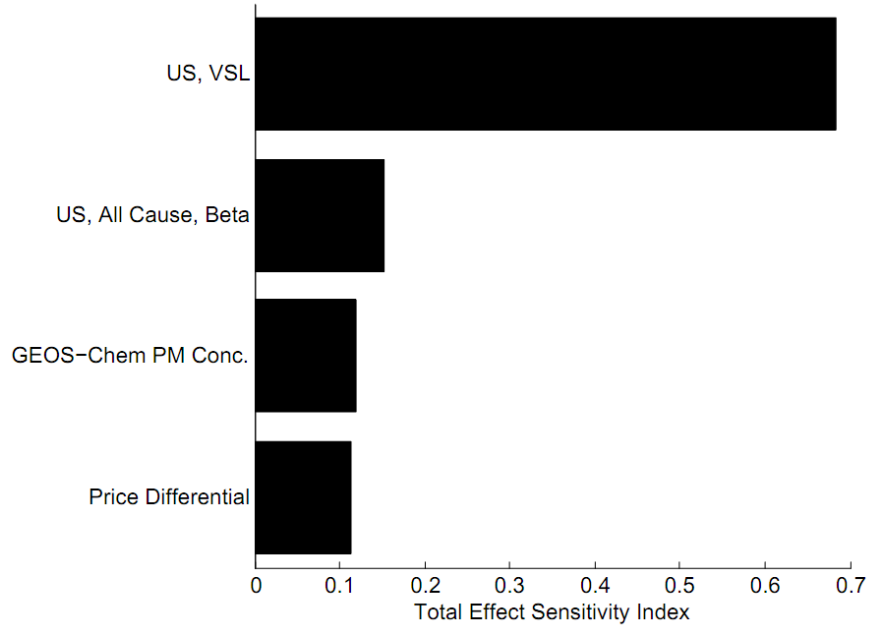

Figure T26: US Implementation GSA total effect sensitivity index results.

H. Additional Operational Concerns

H.1. *Change in Fuel Properties*

One of the major operational concerns of ULSJ is the impact on fuel energy density and specific energy given the additional processing required for desulfurizing jet fuel. From Hileman et al.,[T52] a 1% reduction in energy density and a 0.3% increase in specific energy of the fuel are expected post-processing of a fuel with an average FSC of 600-700 ppm. These changes in fuel properties are most likely brought on by the breakdown of aromatic rings that constitute approximately 20% of jet fuel.[T52] Thus, more fuel will be burned by volume, but less by mass. This has two potential consequences. First, if more fuel is required to be burned by volume, then it is possible that airlines will have to purchase more fuel by the gallon at a given price. The impact of this effect is unclear as market adjustments could take place given that the consumers know the fuel has reduced energy density, and thus airlines may not incur any cost penalty as a result.

Second, if less fuel is burned by mass (assuming that the total fleet energy requirement remains the same and there are no airline operational impacts given the increase in fuel volume carried), there is a potential reduction in climate and health impacts due to a reduction in overall emissions, although this is uncertain and not considered in this analysis.

The reduction in fuel energy density may cause a higher percentage of fuel to fall below standard jet fuel specifications, which in turn has an effect on profits seen by the refineries given that less fuel can be sold as jet fuel. Based on ASTM turbine fuel specifications for Jet A or A1,[T97] jet fuel must have a specific energy content of at least 42.8 MJ/kg and a density between 0.775 and 0.840 kg/L, which implies that the lowest possible energy density that is within specification is 33.2 MJ/L. Fuel data for JP-8 was obtained through the Petroleum Quality Information System (PQIS) database.[T98] Given the similarities between Jet A and JP-8, it is assumed that the fuel specifications mentioned above could also be applied to the PQIS data. The values in the data set are shifted by the expected reduction in energy density. A 1% energy density reduction corresponds to an energy density of 34.4 MJ/L, thus a 0.4 MJ/L shift is applied to all values in the data set and compared against the minimum fuel specification value of 33.2 MJ/L. No energy density values fall below the fuel specification. As a limiting case, a 2% energy density reduction shift is also applied to all the data points. Of the available data where energy density could be

computed, three points fell below the fuel specification, which corresponds to 0.07% of the total fuel volume. It is assumed that no significant additional costs would be seen by refineries or consumers with regards to meeting fuel specification standards.

H.2. *Fuel Lubricity*

One other operational issue is a potential decrease in fuel lubricity. Decrease in fuel lubricity can lead to engine fuel pump failure as these components tend to be partially fuel lubricated. Decreased fuel lubricity can cause more rapid fatigue of the mechanical components due to an increase in wear scar diameter (WSD). An example of this was the full or partial failure of at least eight pumps on New Zealand airlines flights due to poor lubricity fuel delivered from a local New Zealand refinery. Tests indicated excessive wear in the spline-drives, which connect the fuel-pumps to the fuel-control units, from at least three different manufacturers. These splines were expected to have a service life of 3000-5000 hours, but were wearing out in 150 hours.[T99]

This issue was addressed in several ways. First, the refinery added 5% (although 30% has also been suggested[T100]) straight-run (non-hydroprocessed) kerosene to production when possible to hydroprocessed streams which resulted in a reduction of hydrotreater severity. As a result, WSD decreased from 0.78 mm to 0.65 mm from June 1994 to December 1996. Of the airlines affected, one was supplied with DCI-4A (corrosion inhibitor for use in jet fuels) doped fuel, one added a different, unspecified corrosion inhibitor, and one did not use any additive. In addition, hardware modifications were made by the engine manufacturers by offering improved pump splines. There have not been any further reported lubricity issues with this fuel since these changes were implemented.[T101]

If it were needed, a fuel additive could be used with ULSJ to improve its lubricity. The US military currently uses a Corrosion Inhibitor/Lubricity Improver (CI/LI) additive in all of its JP8 fuel. This additive is obtained through a contract price of $19.706/gallon when purchased in a 55 gallon drum. CI/LI is typically added at 20 mg/L (25 ppm m/m) of JP8.[T102] It then follows, on a per gallon volumetric basis, the additional price as a result of the CI/LI additive is 0.05 cents/gallon. Given that this additional price is two orders of magnitude less than the cost of

HDS, it is neglected in the benefit-cost analysis. There is also a possible air quality impact due to the additive since it is burned with the fuel during engine operations, but this is unknown.

H.3. *Sulfur Byproduct*

The creation of ULSJ fuel would also result in increased production of elemental sulfur at oil refineries. To understand how this sulfur may be used, Figure T27 was created with historical elemental free on board (FOB) sulfur price and production data obtained from the US Geological Survey,[T103] where a FOB price is defined by the EIA as "a sales transaction in which the seller makes the product available for pick up at a specified port or terminal at a specified price and the buyer pays for the subsequent transportation and insurance." Although the price of elemental sulfur declined in concert with the increased desulfurization of diesel fuel and the end of domestic production of sulfur from the Frasch mining process, prices subsequently rebounded. This rebound in price occurred along with a steady increase in global production of elemental sulfur. In August 2008, the price of elemental sulfur spiked with prices in Tampa Florida reaching $600 per tonne. However, by the end of November 2008, the price had collapsed. At the end of 2009, the price was about $30 per tonne, which is in line with the price data in Figure T27. Considering that sulfur is still mined using the Frasch process and from native sources and pyrites, it appears that any sulfur that would result from the creation of ULSJ could be absorbed by the chemicals industry market. The sulfur from ULSJ would have a value (in 2006 US $) of 0.005 cents/gal, or $3 million globally.

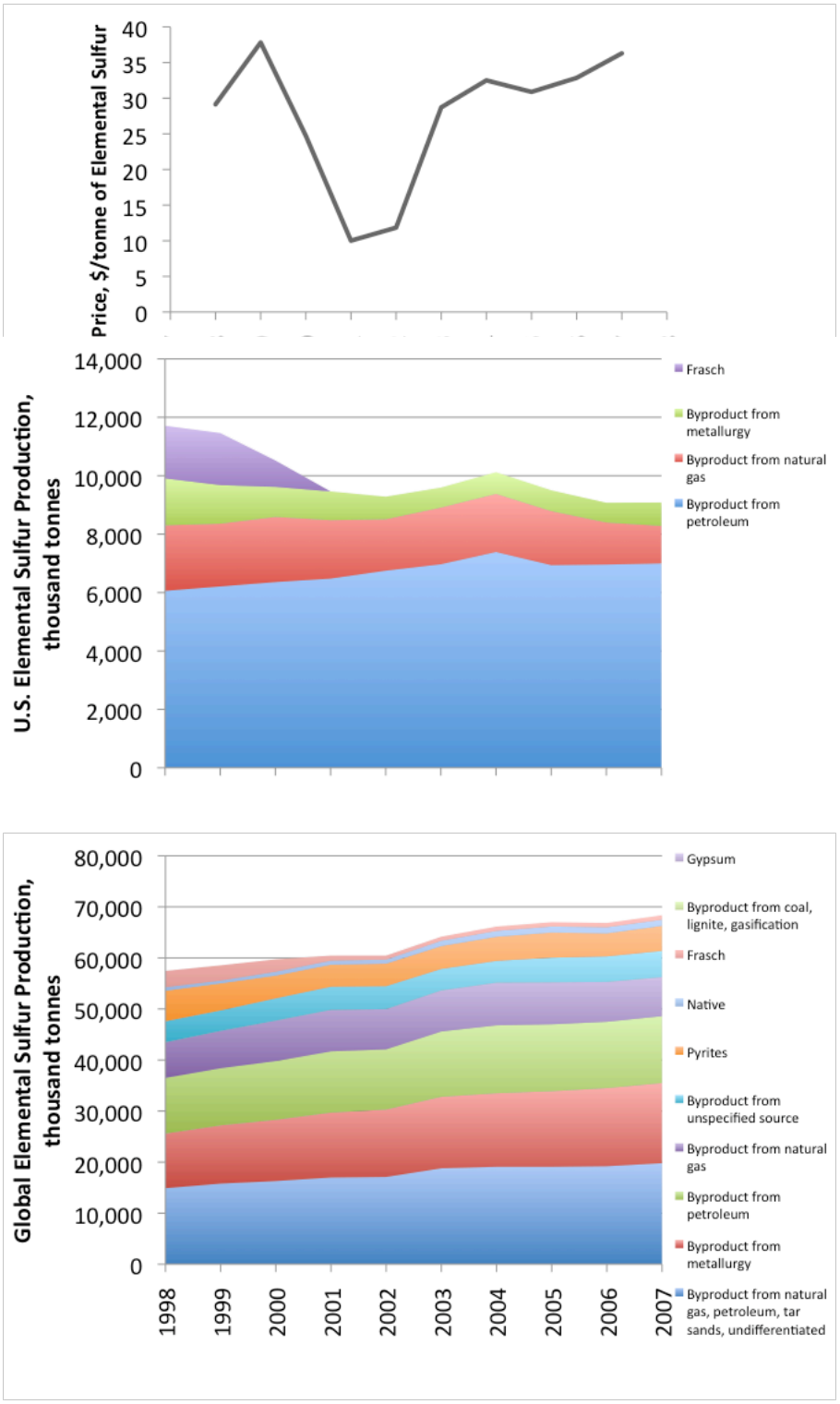

Figure T27: Elemental sulfur prices and production levels.

I. Vertical Transport Assessment

As CTMs have rarely been used to assess the impact of cruise altitude emissions on surface air quality, we apply two approaches to evaluate the performance of GEOS-Chem (the model used for nominal results) with regard to vertical transport from the upper troposphere/lower stratosphere (UT/LS) to the surface. First, we compare vertical profiles of CO, O_3 and PAN from NASA aircraft missions to GEOS-Chem simulation results for 2006. The observations are averaged over chemically and geographically coherent regions described by Wang et al.[T104] and Bey et al.,[T12] with updates from a more recent campaign TRACE-P.[T105] Although all of these aircraft missions took place before 2006, the interannual variability of regionally averaged concentrations is sufficiently small that these observations are still useful to test model vertical transport.[T12]

Second, we simulate beryllium-7 (^{7}Be) production and scavenging using GEOS-Chem. ^{7}Be is produced by cosmic ray spallation of N_2 and O_2 in the UT/LS,[T134] is immediately taken up by aerosol particles, and is subsequently transported until loss by radioactive decay (half-life 53.3 d) or deposition to the surface. Its source distribution is relatively well known and there are extensive climatological observations from a global network of surface sites and from aircraft originally designed by the US Department of Energy (DOE) to monitor radioactive fallout. ^{7}Be has been used in numerous global model studies to test the simulation of vertical transport.[T140,T141,T142,T143,T152] Here we conducted a 6-year GEOS-Chem simulation of ^{7}Be using 2004-2009 GEOS-5 meteorological data and the ^{7}Be source parameterization from Usoskin and Kovaltsov.[T144] The ^{7}Be source depends on solar activity in a predictable manner, and we correspondingly scale the ^{7}Be observations following Koch et al.[T142]

I.1. *GEOS-Chem Results vs. Observation*

Figure T28 shows the comparison between the vertical profiles of observed and (GEOS-Chem) simulated CO concentrations for selected regions. The decrease in concentrations with altitude in the Northern Hemisphere and the uniform vertical distribution in the Southern Hemisphere are generally captured by GEOS-Chem. Similar plots for O_3 and PAN are also included in Figure T29 an T27, respectively. The observed increase in O_3 with altitude is well captured by GEOS-Chem. For PAN, GEOS-Chem can generally reproduce the high near-surface concentrations near

continental source regions such as East Asia, as well as the enhanced concentrations at higher altitudes in remote regions affected by long-range transport. These comparisons indicate no significant bias in the overall model representation of vertical gradients.

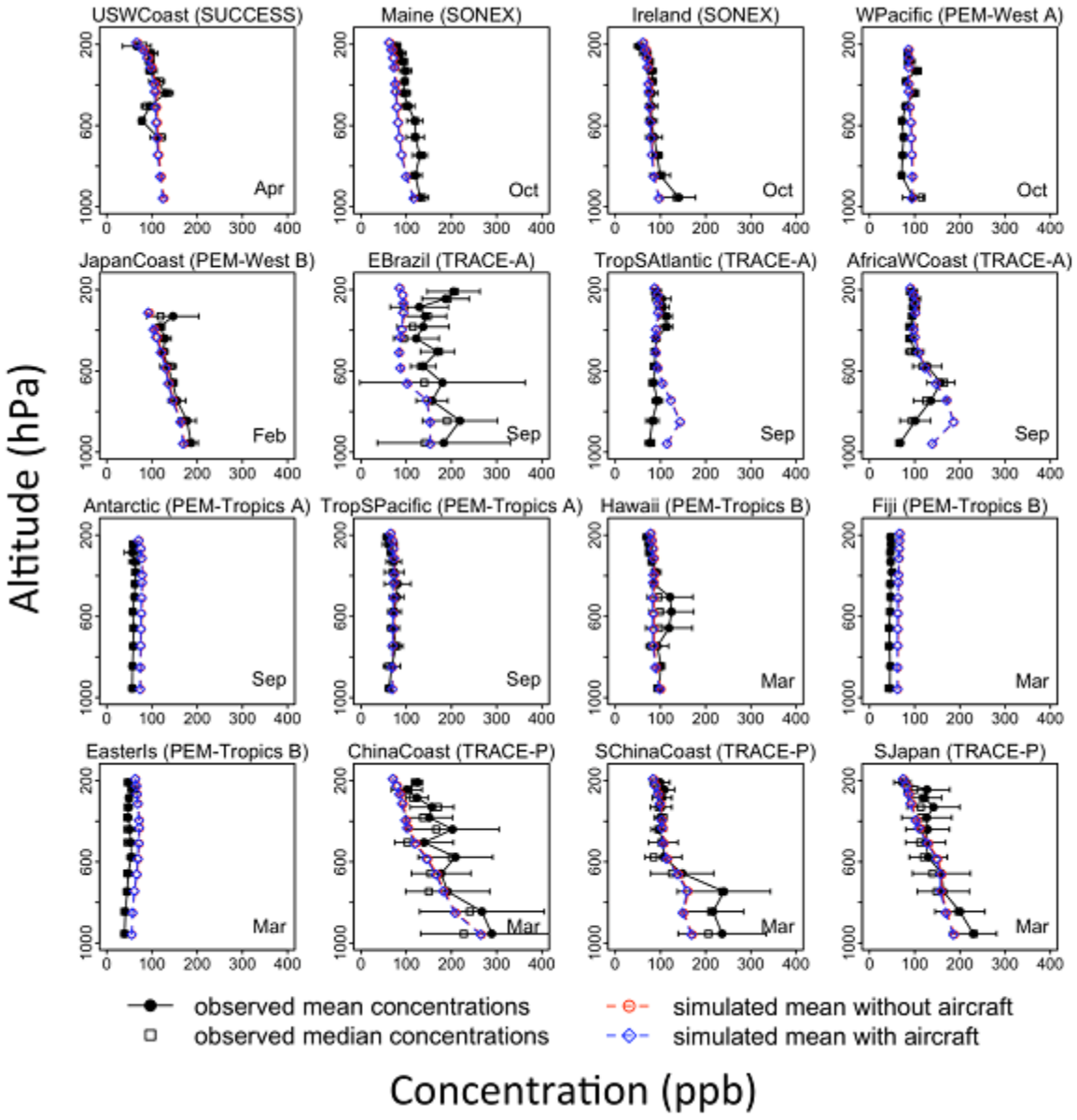

Figure T28: Comparison of observed and simulated vertical profiles of carbon monoxide (CO). Simulated mean concentrations for both scenarios with and without aircraft emissions are shown. Observations are from NASA aircraft missions indicated in brackets and are averaged over coherent regions.

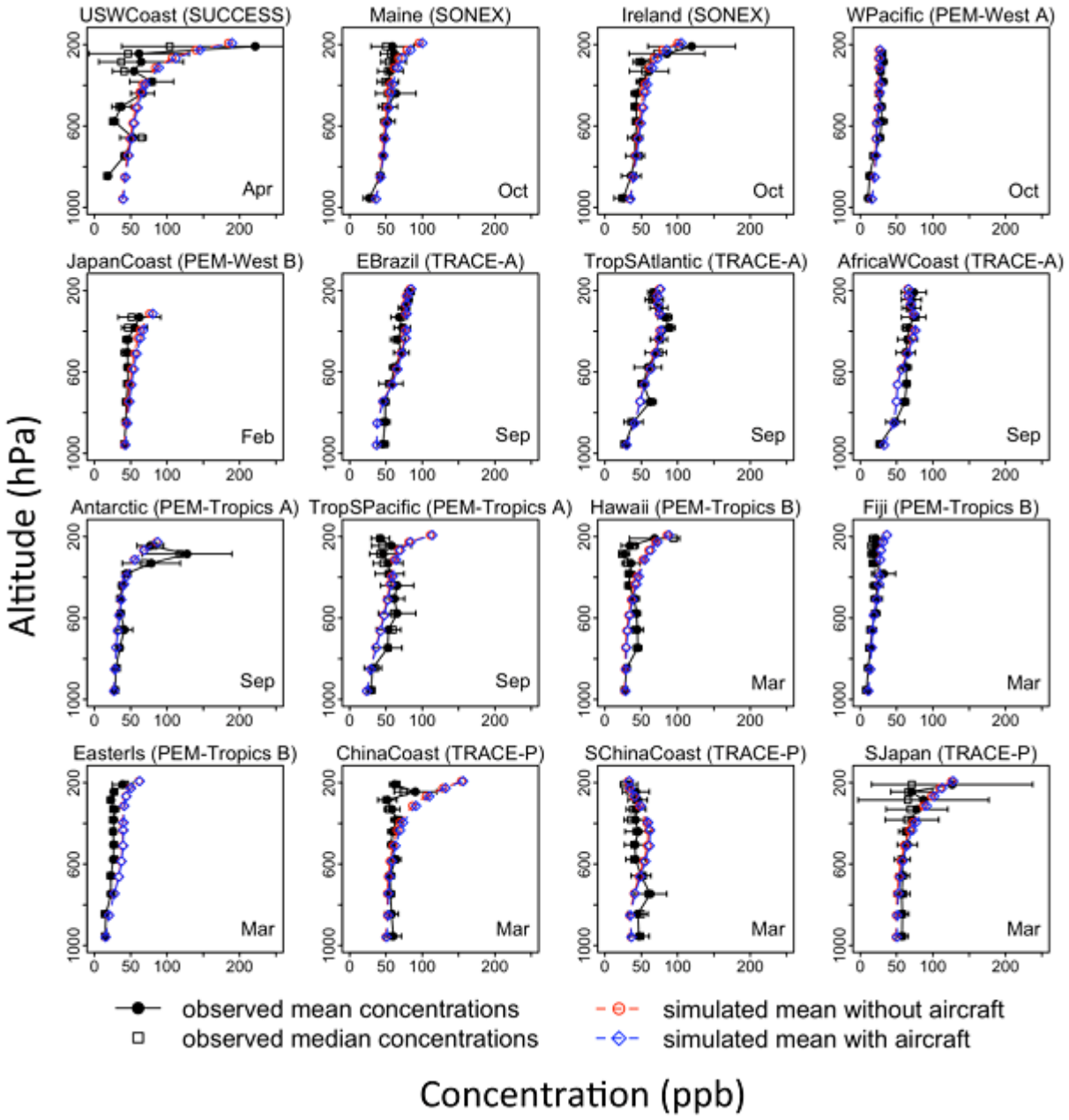

Figure T29: Comparison of observed and simulated vertical profiles of ozone (O_3). Simulated mean concentrations for both scenarios with and without aircraft emissions are shown. Observations are from NASA aircraft missions indicated in brackets and are averaged over coherent regions.

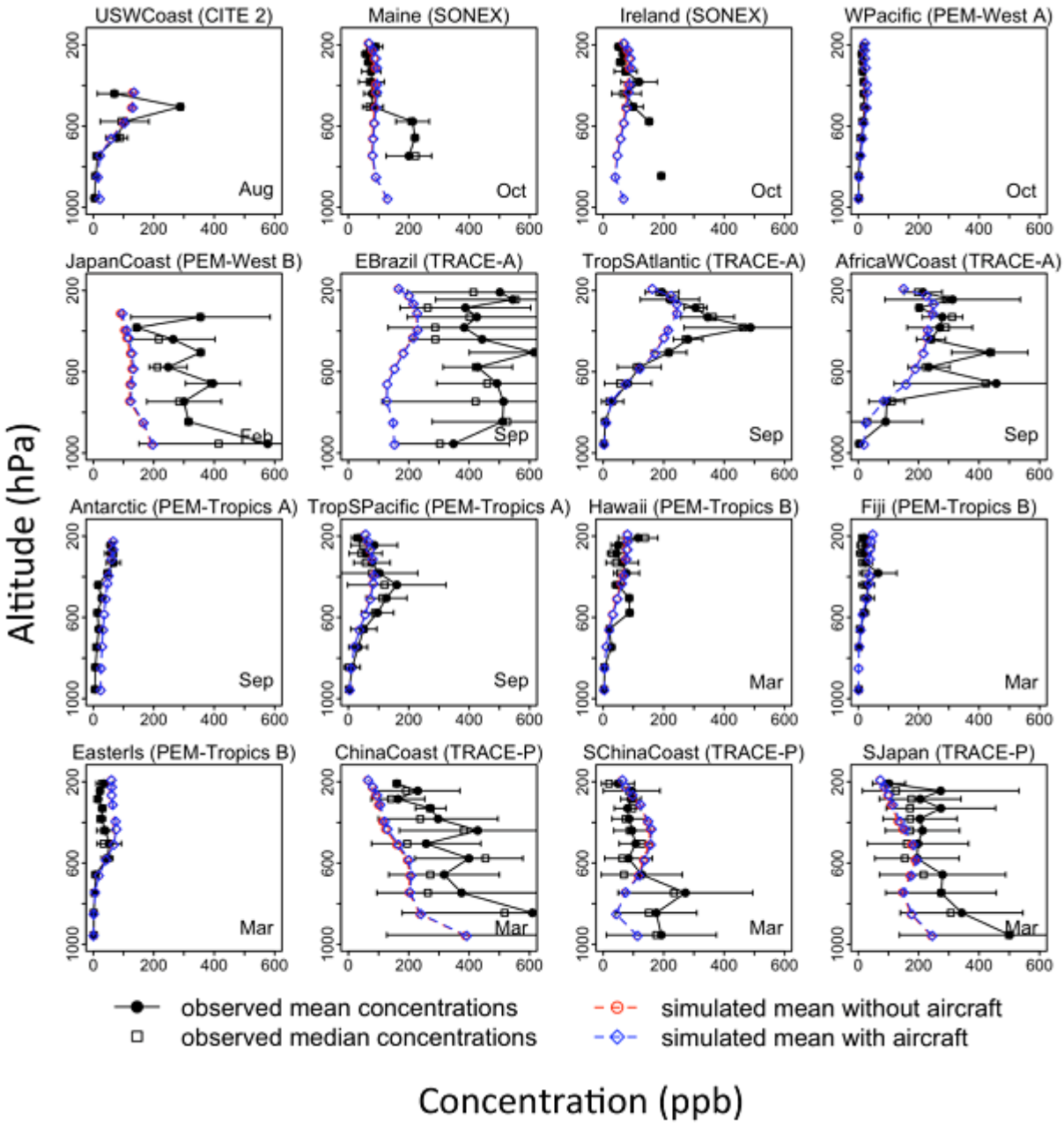

Figure T30: Comparison of observed and simulated vertical profiles of peroxyacetylnitrate (PAN). Simulated mean concentrations for both scenarios with and without aircraft emissions are shown. Observations are from NASA aircraft missions indicated in brackets and are averaged over coherent regions.

I.2. ^{7}*Be Simulations in GEOS-Chem*

Figure T31 compares model results with the climatological observations of ^{7}Be averaged over 10° latitude bins. The model is sampled at the month and location of the observations (solid lines) and the zonal mean is also given (dotted lines). The top panel evaluates the model ^{7}Be emissions source by comparing with the UT/LS aircraft observations of the DOE Radionuclide Database (RANDAB).[T106] The middle panel compares model results with the ^{7}Be wet deposition fluxes aggregated by Koch et al.,[T142] which provide an additional test of the model source since the dominant ^{7}Be removal in the troposphere is by wet deposition. The bottom panel compares the model surface air concentrations with long-term observations from the DOE Surface Air Sampling Program.[T107] We see from Figure T31 that GEOS-Chem reproduces successfully the magnitudes and latitudinal patterns of the ^{7}Be observations. Comparison to RANDAB indicates a model source bias of -4 ± 2%. Comparison to observed surface air concentrations indicates a bias of -18 ± 6% globally and <10% over the US. The ^{7}Be source on average is 60% stratospheric and 40% tropospheric, and Dutkiewicz and Husain[T186] deduced from observed ^{90}Sr/^{7}Be ratios that approximately 25% of surface ^{7}Be at northern mid-latitudes is of stratospheric origin. We find the same fraction in GEOS-Chem, which tests the model simulation of stratosphere-troposphere exchange and implies that the model biases estimate above should be insensitive to the precise distribution of the aerosol source within the UT/LS.

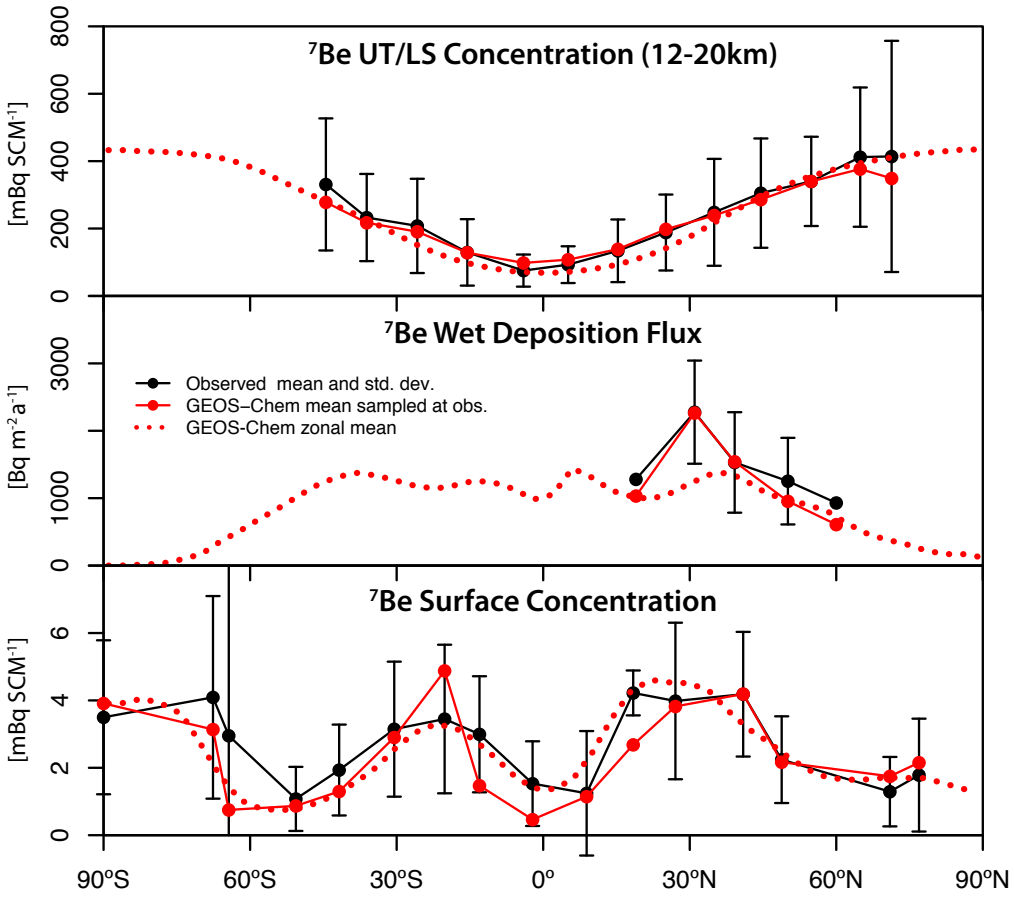

Figure T31: Latitudinal profiles of cosmogenic ^{7}Be as a test of the GEOS-Chem model simulation of vertical transport of aerosols from the UT/LS to the surface. Observations (black lines) are averaged over 10° latitude bins. GEOS-Chem results for 2004-2009 are sampled at the month and location of observations (red lines) and the model zonal mean is also given (dotted lines). The top panel shows DOE RANDAB UT/LS aircraft data from 1957-1983, the middle panel shows annual mean wet deposition flux data compiled by Koch et al.,[T142] and the bottom panel shows DOE SASP surface air concentration data for 1957-1999. Error bars indicate the variability (±σ) across sites in the wet deposition flux data, and across the spatial, seasonal, and interannual variability of the RANDAB and SASP samples for each bin. The GEOS-Chem simulation is conducted for average solar activity conditions (Φ = 670 MV with Usokin and Kovaltsov[T144]). The RANDAB and wet deposition flux data are adjusted for average solar activity following Koch et al.,[T142] while the surface air observations are filtered for average solar activity (Φ = 520-820 MV from Usoskin et al.[T156]). Concentrations are represented by the S.I. unit for radioactivity per cubic meter air at 0°C and 1 atm.

I.3. *Evaluating the Vertical Transport in GEOS-Chem*

I.3.1. Vertical Mixing in the Atmosphere

Motions that effect the vertical distributions of trace gases and particles of upper troposphere / lower stratosphere (UT/LS) origin to the surface include (1) turbulent mixing of the planetary boundary layer, (2) moist deep convection, (3) large scale advection, and (4) stratospheric-tropospheric exchanges (STE). The planetary boundary layer (PBL) represents the lowest 1-2 km of the atmosphere, and is in direct contact with the surface of the Earth, where various thermal and mechanical forcings drive a mostly turbulent and vertically well-mixed regime that rapidly responds (< 1 h) to changes.[T108] Above the PBL is the free troposphere, a region that is predominantly non-turbulent. Large-scale advection from dominant climate features (e.g., the Hadley and Walker circulations) will mix the troposphere on the order of 1 month. However, intermittent turbulent mixing from moist deep convection (thunderstorms) plays an important role in the general mixing of the troposphere by locally mixing on time scales of 0.5-2 hours.[T109] The troposphere is capped by a strong thermal inversion at the tropopause (10-12 km extratropics; 16-18 km tropics), impeding vertical exchanges between the troposphere and the overhead stratosphere. Nevertheless, mixing between the stratosphere and troposphere ultimately occurs on time scales of 5-6 years following the Brewer-Dobson Circulation.[T110]

I.3.2. Vertical Mixing in GEOS-Chem

The GEOS-Chem chemical transport model (CTM)[T111] has transport driven by assimilated meteorological fields from the GEOS-5 DAS global circulation model (GCM).[T112] The meteorological data are 6 h means (3 h for surface fields) and have horizontal resolution of 0.5º latitude by 0.667º longitude with 72 layers in the vertical (~37 in the troposphere). The horizontal resolution is degraded to either 4º × 5º or 2º × 2.5º for input to global GEOS-Chem simulations, or may be run at native model resolution for nested regions (e.g., North America, East Asia). For large-scale vertical and horizontal mixing, GEOS-Chem uses the same flux-form semi-Lagrangian advection scheme[T113] as the GEOS-5 DAS parent GCM. Sub-resolution processes must be parameterized. Convective transport is that of Lin[T114] and driven by convective mass fluxes determined within the GCM assimilation using a relaxed Arakawa-Schubert scheme.[T115] Boundary layer mixing by default is parameterized by uniformly mixing

the boundary layer each dynamic time step. An optional alternative PBL-mixing scheme using a representation of local turbulent mixing is also implemented.[T116]

I.3.3. Radon-222

Terrigenic ^{222}Rn is an inert, insoluble, short-lived (half-life 3.8 d) noble gas produced from the slow decay of ^{226}Ra (half-life 1600 a) found in uranium ores. Its insolubility and time scale of decay make it a useful and sensitive tracer for diagnosing quick vertical mixing within atmospheric models from moist convection and boundary layer mixing and ventilation.[T117,T118,T119,T120,T121,T122,T123,T124,T125,T126]

Emissions of ^{222}Rn within GEOS-Chem are those of Jacob et al.[T123] We assume a uniform 1.0 atom cm^{-2} s^{-1} from land 60ºS-60ºN, and 0.05 atom cm^{-2} s^{-1} from 60-70ºN and 60-70ºS. Oceans are assumed to have uniform emission of 0.05 atom cm^{-2} s^{-1}. There are no emissions poleward of 70º in either hemisphere. We reduce all fluxes by a factor of three under freezing conditions following Jacob and Prather.[T122] We simulate GEOS-Chem over every available full year of the GEOS5 DAS meteorology (2004-2009) to compare climatological monthly profiles with the observations. Vertical profile measurements of ^{222}Rn are scarce, and only available at northern extratropical locations. We aggregate those from Ohio,[T127] Central Asia,[T128] Central Illinois,[T129] Eastern Ukraine and Moscow,[T130] Central New Mexico,[T131] Colorado, Nebraska, Kansas, Utah,[T132] and Moffett Field, California.[T133]

Figure T32 shows GEOS-Chem mean 2005-2009 climatological ^{222}Rn profiles sampled at the month and location of the observations, also plotted. We use here units common to the radioactivity community: mBq per standard cubic meter (at 273.15 K and 1 atm), a linear transformation of the molar mixing ratio (e.g., 5.637 mBq SCM^{-1} = 1.0x10^{-22} mol ^{222}Rn / mol air). In the absence of convective transport and PBL mixing within the model (green line), there is an expected overestimate of ^{222}Rn at the surface near its sources, and an underestimate at altitude. In an overly convective atmosphere, the vertical gradient would disappear. Therefore, the observed vertical gradient is determined by the amount of vertical mixing. The model with convection and PBL-mixing (red line) well represents the climatological median of the measurements. There is a slight overestimate within the PBL and overestimate above, implying a slight underestimate in vertical mixing. However, this performance is comparable to or better

than other CTMs/GCMs [e.g., Fig. 5 and 6, Considine et al.[T119]]. The choice of boundary layer mixing parameterization (i.e., default vs. turbulent scheme) has no influence on the simulated ^{222}Rn profiles (not shown).

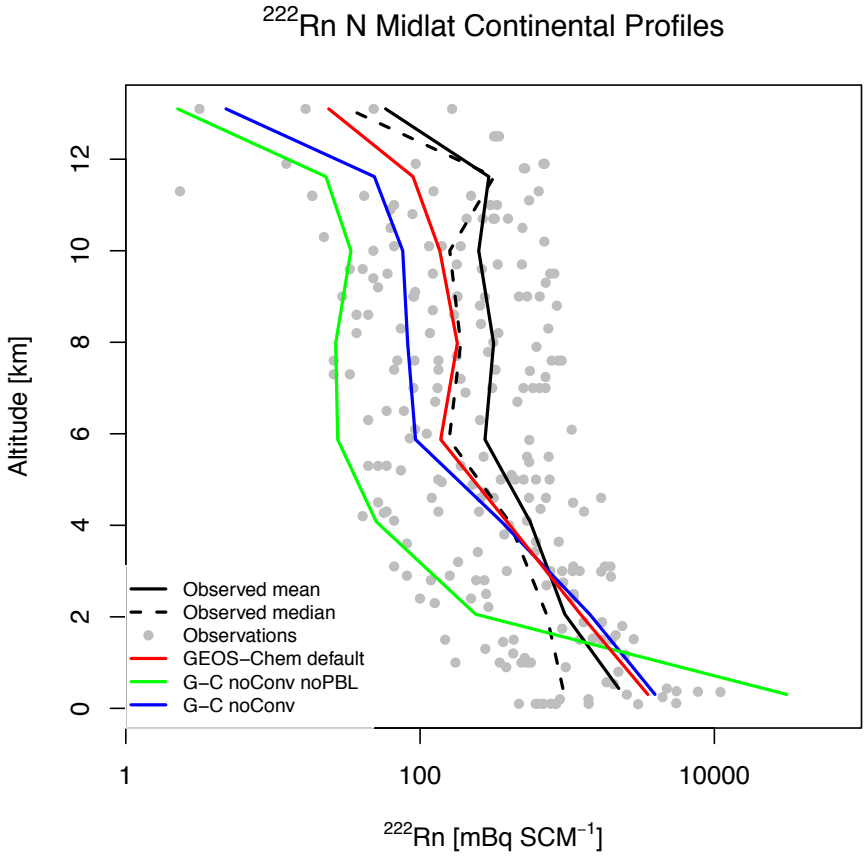

Figure T32: Mean observed vertical profile of ^{222}Rn (black lines) compared with GEOS-Chem sampled at month and location of observations. Model results are shown for the standard simulation (red line), as well as simulations with no convection (blue line) and neither convection nor PBL-mixing (green).

Though profiles of ^{222}Rn are useful in demonstrating that there are no egregious problems with the model vertical transport, the observations are sparse, and its source at the surface makes it a better tracer for upward vertical motions. For additional insight, we turn to a tracer of UT/LS origin.

I.3.4. Beryllium-7

Cosmogenic ^{7}Be is produced by the cosmic ray spallation of N_2 and O_2, predominantly in the polar UT/LS.[T134] It is immediately and indiscriminately taken up into submicron aerosol particles where it remains chemically inert.[T135,T136,T137,T138,T139] It is subsequently transported until removal from the atmosphere via tropospheric rainout, surface deposition, or radioactive decay (half-life 53.3 d) as depicted in Figure T33. It has been used in numerous global model studies to constrain model vertical transport, wet deposition fluxes, and STE.[T140,T141,T142,T143]

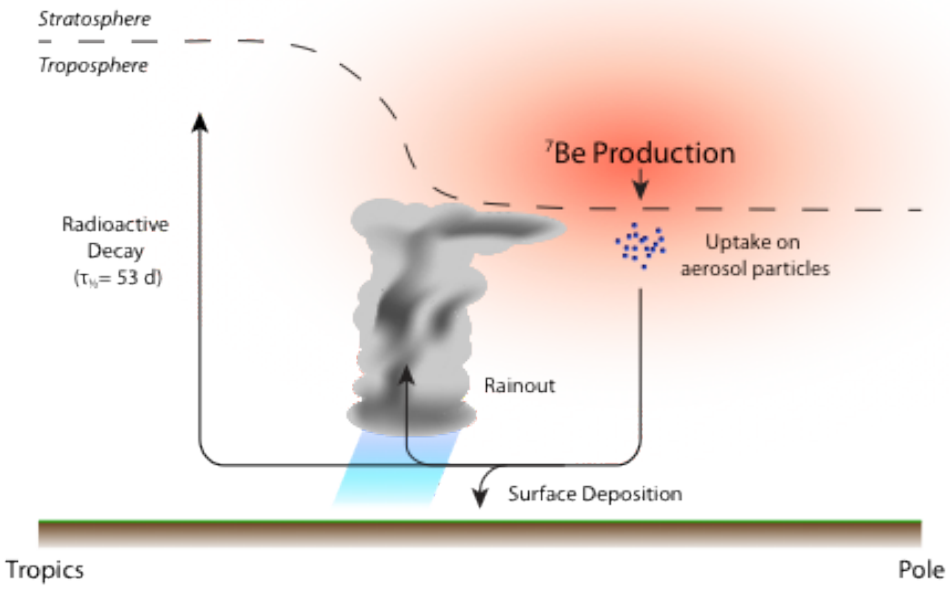

Figure T33: Typical beryllium-7 atmospheric source, transport pathways, and losses.

I.3.5. Simulating Comogenic Production of ^{7}Be

We simulate the source of ^{7}Be using the parameterization of Usoskin and Kovaltsov,[T144] who determine ^{7}Be production as a function of atmospheric depth, geomagnetic cutoff rigidity, and solar modulation potential. We determine the geomagnetic cutoff rigidity as a function of geomagnetic latitude using the dipole approximation.[T145] During periods of high solar activity, cosmic rays are defected away from Earth. The solar modulation potential, Φ, is a single parameter representing this ability, and has been reconstructed from long-term ground-based neutron monitors.[T144]

GEOS-5 DAS assimilated meteorological fields are only available for 2005-present, and not cover a full 11-year solar cycle. Therefore we perform multi-year simulations with constant solar modulation potentials for mean solar activity (Φ = 670 MV), solar minimum (Φ = 280 MV), and solar maximum (Φ = 1200 MV). Our average simulation leads to a production of 0.05 atoms cm^{-2} s^{-1}; 60% in the stratosphere and 40% in the troposphere. This falls amongst the wide range of previous studies: 0.08[T146,T147] atoms cm^{-2} s^{-1}; 0.063[T148,T149] atoms cm^{-2} s^{-1}; 0.035[T150] atoms cm^{-2} s^{-1}; 0.055-0.062[T151] atoms cm^{-2} s^{-1}; 0.035[T152,T153] atoms cm^{-2} s^{-1}; 0.062[T144] atoms cm^{-2} s^{-1}. Earlier ^{7}Be studies using GEOS-Chem[T142,T143,T154] use the Lal and Peters[T146] fixed latitude-altitude production tables yielding 0.08 atoms cm^{-2} s^{-1} at solar maximum, with 67% of production in the stratosphere and 33% in the troposphere.

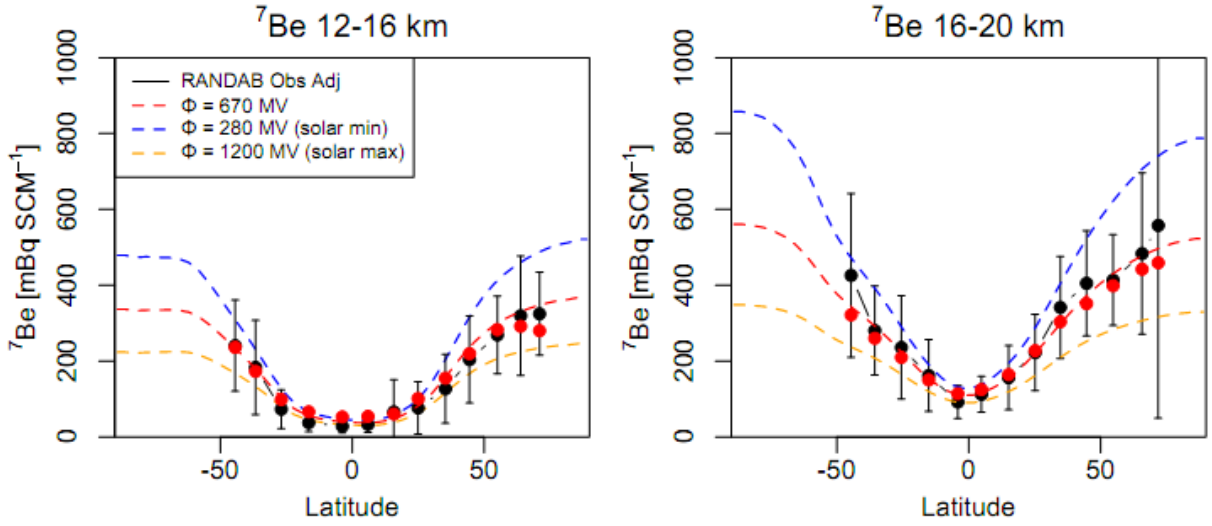

Figure T34: Comparison of model ^{7}Be source parameterization with UT/LS aircraft observations from DOE RANDAB for two different altitude ranges. Observations are adjusted for mean solar activity and averaged over 10º latitude bins (black dots) with error bars representing the standard deviation. The model is sampled at the month and location of the observations (red dots). Mean zonal concentrations (dashed lines) are also shown for simulations using average solar activity (red), as well as solar minimum (blue) and solar maximum (orange).

Figure T34 compares the simulated zonal ^{7}Be UT/LS concentrations of this work with that of the DOE RAdioNuclide DAtaBase (RANDAB). RANDAB is the largest collection of stratospheric and upper tropospheric radionuclide data, sampled from meridional aircraft campaigns from

1957-1983, and available online from the Oak Ridge National Laboratory Carbon Dioxide Information Analysis Center.[T155] The 10º latitudinal bins of the UT/LS observations are plotted as black dots. We adjust the observations to solar mean for comparison, assuming an inverse linear relationship in concentration with the reconstructed monthly Φ time series of Usoskin et al.[T156] as

$$^{7}Be_{adj} = {}^{7}Be_{obs} \bullet \Phi_{obs} / 670 \quad (26).$$

Red dots represent GEOS-Chem values sampled at the month and location of the RANDAB observations for a simulation of average solar activity for the period 2005-2009. The red, orange and blue-dashed lines represent the zonal mean concentration for the same period for average, maximum and minimum solar activity. The model well-represents the observed meridional gradients at both 12-16 km, where the tropics are still in the UT (and the oldest air with respect to ^{7}Be, and minimum atmospheric concentration), and 16-20 km, in the region of greatest production. The variability associated with solar minimum and maximum are within the variability of the observations; the black vertical bars represent the standard deviations of the latitude-binned adjusted observations. We use the Koch et al.[T142] definition of model bias, γ, as the signed model residuals normalized by the mean observed concentration, i.e.,

$$\gamma = \Sigma(X_{mod} - X_{obs}) / \Sigma(X_{obs}) \quad (27)$$

where X_{mod} and X_{obs} represent the vectors of simulated and observed concentrations, and determine there to be a bias of -4% (standard error ±2%) in the simulated UT/LS ^{7}Be source.

I.3.6. Constraining Loss Processes

The dominant loss mechanism for tropospheric ^{7}Be is the wet deposition (rainout) of the radionuclide-containing aerosol particles (approximately 60% total tropospheric loss in this work). Therefore, it is important that we have a reasonable representation of the aerosol wet deposition flux for correct interpretation of atmospheric concentrations. The aerosol wet scavenging scheme used in GEOS-Chem is described by Liu et al.,[T143] with minor changes for GEOS5-driven simulations (convective anvil scavenging is treated elsewhere).

The standard test for tropospheric wet deposition of aerosols is from ^{210}Pb,[T157,T121,T142,T143,T158] a decay daughter of terrigenic ^{222}Rn. Like ^{7}Be, it is chemically inert, but readily taken up by aerosols and subsequently removed from the atmosphere by deposition or decay[T135,T136,T159,T139]. Because of its relatively long lifetime (half-life 22.2 a), nearly all of ^{210}Pb is removed via deposition. This coupled with a relatively well-known source and the availability of a global and long-term surface deposition flux and concentration inventory,[T159] make it a robust test of model aerosol deposition performance.

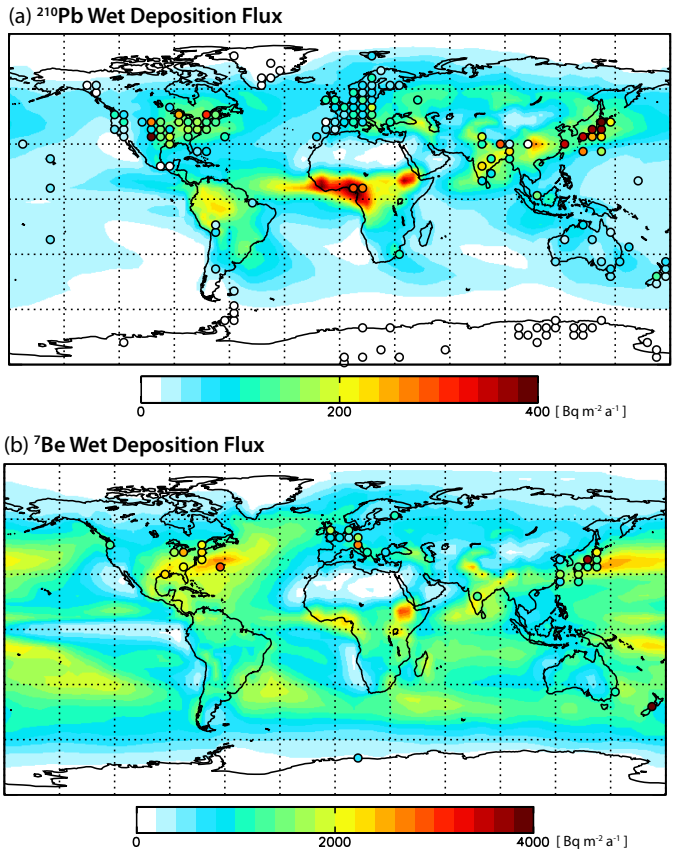

Figure T35: GEOS-Chem annual average aerosol wet deposition flux for (a) ^{210}Pb and (b) ^{7}Be. Observations are aggregated to model resolution and overplotted.

Figure T35 compares the annual 2004-2009 mean ^{210}Pb wet deposition flux with that of the climatological annual average fluxes determined from rainfall collectors, soil cores, and snow samples aggregated by Preiss et al.[T159] The observations are available from the Laboratoire Glaciologie et Géophysique de l'Environnement,[T160] and have been aggregated to GEOS-Chem

model resolution and overplotted as dots for comparison. GEOS-Chem well represents the magnitude and global spatial distribution of the ^{210}Pb deposition flux, with the exception of the East Asian outflow. The highest observed ^{210}Pb fluxes are over the Japanese archipelago, and attributed to the winter southwest monsoon where dry continental air masses from northern China and Mongolia become humidified over the Sea of Japan and orographic forcing causes large fluxes.[T161] This simulation does not consider possible primary emission and transport of dust containing ^{210}Pb from in-soil decay of ^{222}Rn, which could explain the regional underestimate. Overall, there is a low bias of -15% in the wet deposition flux of ^{210}Pb (-11% sans East Asia) with a model-observation correlation of $R^2 = 0.67$. We find a tropospheric residence time for ^{210}Pb-containing aerosols against deposition of 9.5 d. This is comparable to other model studies: 7.2[T162] d; 6.5[T124] d; 8.8-12.5[T157] d; 9[T142] d; 7.2-9.5[T163,T164] d; 9[T143] d.

Figure T35b also examines the more sparsely-sampled ^{7}Be wet deposition fluxes, compared against aggregated available observations.[T165,T166,T167,T168,T169,T170,T171,T172,T173,T174,T175,T176,T177,T178,T179,T180] Similar results (-20% low bias) are found as with the ^{210}Pb fluxes, though there is large variability in the observed fluxes from the dependence on solar activity. We determine a tropospheric lifetime against wet deposition of 42 d, the longer lifetime reflecting the drier UT. This is longer than prior findings, e.g., 23[T142] d and 21[T143] d, but within the variability expected from the sensitivity of the calculation to model vertical resolution and tropopause definition, since the majority of the ^{7}Be burden straddles the tropopause.

I.3.7. Stratosphere-Troposphere Exchange

Beryllium-7 has often been used as a tracer of downward transport from the stratosphere.[T181,T182,T183,T184,T139,T185] It has been previously used as an indicator of STE performance within global atmospheric models.[T140,T143,T154] Dutkiewcz and Husain[T186] observationally determined that about 25% of annual average surface ^{7}Be concentrations in the northern midlatitudes (38-51ºN) were of stratospheric origin, using ^{90}Sr/^{7}Be surface observations. Liu et al.[T143] used this constraint in an earlier version of GEOS-Chem using a different meteorological product (GEOS1-STRAT) to infer 3.5 to 4 times excessive stratospheric to tropospheric transport, and downscaled their stratospheric ^{7}Be production to artificially correct the STE flux.

Liu et al.[T154] repeat their analysis using both GEOS-Chem and the NASA Global Modeling Initiative (GMI) CTM tested within an ensemble of meteorological frameworks, using the Lal and Peters[T146] source. They conclude that GEOS-Chem driven by GEOS5-DAS for the year 2004 represents the impact of cross-tropopause transport on surface ^{7}Be concentrations without adjustment. Figure T36 shows comparable results with Liu et al.[T154] using the Usoskin and Kovaltsov[T144] source parameterization. Plotted is the zonal 2004-2009 annual average fraction of ^{7}Be of stratospheric origin following transport, deposition, and decay. Our simulated surface 38º-51ºN concentrations are 24-26% of stratospheric origin, suggesting the model can reproduce the transport of lower stratospheric-sourced tracers across the tropopause and to the surface.

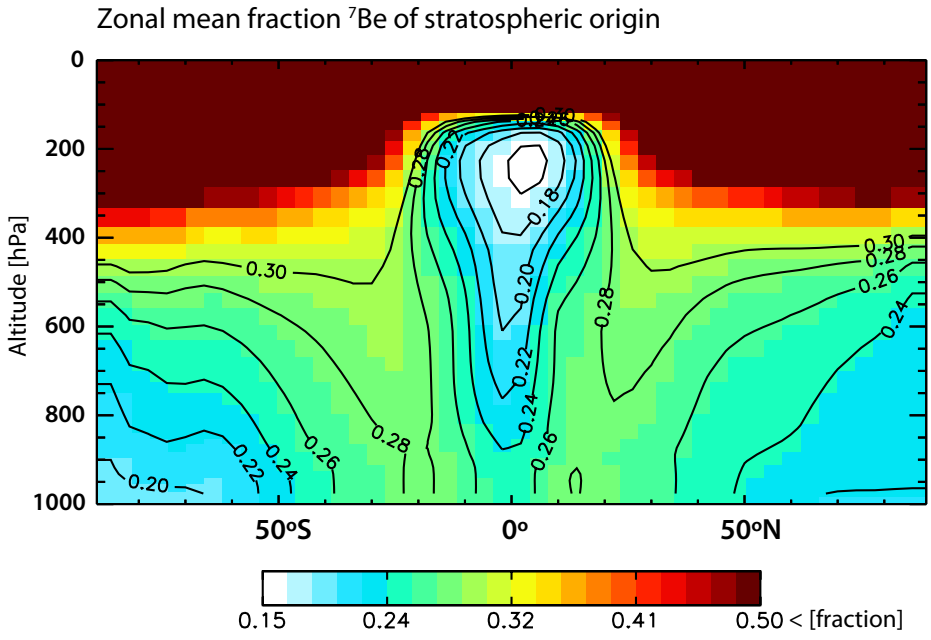

Figure T36: Zonal annual mean fraction ^{7}Be of stratospheric origin in GEOS-Chem.

I.3.8. Tropospheric Mixing

To understand the influence of the model's vertical transport on surface ^{7}Be concentrations, we turn to the long-term surface monitoring stations of the then-DOE Environmental Measurements Laboratory (EML) Surface Air Sampling Program (SASP).[T187] The SASP database recorded the spatial and temporal distribution of various natural and anthropogenic radionuclides in surface ambient air from 1957 until 1999.

Figure T37 compares the simulated radionuclide concentrations with the SASP observations during periods of average solar activity (Φ = 670 ± 50 MV from the Usoskin et al.[T156] monthly time series). Figure T37a shows the annual mean surface concentration of ^{7}Be for 2004-2009 simulated with mean solar activity (Φ = 670 MV). Overplotted as dots are the concentrations of the SASP stations aggregated during periods of average solar activity. (Note that this is not necessarily representative of an annual average concentration.)

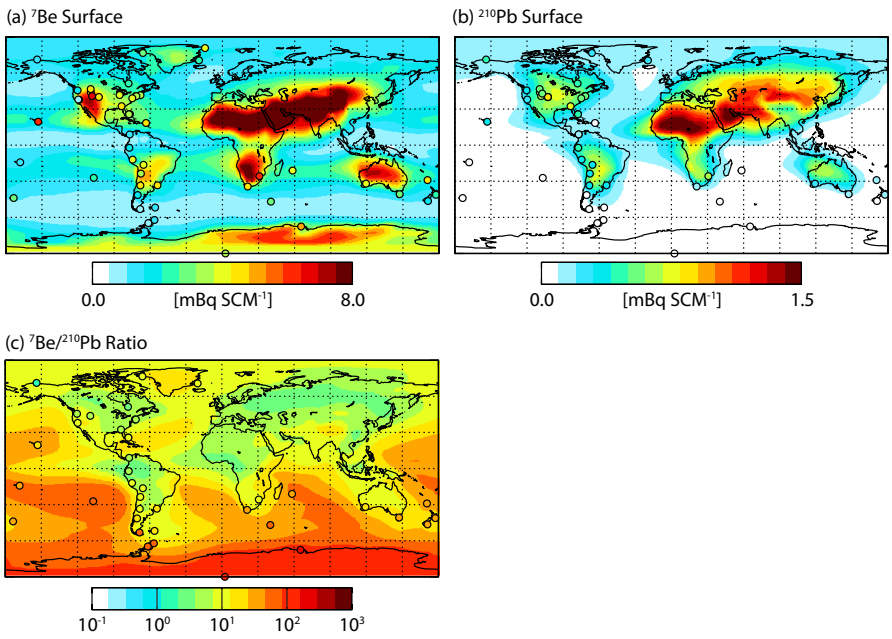

Figure T37: Mean GEOS-Chem surface concentrations of (a) ^{7}Be and (b) ^{210}Pb, and (c) the ^{7}Be/^{210}Pb ratio. Long-term mean observations from the DOE SASP network are overplotted. ^{7}Be observations have been selected for periods of average solar activity.

Figure T38 compares the same observations, now with the model average weighted by the months observed. GEOS-Chem has a global bias (± std. error) of -18 ± 6% when compared with the SASP surface concentrations (excluding mountain sites that sample free tropospheric air and are not indicative of the surface, e.g., Mauna Loa). The bias is mostly driven by relatively poor performance over South America and the Southern Ocean. Over the continental United States, the model performs better, with an average bias of -3 ± 10%. A regional high bias (29 ± 18%) in the western US offsets the low bias (-23 ± 8%) in the eastern US for the national mean.

Additionally, given the UT/LS origins of ^{7}Be and the surface origins of ^{210}Pb, and equal affinity for uptake by aerosol and wet scavenging, the ratio of $^{7}Be/^{210}Pb$ (unaffected by scavenging) in surface air is a useful proxy for the amount of tropospheric vertical mixing.[T142] Given faith in the simulated sources via comparison with the RANDAB UT/LS ^{7}Be (Figure T34) and SASP surface ^{210}Pb concentrations (Figure T37b), a persistent high bias could indicate excessive downward transport or insufficient upward transport. The distribution of the SASP $^{7}Be/^{210}Pb$ ratio is reproduced well in GEOS-Chem (Figure T37c), with poorer performance in the Southern Hemisphere, particularly near the Drake Passage.

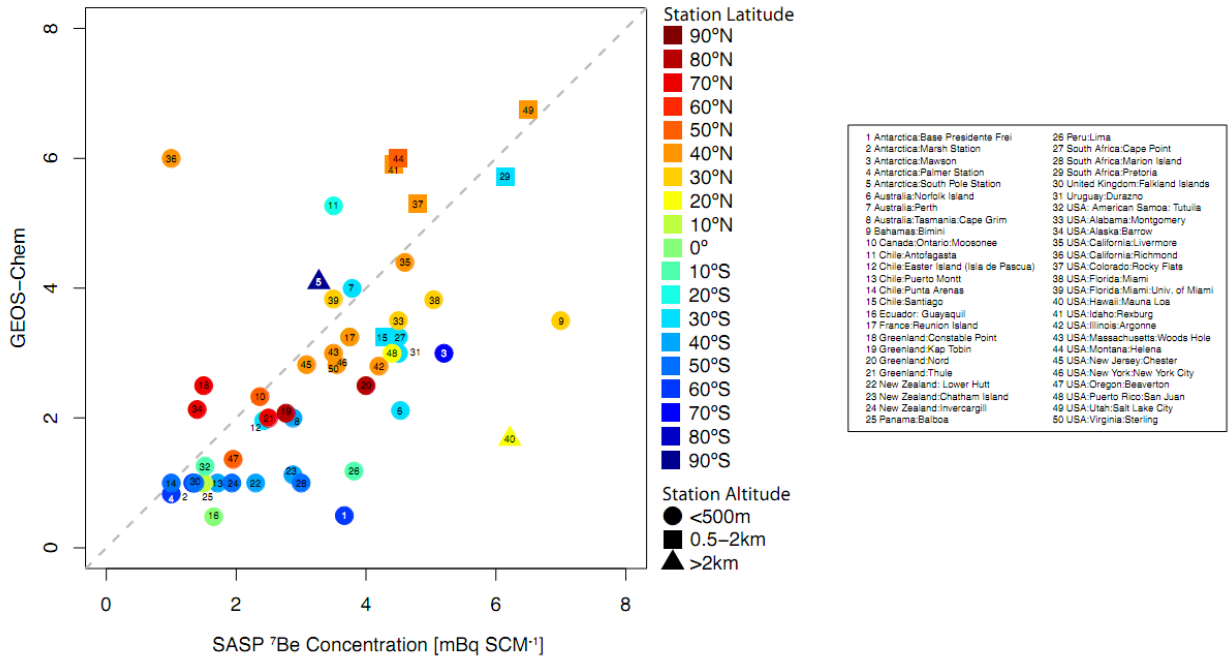

Figure T38: Model comparison of ^{7}Be surface concentrations with SASP concentrations by site. The model has been sampled at the month and location of the SASP observations.

I.3.9. GEOS-Chem vs. GATOR-GCMOM Vertical Transport

Recently, Whit 2011[T188] stated the ground-level cruise emissions impact quantified in Barrett et al.[T80] was being overestimated due to the lack of meteorological feedback as well as coarse vertical grid resolutions within GEOS-Chem in relation to GATOR-GCMOM given differences in ground-level concentrations of aircraft-attributable$PM_{2.5}$. The following figures show a comparison of vertical transport between the two models using an inert tracer with no deposition.

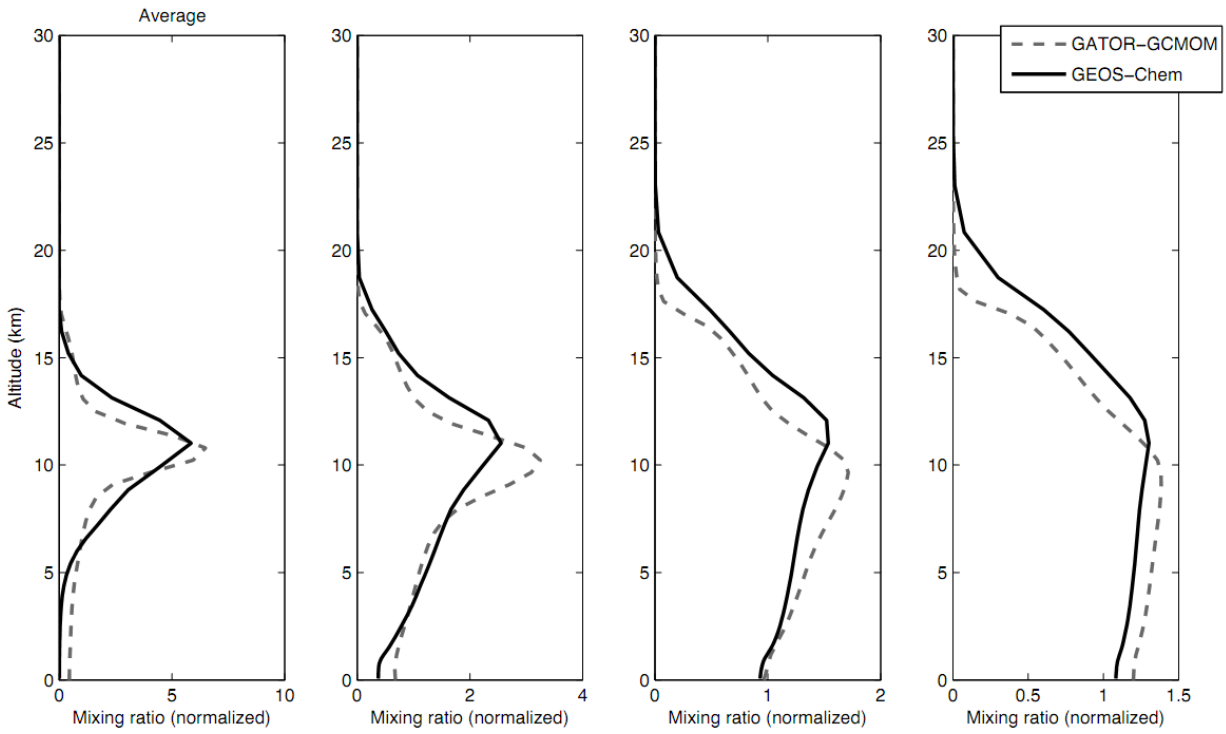

Figure T39: Globally averaged tracer mixing ratio vertical profile comparison between GATOR-GCMOM and GEOS-Chem 7, 21, 49, and 77 days after the introduction of an inert tracer.

Figure T39 shows the globally averaged tracer mixing ratio vertical profile comparison between the two models. Although the vertical profiles do differ slightly, particularly in the UT/LS region, the ground-level mixing ratios due to vertical transport are similar as time progresses.

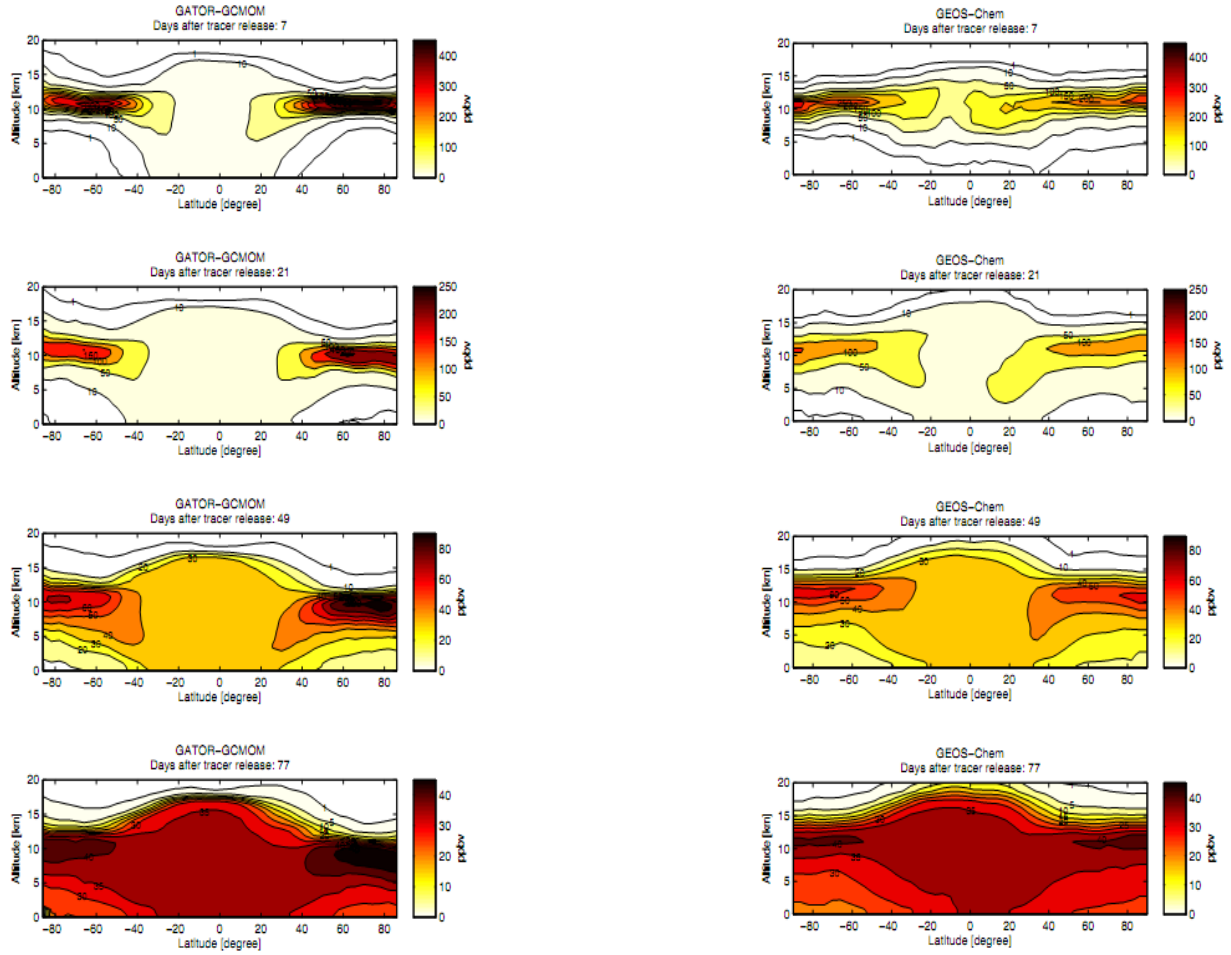

Figure T40: Time evolution of tracer mixing ratio compared between GATOR-GCMOM (left) and GEOS-Chem (right).

Figure T40 shows the evolution of the tracer for both models averaged zonally. Spacial tracer distribution is very similar in both models, but observed concentrations are consistently higher by 10 to 40% in GATOR-GCMOM than in GEOS-Chem in the UT/LS region. Ground-level concentrations are similar in magnitude (approximately 20-30 ppbv after 77 days).

Based on the results of this comparison tracer study, there is no significant difference in vertical transport rates between GEOS-Chem and GATOR-GCMOM and differences in ground-level concentration values may be explained by other factors, such as climate feedbacks which GATOR-GCMOM accounts for but GEOS-Chem does not. Additional research is currently being conducted with the goal of quantifying vertical transport rates and their impact on ground-level air quality.

J. References

T1 Hileman, J.I.; Ortiz, D.S.; Bartis, J.T.; Wong, H.M.; Donohoo, P.E.; Weiss, M.A.; Waitz, I.A. *Near-Term Feasibility of Alternative Jet Fuels.* RAND and Massachusetts Institute of Technology, 2009.

T2 US Environmental Protection Agency, Fuels and Fuel Additives; http://www.epa.gov/oms/regs/fuels/diesel/diesel.htm.

T3 Clean Diesel Fuel Alliance; http://www.clean-diesel.org/.

T4 QinetiQ. *Reduction of sulphur limits in aviation fuel standards*. EASA, 2010.

T5 Department for Transport. *Britain's Transport Infrastructure - Adding Capacity at Heathrow: Decisions Following Consultation.* DfT, 2009.

T6 International Civil Aviation Organization. *Airport Air Quality Guidance Manual*, 2007.

T7 Energy Information Administration. *The Transition to Ultra-Low-Sulfur Diesel Fuel: Effects on Prices and Supply*. EIA, 2001.

T8 US Environmental Protection Agency. *Regulatory Impact Analysis: Heavy-Duty Engine and Vehicle Standards and Highway Diesel Fuel Sulfur Requirements*. EPA, 2000.

T9 Corbett, J.J.; Winebrake, J.J. Emissions tradeoffs among alternative marine fuels: Total fuel cycle analysis of residual oil, marine gas oil, and marine diesel oil. *Journal of the Air and Waste Management Association*. **2008,** 58 (4), 538-542.

T10 Winebrake, J.J.; Corbett, J.J.; Green, E.H.; Lauer, A.; Eyring, V. Mitigating the health impacts of pollution from oceangoing shipping: An assessment of low-sulfur fuel mandates. *Environmental Science and Technology*. **2009,** 43 (13), 4776-4782.

T11 Barrett, S.; et al. Guidance on the use of AEDT Gridded Aircraft Emissions in Atmospheric Models Version 2.0, FAA, Washington DC, August 17, 2010.

T12 Bey, I.; Jacob, D. J.; Yantosca, R. M.; Logan, J. A.; Field, B.; Fiore, A. M., et al. Global modeling of tropospheric chemistry with assimilated meteorology: Model description and evaluation. *J. Geophys. Res*. **2001,** 106 (23),073-096.

T13 Chin, M.; Diehl, T.; Ginoux, P.; Malm, W. Intercontinental transport of pollution and dust aerosols: Implications for regional air quality. *Atmos. Chem. Phys*. **2007,** 7 (21), 5501-5517.

T14 Heald, C. L.; Jacob, D. J.; Park, R. J.; Alexander, B.; Fairlie, T. D.; Yantosca, R. M., et al. Transpacific transport of Asian anthropogenic aerosols and its impact on surface air quality in the United States. *J. Geophys. Res.* **2006,** 111 (14), D14310.

T15 Park, R. J.; Jacob, D. J.; Kumar, N.; Yantosca, R. M. Regional visibility statistics in the United States: Natural and transboundary pollution influences, and implications for the Regional Haze Rule. *Atmospheric Environment*. **2006,** 40 (28), 5405-5423.

T16 Park, R. J.; Jacob, D. J.; Chin, M.; Martin, R. V. Sources of carbonaceous aerosols over the United States and implications for natural visibility. *J. Geophys. Res.* **2003,** 108 (D12), 4355.

T17 Park, R. J.; Jacob, D. J.; Field, B. D.; Yantosca, R. M.; & Chin, M. Natural and transboundary pollution influences on sulfate-nitrate-ammonium aerosols in the United States: Implications for policy. *J. Geophys. Res.* **2004,** 109 (15), D15204.

T18 Duncan Fairlie, T.; Jacob, D. J.; Park, R. J. The impact of transpacific transport of mineral dust in the United States. *Atmos. Environ.* **2007**, 41 (6), 1251-1266.

T19 Corbett, J. J.; Winebrake, J. J.; Green, E. H.; Kasibhatla, P.; Eyring, V.; Lauer, A. Mortality from ship emissions: A global assessment. *Environ. Sci. Technol,* **2007,** 41 (24), 8512-8518.

T20 IPCC. *Aviation and the Global Atmosphere*. Cambridge University Press, 1999.

T21 Liu, H.; Jacob, D. J.; Bey, I.; Yantosca, R. M. Constraints from 210Pb and 7Be on wet deposition and transporting a global threee-dimensional chemical tracer model driven by assimilated meteorological fields. *J. Geophys. Res*. **2001,** 106 (D11), 12109-12128.

T22 Liao, H.; Henze, D. K.; Seindeld, J. H.; Wu, S.; Mickley, L. J. Biogenic secondary organic aerosol over the United States: Comparison of climatological simulations with observations. *J. Geophys. Res.* **2007,** 112, D06201.

T23 University of North Carolina – Chapel Hill. CMAQ 4.6 Operational Guidance Document, 2009.

T24 Grell, G. A.; Dudhia, J.; Stauffer, D.. A description of the Fifth-Generation Penn State/NCARMesoscaleModel (MM5). NCAR Tech. Note NCAR/TN-3981STR, 122 pp, 1994.

T25 O'Connor, F.M.; Carver, G.D.; Savage, N.H.; Pyle, J.A.; Methven, J.; Arnold, S.R.; Dewey, K.; Kent, J. Comparison and visualisation of high-resolution transport modelling with aircraft measurements. *Atmospheric Science Letters*. **2005,** 6 (3), 164-170.

T26 Cook, P.A.; Savage, N.H.; Turquety, S.; Carver, G.D.; O'Connor, F.M.; Heckel, A.; Stewart, D.; Whalley, L.K.; Parker, A.E.; Schlager, H.; Singh, H.B.; Avery, M.A.; Sachse, G.W.; Brune, W.; Richter, A.; Burrows, J.P.; Purvis, R.; Lewis, A.C.; Reeves, C.E.; Monks, P.S.; Levine, J.G.; Pyle, J.A. Forest fire plumes over the North Atlantic: p-TOMCAT model simulations with aircraft and satellite measurements from the ITOP/ICARTT campaign. *Journal of Geophysical Research D: Atmospheres.* **2007,** 112 (10), D10S43.

T27 Law, K. S.; Plantevin, P. -H.; Shallcross, D. E.; Rogers H. L.; Pyle, J. A.; Grouhel, C.; Thouret, V.; Marenco, A. Evaluation of modeled O3 using Measurement of Ozone by Airbus In-Service Aircraft (MOZAIC) data. *J. Geophys. Res*. **1998,** 103 (25), 721–737.

T28 Law, K. S .; Plantevin, P. -H .; Thouret, V .; Marenco, A .; Asman, W. A. H .; Lawrence, M .; Crutzen P. J .; Muller, J. -F .; Hauglustaine, D. A .; Kanakidou, M.: Comparison between global chemistry transport model results and Measurement of Ozone by Airbus In-Service Aircraft (MOZAIC) data. *J. Geophys. Res.* **2000,** 105, 1503–1525.

T29 Savage, N.H.; Law, K.S.; Pyle, J.A.; Richter, A.; Nub, H.; Burrows, J.P. Using Gome NO_2 satellite data to examine regional differences in TOMCAT model performance. *Atmos. Chem. Phys.* **2004**, 4, 2569-2613.

T30 Law, K.S.; Pyle, J.A. Modeling Trace Gas Budgets in the Toposphere. *J. Geophys. Res.-Atmos.* **1993,** 98, 18401-18412.

T31 Berglen, T. F .; Berntsen, T. K .; Isaksen, I. S. A .; Sundet, J. K. A global model of the coupled sulfur/oxidant chemistry in the troposphere: The sulfur cycle. *J. Geophys. Res.-Atmos.* **2004,** 109, doi:10.1029/2003JD003948.

T32 Brunner, D .; Staehelin, J .; Rogers, H. L .; Kohler, M. O .; Pyle, J. A .; Hauglustaine, D .; Jourdain, L .; Berntsen, T. K .; Gauss, M .; Isak-sen, I. S. A .; Meijer, E .; van Velthoven, P .; Pitari, G .; Mancini, E .; Grewe, V .; Sausen, R. An evaluation of the performance of chemistry transport models by comparison with research aircraft observations, Part 1: Concepts and overall model performance. *Atmos. Chem. Phys.* **2003,** 3, 1609–1631.

T33 Brunner, D .; J. Staehelin, H.L.; Rogers, M.O.; Kohler, J.A.; Pyle, D.A.; Hauglustaine, L.; Jourdain, T.K.; Bernsten, M.; Gauss, I.S.A.; Isaksen, E.; Meijer, P.; Van Velthoven, G.; Pitari, E.Mancini,; V. Grewe,; R. Sausen, An evaluation of the performance of chemistry transport models - Part 2: Detailed comparison with two selected campaigns. *Atmos. Chem. Phys.* **2005,** 5, 107–129.

T34 Lee, D.S.; Fahey, D.W.; Forster, P.M.; Newton, P.J.; Wit, R.C.N.; Lim, L.L.; Owen, B.; Sausen, R. Aviation and global climate change in the 21st century. *Atmospheric Environment*. **2009,** 43 (22-23), 3520-3537.

T35 Stratton, R.W.; Wong, H.M.; and Hileman, J.I. *Life Cycle Greenhouse Gas emissions from Alternative Jet Fuels.* PARTNER, 2010.

T36 Charlson, R.J.; S.E. Schwartz; J.M. Hales; R.D. Cess; J.A. Coakley, Jr.; J.E. Hansen; D.J. Hoffman. Climate forcing by anthropogenic aerosols. *Science*. **1992,** 255, 423-430.

T37 Wang, J.; Jacob, D.J.; Martin, S.T. Sensitivity of sulfate direct climate forcing to the hysteresis of particle phase transitions. *J. Geophys. Res.* **2008,** 113, D11207.

T38 J. H. Seinfeld, S. N. Pandis. *Atmospheric Chemistry and Physics*; John Wiley & Sons, Inc.: Hoboken, NJ, 2006.

T39 Heald, C. GEOS-Chem Optics Description, 2010.

T40 Kiehl, J.T.; Schneider, T.L.; Rasch, P.J.; Barth, M.C. Radiative forcing due to sulfate aerosols from simulations with the National Center for Atmospheric research Community Climate Model, Version 3. *J.* Geophys*. Res.* **2000,** 105*,* 1441-1458.

T41 Wiscombe, W.J.; Grams, G.W. The backscattered fraction in two-stream approximations. *J. Atmos. Sci.* **1976,** 33, 2440.

T42 Nemesure, S.; Wagener, R.; Schwartz, S.E. Direct shortwave forcing of climate by the anthropogenic sulfate aerosol: Sensitivity to particle size, composition, and relative humidity. *J. of Geophysical Research*. **1995,** 100 (D12), 26105-26116.

T43 Curci, G. FlexAOD, http://pumpkin.aquila.infn.it/flexaod/.

T44 Adams, P.J.; Seinfeld, J.H.; Koch, D.; Mickley, L.; Jacob, D. General circulation model assessment of direct radiative forcing by the sulfate-nitrate-ammonium-water inorganic aerosol system. *J. of Geo. Res.* **2001,** 106 (D1), 1097-1111.

T45 IPCC. IPCC Third Assessment Report: Working Group I, The Scientific Basis, 2001.

T46 Penner, J.E.; Charlson, R.J.; Hales, J.M.; Laulainen, N.S.; Leifer, R.; Novakov, T.; Ogren, J.; Radke, L.F.; Schwartz, S.E.; Travis, L. Quantifying and Minimizing Uncertainty of Climate Forcing by Anthropogenic Aerosols. *Bulletin of the American Meteorological Society*. **1994,** 75, 375.

T47 IPCC. IPCC Fourth Assessment Report: Working Group I Report, The Physical Scientific Basis, 2007.

T48 Martin, S.T.; Hung H.-M.; Park, R.J.; Jacob D.J.; Spurr, R.J.D.; Chance, K.V. Chin, M. *Atmos. Chem. Phys.* **2004,** 4, 183-214.

T49 Liao, H.; Seinfel, J.H.; Adams, P.J.; Mickley, L.J. Global radiative forcing of coupled tropospheric ozone and aerosols in a unified general circulation model. *J. of Geo. Res.* **2004,** 109 (D16207), doi:10.1029/2003JD004456.

T50 Sausen, R.; Isaksen, I.; Grewe, V.; Hauglustaine, D.; Lee, D.S.; Myhre, G.; Kohler, M.O.; Pitari, G.; Schumann, U.; Stordal, F.; Zerefos, C. Aviation radiative forcing in 2000: an update of IPCC (1999). *Meteorol. Zeit*. **2005,** 114, 555–561.

T51 General Motors Corporation, Well-to-Tank Energy Use and Greenhouse Gas Emissions of Transportation Fuels - North American Analysis, Volume 3, General Motors Corporation,

Argonne National Labs, British Petroleum, Exxon Mobile, Shell, 2001; http://www.transportation.anl.gov/pdfs/TA/165.pdf (accessed October 12, 2009).

T52 Hileman, J. I.; Stratton, R. W.; Donoho, P. E. Energy Content and Alternative Jet Fuel Viability *Journal of propulsion and power.* **2010,** 26 (6), 1184-1195.

T53 Marais, K.; Lukachko, S.P.; Jun, M.; Mahashabde, A.; Waitz, I.A. Assessing the impact of aviation on climate. *Meterologische Zeitschrift*. **2008,** 17 (2), 157-172.

T54 Mahashabde, A. Assessing Environmental Benefits and Economics Costs of Aviation Environmental Policy Measures. Ph.D. Dissertation, Massachusetts Institute of Technology, Cambridge, MA, 2009.

T55 Shine, K.P.; Fuglestvedt, J.S.; Hailemariam, K.; Stuber, N. Alternatives to the global warming potential for comparing climate impacts of emissions of greenhouse gases. *Climatic Change.* **2005,** 68(3), 281-302.

T56 W. D. Nordhaus. *A Question of Balance: Weighing the Options on Global Warming Policies*. Yale University Press, New Haven, 2008.

T57 US Environmental Protection Agency. *The Benefits and Costs of the Clean Air Act: 1990 to 2020*. Washington, DC: Office of Air and Radiation; 2011.

T58 Pope, C. A., 3rd; Thun, M. J.; Namboodiri, M. M.; Dockery, D. W.; Evans, J. S.; Speizer, F. E.; Heath, C. W., Jr., Particulate air pollution as a predictor of mortality in a prospective study of U.S. adults. *Am J Respir Crit Care Med* **1995,** *151*, (3 Pt 1), 669-674.

T59 Pope, C. A.; Burnett, R. T.; Thun, M. J.; Calle, E. E.; Krewski, D.; Ito, K.; Thurston, G. D., Lung cancer, cardiopulmonary mortality, and long-term exposure to fine particulate air pollution. *JAMA* **2002,** *287*, (9), 1132-1141.

T60 Dockery, D. W.; Pope, C. A.; Xu, X.; Spengler, J. D.; Ware, J. H.; Fay, M. E.; Ferris, B. G. J.; Speizer, F. E., An association between air pollution and mortality in six U.S. cities. *N Engl J Med* **1993,** *329*, (24), 1753-1759.

T61 Laden, F.; Schwartz, J.; Speizer, F. E.; Dockery, D. W., Reduction in fine particulate air pollution and mortality: Extended follow-up of the Harvard Six Cities study. *Am J Respir Crit Care Med* **2006,** *173*, (6), 667-672.

T62 Industrial Economics *Expanded expert judgment assessment of the concentration-response relationship between PM2.5 exposure and mortality*; Prepared for Office of Air Quality Planning and Standards, U.S. Environmental Protection Agency: Cambridge, MA, 2006.

T63 Pope III, C.A.; Dockery, D.W. Health effects of fine particulate air pollution: Lines that connect. *Journal of the Air and Waste Management Association*, **2006,** 56 (6), 709-742.

T64 Brauer, M.; Avila-Casado, C.; Fortoul, T.I.; Vedal, S.; Stevens, B.; Churg, A. Air Pollution and Retained Particles in the Lung. *Environ. Health Perspect*. **2001,** 109, 1039-1043.

T65 Churg, A.; Brauer, M.; Avila-Casada, C.; Fortoul, T.I.; Wright, J.L. Chronic Exposure to High Levels of Particulate Air Pollution and Small Airway Remodeling. *Environ. Health Perspect*. **2003,** 111, 714-718.

T66 Libby, P.; Ridker, P.M.; Maseri, A. Inflammation and Atherosclerosis. *Circulation*. **2002,** 105, 1135-1143.

T67 Cohen, A.J.; Pope, C.A., III. Lung Cancer and Air Pollution. *Environ. Health Perspect.* **1995,** 103, 219-224.

T68 Samet, J.M.; Cohen, A.J. Air Pollution and Lung Cancer. In Air Pollution and Health; Holgate, S.T.; Samet, J.M.; Koren, H.S.; Maynard, R.L., Eds.; Academic Press: London, United Kingdom, 1999; 841-864.

T69 Cohen, A.J. Air Pollution and Lung Cancer: What More Do We Need to Know?. *Thorax*. **2003,** 58, 1010-1012.

T70 Schwartz, J.; Coull, B.; Laden, F.; Ryan, L., The effect of dose and timing of dose on the association between airborne particles and survival. *Environ Health Perspect.* **2008,** *116*, (1), 64-69.

T71 Reiss, R.; Anderson, E. L.; Cross, C. E.; Hidy, G.; Hoel, D.; McClellan, R.; Moolgavkar, S., Evidence of health impacts of sulfate- and nitrate-containing particles in ambient air. *Inhal Toxicol.* **2007,** *19*, (5), 419-449.

T72 Luttmann-Gibson, H.; Suh, H. H.; Coull, B. A.; Dockery, D. W.; Sarnat, S. E.; Schwartz, J.; Stone, P. H.; Gold, D. R., Short-term effects of air pollution on heart rate variability in senior adudts in Steubenville, Ohio. *Journal of Occupational and Environmental Medicine.* **2006,** *48*, (8), 780-788.

T73 Sarnat, S. E.; Suh, H. H.; Coull, B. A.; Schwartz, J.; Stone, P. H.; Gold, D. R., Ambient particulate air pollution and cardiac arrhythmia in a panel of older adults in Steubenville, Ohio. *Occupational and Environmental Medicine.* **2006,** *63*, (10), 700-706.

T74 O'Neill, M. S.; Veves, A.; Zanobetti, A.; Sarnat, J. A.; Gold, D. R.; Economides, P. A.; Horton, E. S.; Schwartz, J., Diabetes enhances vulnerability to particulate air pollution - Associated impairment in vascular reactivity and endothelial function. *Circulation* **2005,** *111*, (22), 2913-2920.

T75 US Environmental Protection Agency Science Advisory Board Advisory on Plans for Health Effects Analysis in the Analytical Plan for EPA's Second Prospective Analysis -

Benefits and Costs of the Clean Air Act, 1990-2020; EPA-SAB-COUNCIL-ADV-04-002; Washington, DC, 2004.

T76 Hedley, A.J.; Wong, C.-M.; Thach, T.Q.; Ma, S.; Lam, T.-H.; Anderson, H.R. Cardiorespiratory and all-cause mortality after restrictions on sulphur content of fuel in Hong Kong: An intervention study. *Lancet*. **2002,** 360 (9346), 1646-1652.

T77 Center for International Earth Science Information Network (CIESIN), Centro Internacional de Agricultura Tropical (CIAT). *Global Rural-Urban Mapping Project (GRUMP).* Columbia University, 2004.

T78 World Health Organization. *Global Burden of Disease (GBD)*; http://www.who.int/healthinfo/global_burden_disease/en/.

T79 B. Ostro. Outdoor air pollution: Assessing the environmental burden of disease at national and local levels. Environmental Burden of Disease Series, No. 5 World Health Organization, 2004.

T80 Barrett, S.R.H.; Britter, R.E.; Waitz, I.A. Global mortality attributable to aircraft cruise emissions. *Environmental Science and Technology*. **2010,** 44 (19), 7736-7742.

T81 US Census Bureau. *International Data Base (IDB)*; http://www.census.gov/population/international/data/idb/informationGateway.php.

T82 US Environmental Protection Agency. *Guidelines for Preparing Economic Analyses*. EPA, 2010.

T83 Miller, T.R. Variations between countries in values of statistical life. *Journal of Transport Economics and Policy*. **2000,** 34 (2), 169-188.

T84 Viscusi, W.K.; Aldy, J.E. The Value of a Statistical Life: A Critical Review of Market Estimates Throughout the World (2003) Journal of Risk and Uncertainty, 27 (1), 5-76.

T85 Hammitt, J.K.; Robinson, L.A. The Income Elasticity of the Value per Statistical Life: Transferring Estimates between High and Low Income Populations. *Journal of Benefit-Cost Analysis*. **2011,** 2(1).

T86 US Department of Transportation. Treatment of the Value of Preventing Fatalities and Injuries in Preparing Economic Analyses: http://ostpxweb.dot.gov/policy/reports/080205.htm.

T87 The World Bank. *GNI per capita, PPP*; http://data.worldbank.org/indicator/NY.GNP.PCAP.CD.

T88 US Energy Information Administration; http://www.eia.gov/.

T89 Argonne National Laboratory. *GREET Model v1.8A*; http://greet.es.anl.gov/.

T90 Gary, J.H.; Handwerk, G.E.; Kaiser, M.J. *Petroleum Refining: Technology and Economics*, 5th, ed; CRC Press: Boca Raton, Fl, 2007.

T91 Department Of Treasury Internal Revenue Service. *Publication 946: How to Depreciate Property*. Department of Treasury, Washington, DC, 2009.

T92 Allaire, D.; Willcox, K. Surrogate modeling for uncertainty assessment with application to aviation environmental system models. *AIAA Journal*. **2010,** 48 (8), 1791-1803.

T93 Interagency Working Group on Social Cost of Carbon United States Government. *Appendix 15A. Social Cost of Carbon for Regulatory Impact Analysis Under Executive Order 12866*, 2010.

T94 Schwartz, S.E. Heat capacity, time constant, and sensitivity of Earth's climate system. *J. Geosphys. Res.* **2007,** 112 (24), D24S05.

T95 Jun, Mina. Uncertainty Analysis of an Aviation Climate Model and an Aircraft Price Model for Assessment of Environmental Effects. Masters Thesis, Massachusetts Institute of Technology, Cambridge, MA, 2007.

T96 Saltelli, A.; Ratto, M.; Andres, T.; Campolongo, F.; Cariboni, J.; Gatelli, D.; Saisana, M.; Tarantola, S. *Global Sensitivity Analysis: The Primer*; Wiley and Sons: England, 2008.

T97 ExxonMobil Aviation. *World Jet Fuel Specifications: 2005 Edition*. Exxon Mobil, U.S., 2005.

T98 Defense Energy Support System. *Petroleum Quality Information System*, 2008.

T99 Phelan, P. 'Green' fuel sparks off fears of engine failure. *Flight International*, 17-23 August 1994.

T100 Coordinating Research Council, Inc. *CRC Fuel Lubricity Workshop*. CRC, Alexandria, VA, 1996.

T101 Coordinating Research Council, Inc. *CRC Fuel Lubricity Workshop*. CRC, Alexandria, VA, 1996.

T102 Baniszewski, D. "Question about cost of CI/LI additive for JP-8." Correspondence with Hileman, J. November 16, 2010.

T103 US Geological Survey. *Sulfur Statistics and Information*; http://minerals.usgs.gov/minerals/pubs/commodity/sulfur/index.html#mcs.

T104 Wang, Y., Logan, J. A.; Jacob, D. J. Global simulation of tropospheric O3-NOx-hydrocarbon chemistry, 2. Model evaluation and global ozone budget. *J. Geophys. Res.* **1998,** 103/D9, 10,727-10,756.

T105 Jacob, D. J.; Crawford, J. H.; Kleb, M. M.; Connors, V. S.; Bendura, R. J.; Raper, J. L.; Sachse, G. W.; Gille, J. C.; Emmons, L.; Heald, C. L. The Transport and Chemical Evolution over the Pacific (TRACE-P) aircraft mission: design, execution, and first results. *J. Geophys. Res.* **2003,** 108, 9000, DOI: 10.1029/2002JD003276.

T106 Carbon Dioxide Information Analysis Center. *The Environmental Measurements Laboratory's Stratospheric Radionuclide Database (RANDAB)*; http://cdiac.ornl.gov/epubs/db/db1019/db1019.html.

T107 National Urban Security Technology Laboratory. *Surface Air Sampling Program (SASP)*; http://www.eml.st.dhs.gov/databases/.

T108 Stull, R. B. (2003), *An introduction to boundary layer meteorology*, Kluwer Academic, Boston.

T109 Holton, J. (2004), *An introduction to dynamic meteorology*, 4 ed., 535 , Elsevier Academic Press, Burlington, MA.

T110 Holton, J.; Haynes, P.; McIntyre, M.; Douglass, A.R.; Rood, R.; Pfister, L. Stratosphere-troposphere exchange, *Rev Geophys*, **1995,** 33 (4), 403-439.

T111 Bey, I.; Jacob, D.J.; Yantosca, R.M.; Logan, J.A.; Field, B.; Fiore, A.M.; Li, Q.; Liu, H.; Mickley, L.J.; Schultz, M. Global modeling of tropospheric chemistry with assimilated meteorology: Model description and evaluation. *J Geophys Res*, **2001,** 106 (D19), 23073-23095.

T112 Zhu, Y.; Gelaro, R. Observation sensitivity calculations using the adjoint of the Gridpoint Statistical Interpolation (GSI) analysis system. *Mon Weather Rev*, **2008,** 136 (1), 335-351.

T113 Lin, S.; Rood, R. Multidimensional flux-form semi-Lagrangian transport schemes, *Mon Weather Rev*, **1996,** 124 (9), 2046-2070.

T114 Lin, S. Description of the parameterization of cumulus transport in the 3D Goddard chemistry transport model. *Rep.*, **1996** NASA/GSFC.

T115 Moorthi, S.; Suarez, M. Relaxed Arakawa-Schubert – a parameterization of moist convection for general circulation models. *Mon Weather Rev*. **1992,** 120 (6), 978-1002.

T116 Lin, J.-T.; Youn, D.; Liang, X.-Z.; Wuebbles, D.J. Global model simulation of summertime US ozone diurnal cycle and its sensitivity to PBL mixing, spatial resolution, and emissions. *Atmospheric Environment*. **2008,** 42 (36), 8470-8483.

T117 Allen, D. J.; Rood, R.; Thompson, A.M.; Hudson, R. Three-dimensional radon 222 calculations using assimilated meteorological data and a convective mixing algorithm. *J Geophys Res*. **1996,** 01(D3), 6871-6881.

T118 Brost, R.; Chatfield, R. Transport of radon in a 3-dimensional, subhemispheric model. *J Geophys Res*. **1989,** 94 (D4), 5095-5119.

T119 Considine, D.; Bergmann, D.J.; Liu, H. Sensitivity of Global Modeling Initiative chemistry and transport model simulations of radon-222 and lead-210 to input meteorological data. *Atmos Chem Phys*. **2005,** 5, 3389-3406.

T120 Feichter, J.; Crutzen, P.J. Parameterization of vertical tracer transport due to deep cumulus convection in a global transport model and its evaluation with 222Radon measurements. *Tellus B*. **1990,** 42 (1), 100-117.

T121 Hauglustaine, D. A. Interactive chemistry in the Laboratoire de Météorologie Dynamique general circulation model: Description and background tropospheric chemistry evaluation. *J Geophys Res*. **2004,** 109 (D4), D04314.

T122 Jacob, D. J.; Prather, M.J. Radon-222 as a test of convective transport in a general circulation model. *Tellus B*. **1990,** 42 (1), 118-134.

T123 Jacob, D. J., et al. Evaluation and intercomparison of global atmospheric transport models using Rn-222 and other short-lived tracers. *J Geophys Res*. **1997,** 102 (D5), 5953-5970.

T124 Lambert, G.; Polian, G.; Sanak, J.; Ardouin, B.; Buisson, A.; Jegou, A.; Leroulley, J. Cycle du radon et de ses descendants: application à l'étude des échanges troposphère-stratosphère. *Ann Geophys*. **1982,** 38 (4), 497-531.

T125 Mahowald, N. M.; Rasch, P.; Prinn, R.G. Cumulus parameterizations in chemical transport models. *J Geophys Res*. **1995,** 100 (D12), 26173-26189.

T126 Stockwell, D.; Kritz, M.; Chipperfield, M.P.; Pyle, J.A. Validation of an off-line three-dimensional chemical transport model using observed radon profiles - 2. Model results. *J Geophys Res*. **1998,** 103 (D7), 8433-8445.

T127 Wexler, H.; Machta, L.; Pack, D.H.; White, F.D. Atomic energy and meteorology, paper presented at First Intern. Conf. Peaceful Uses At. Energy, Geneva, 1956.

T128 Kirichenko, L. V. The vertical distribution of the products of decay of radon in the free atmosphere. *Problems of Nuclear Meteorology*. **1962,** edited, 92-124.

T129 Bradley, W.; Pearson, J. Aircraft measurements of vertical distribution of radon in lower atmosphere. *J Geophys Res*. **1970,** 75 (30), 5890-&.

T130 Nazarov, L. E.; Kuzenkov, A.F.; Malakhov, S.G.; Volokitina, L.A.; Gaziyev, Y.I.; Vasil'yev A. Radioactive aerosol distribution in middle and upper troposphere over USSR in 1963-1968. *J Geophys Res*. **1970,** 75 (18), 3575-&.

T131 Wilkening, M. H. Rn-222 concentration in convective patterns of a mountain environment. *J Geophys Res*. **1970,** 75 (9), 1733-&.

T132 Moore, H.; Poet, S.; Martell, E. Rn-222, Pb-210, Bi-210, and Po-210 profiles and aerosol residence times versus altitude. *J Geophys Res*. **1973,** 78 (30), 7065-7075.

T133 Kritz, M.; Rosner, S.; Stockwell, D. Validation of an off-line three-dimensional chemical transport model using observed radon profiles - 1. Observations. *J Geophys Res*. **1998,** 103 (D7), 8425-8432.

T134 Lal, D. M.; Malhotra, P.; Peters, B. On the production of radioisotopes in the atmosphere by cosmic radiation and their application to meteorology. *J Atmos Terr Phys*. **1958,** 12 (4), 306-328.

T135 Bondietti, E.; Brantley, J.; Rangarajan, C. Size distributions and growth of natural and Chernobyl-derived sub-micron aerosols in Tennessee. *J Environ Radioactiv*. **1998,** 6 (2), 99-120.

T136 Maenhaut, W.; Zoller, W.; Coles, D. Radionuclides in the south pole atmosphere. *J Geophys Res-Oc Atm*. **1979,** 84 (NC6), 3131-3138.

T137 Papastefanou, C. Beryllium-7 Aerosols in Ambient Air. *Aerosol Air Qual Res*. **2009,** 9 (2), 187-197.

T138 Papastefanou, C.; Joannidou, A. Beryllium-7 aerosols in ambient air. *Environment International*. **1996,** *22*, 125-130.

T139 Sanak, J.; Gaudry, A.; Lambert, G. Size distribution of Pb-210 aerosols over oceans. *Geophys Res Lett*. **1981,** 8 (10), 1067-1069.

T140 Allen, D. J.; Dibb, J.E.; Ridley, B.; Pickering, K.E.; Talbot, R.W. An estimate of the stratospheric contribution to springtime tropospheric ozone maxima using TOPSE measurements and beryllium-7 simulations. *J Geophys Res*. **2003,** 108 (D4), 8355.

T141 Brost, R.; Feichter, J.; Heimann, M. 3-dimensional simulation of Be-7 in a global climate model. *J Geophys Res*. **1991,** 96 (D12), 22423-22445.

T142 Koch, D.; Jacob, D.J.; Graustein, W. Vertical transport of tropospheric aerosols as indicated by Be-7 and Pb-210 in a chemical tracer model. *J Geophys Res*. **1996,** 101 (D13), 18651-18666.

T143 Liu, H., Jacob, D.J.; Bey, I.; Yantosca, R.M. Constraints from Pb-210 and Be-7 on wet deposition and transport in a global three-dimensional chemical tracer model driven by assimilated meteorological fields. *J Geophys Res*. **2001,** 106 (D11), 12109-12128.

T144 Usoskin, I. G.; Kovaltsov, G.A. Production of cosmogenic Be-7 isotope in the atmosphere: Full 3-D modeling. *J Geophys Res*. **2008,** 113 (D12), D12107.

T145 Smart, D.; Shea, M. A review of geomagnetic cutoff rigidities for earth-orbiting spacecraft. *Adv Space Res*. **2005,** 36 (10), 2012-2020.

T146 Lal, D. M.; Peters, B. Cosmic ray produced radioactivity on the Earth. *Hanbuch der Physik*. **1967,** edited by K. Sitte, 551-612, Springer-Verlag, New York.

T147 Lal, D. M.; Suess, H. Radioactivity of atmosphere and hydrosphere. *Ann Rev Nucl Sci*. **1968,** 18, 407-&.

T148 O'Brien, K. Secular variations in the production of cosmogenic isotopes in thte Earth's atmosphere. *J Geophys Res-Space*. **1979,** 84 (NA2), 423-431.

T149 O'Brien, K.; de La Zerda, A.; Shea, M.; Smart, D. The production of cosmogenic isotopes in the Earth's atmosphere and their inventories, in *The Sun in Time*, edited by C. P. Sonett and M. S. Giampapa, **1991,** 317-342, Univ. of Ariz. Press, Tucson.

T150 Masarik, J.; Beer, J. Simulation of particle fluxes and cosmogenic nuclide production in the Earth's atmosphere. *J Geophys Res*. **1999,** 104 (D10), 12099-12111.

T151 Nagai, H.; Tada, W.; Kobayashi, T. Production rates of Be-7 and Be-10 in the atmosphere. *Nucl Instrum Meth B*. **2000,** 172, 796-801.

T152 Webber, W. R., Higbie, P. Production of cosmogenic Be nuclei in the Earth's atmosphere by cosmic rays: Its dependence on solar modulation and the interstellar cosmic ray spectrum. *J Geophys Res-Space*. **2003,** 108 (A9), 1355.

T153 Webber, W. R.; Higbie, P.R.; McCracken, K.G. Production of the cosmogenic isotopes H-3, Be-7, Be-10, and Cl-36 in the Earth's atmosphere by solar and galactic cosmic rays. *J Geophys Res-Space*. **2007,** 112 (A10), A10106.

T154 Liu, H.; Considine, D.; Horowitz, L.W.; Crawford, J.H.; Strahan, S.; Damon, M.R.; Rodriguez, J.M.; Xu, X.; Carouge, C.; Yantosca, R.M. Using beryllium-7 to assess cross-tropopause transport in global models. *J Geophys Res*. Submitted.

T155 Environmental Measurements Laboratory. *Stratospheric Radionuclide (RANDAB) and Trace Gas (TRACDAB) Databases*; http://cdiac.ornl.gov/ndps/db1019.html.

T156 Usoskin, I. G.; Alanko-Huotari, K.; Kovaltsov, G.A.; Mursula, K. Heliospheric modulation of cosmic rays: Monthly reconstruction for 1951-2004. *J Geophys Res-Space*. **2005,** 110 (A12), A12108.

T157 Balkanski, Y. J.; Jacob, D.J.; Gardner, G.; Graustein, W.; Turekian, K. Transport and residence times of tropospheric aerosols inferred from a global 3-dimensional simulation of Pb-210. *J Geophys Res*. **1993,** 98 (D11), 20573-20586.

T158 Preiss, N.; Genthon, C. Use of a new database of lead 210 for global aerosol model validation. *J Geophys Res*. **1997,** 102 (D21), 25347-25357.

T159 Preiss, N.; Melieres, M.; Pourchet, M. A compilation of data on lead 210 concentration in surface air and fluxes at the air-surface and water-sediment interfaces. *J Geophys Res*. **1996,** 101 (D22), 28847-28862.

T160 Laboratoire Glaciologie et Geophysique Environnement. *Database on Lead 210*; http://www-lgge.ujf-grenoble.fr/axes/radioactivite/Pb210_database/.

T161 Fukuda, K.; Tsunogai, S. Pb-210 in precipitation in Japan and its implications for transport of continental aerosols across ocean. *Tellus*. **1975,** 27 (5), 514-521.

T162 Turekian, K.; Nozaki, Y.; Benniger, L. Geochemistry of atmospheric radon and radon products. *Annu Rev Earth Pl Sc*. **1997,** 5, 227-255.

T163 Guelle, W.; Balkanski, Y.J.; Dibb, J.E.; Schulz, M.; Dulac, F. Wet deposition in a global size-dependent aerosol transport model 2. Influence of the scavenging scheme on Pb-210 vertical profiles, surface concentrations, and deposition. *J Geophys Res*. **1991a,** 103 (D22), 28875-28891.

T164 Guelle, W.; Balkanski, Y.J.; Schulz, M.; Dulac, F.; Monfray, P. Wet deposition in a global size-dependent aerosol transport model - 1. Comparison of a 1 year Pb-210 simulation with ground measurements. *J Geophys Res*. **1998b,** 103 (D10), 11429-11445.

T165 Baskaran, M.; Coleman, C.; Santschi, P.H. Atmospheric depositional fluxes of Be-7 and Pb-210 at Galveston and College Station, Texas. *J Geophys Res*. **1993,** 98 (D11), 20555-20571.

T166 Bleichrodt, J. Mean tropospheric residence time of cosmic-ray-produced beryllium-7 at north temperate latitudes. *J Geophys Res-Oc Atm*. **1978,** 83 (NC6), 3058-3062.

T167 Brown, L.; Stensland, G.; Klein, J.; Middleton, R. Atmospheric deposition of Be-7 and Be-10. *Geochim Cosmochim Ac*. **1989,** 53 (1), 135-142.

T168 Dibb, J. E. Atmospheric deposition of beryllium-7 in the Chesapeake Bay region. *J Geophys Res*. **1989,** 94 (D2), 2261-2265.

T169 Du, J.; Zhang, J.; Zhang, J.; Wu, Y. Deposition patterns of atmospheric Be-7 and Pb-210 in coast of East China Sea, Shanghai, China. *Atmospheric Environment*. **2008,** 42 (20), 5101-5109.

T170 Harvey, M.; Matthews, K. Be-7 deposition in a high-rainfall area of New Zealand. *J Atmos Chem*. **1989,** 8 (4), 299-306.

T171 Hasebe, N.; Doke, T.; Kikuchi, J.; Takeuchi, Y.; Sugiyama, T. Observation of fallout rates of atmospheric Be-7 and Na-22 produced by cosmic rays concerning estimation of the fallout of atmospheric Al-26. *J Geophys Res-Space*. **1981,** 86 (NA2), 520-524.

T172 Hirose, K.; Honda, T.; Yagishita, S.; Igarashi, Y.; Aoyama, M. Deposition behaviors of Pb-210, Be-7 and thorium isotopes observed in Tsukuba and Nagasaki, Japan. *Atmospheric Environment*. **2004,** 38 (38), 6601-6608.

T173 Igarashi, Y.; Hirose, I.; Otsuji-Hatori, M. Beryllium-7 deposition and its relation to sulfate deposition. *J Atmos Chem*. **1998,** 29 (3), 217-231.

T174 Narazaki, Y.; Fujitaka, K. The Geographical Distribution and Features of 7Be Deposition in Japan. *Japan Health Physics Society*. **2002,** 37 (4), 317-324.

T175 Nijampurkar, V.; Rao, D. Polar fallout of radionuclides Si-32, Be-7 and Pb-210 and past accumulation rate of ice at Indian Station, Dakshin Gangotri, East Antarctica. *J Environ Radioactiv*. **1993,** 21 (2), 107-117.

T176 Olsen, C.; Larsen, I.; Lowry, P.; Cutshall, N.; Todd, J.; Wong, G.; Casey, W. Atmospheric fluxes and marsh soil inventories of Be-7 and Pb-210. *J Geophys Res*. **1985,** 90 (ND6), 10487-10495.

T177 Papastefanou, C.; Ioannidou, A.; Stoulos, S.; Manolopoulou, M. Atmospheric deposition of cosmogenic Be-7 and Cs-137 from fallout of the Chernobyl accident. *Sci Total Environ*. **1995,** 170 (1-2), 151-156.

T178 Schuler, C., et al. A Multitracer Study of Radionuclides in Lake Zurich, Switzerland 1. Comparison of Atmospheric and Sedimentary Fluxes of 7Be, 10Be, 210Pb, 210Po, and 137Cs. *J Geophys Res*. **1991,** 96 (C9), 17051-17017,17065.

T179 Turekian, K.; Benniger, L.; Dion, E. Be-7 and Pb-210 total deposition fluxes at New Haven, Connecticut and Bermuda. *J Geophys Res-Oc Atm*. **1983,** 88 (NC9), 5411-5415.

T180 Wallbrink, P.; Murray, A. Fallout of Be-7 in south eastern Australia. *J Environ Radioactiv*. **1994,** 25 (3), 213-228.

T181 Dibb, J. E.; Talbot, R.W.; Gregory, G. Beryllium-7 and Pb-210 in the western hemisphere arctic atmosphere – observations from 3 recent aircraft-based sampling programs. *J Geophys Res*. **1992,** 97 (D15), 16709-16715.

T182 Dibb, J. E.; Meeker, L; Finkel, R.; Southon, J.; Caffee, M.; Barrie, L. Estimation of stratospheric input to the arctic troposphere – Be-7 and Be-10 in aerosols at Alert, Canada. *J Geophys Res*. **1994,** 99 (D6), 12855-12864.

T183 Husain, L.; Coffey, P.; Meyers, R.; Cederwall, R. Ozone transport from stratosphere to troposphere. *Geophys Res Lett*. **1977,** 4 (9), 363-365.

T184 Rehfeld, S.; Heimann, M. Three dimensional atmospheric transport simulation of the radioactive tracers Pb-210, Be-7, Be-10, and Sr-90. *J Geophys Res*. **1995,** 100 (D12), 26141-26161.

T185 Viezee, W.; Singh, H.B. The distribution of beryllium-7 in the troposphere – implications on stratospheric-tropospheric air exchange. *Geophys Res Lett*. **1980,** 7 (10), 805-808.

T186 Dutkiewicz, V.; Husain, L. Stratospheric and tropospheric components of Be-7 in surface air. *J Geophys Res*. **1985,** 90 (ND3), 5783-5788.

T187 National Urban Security Technology Laboratory. *Surface Air Sampling Program (SASP)*; http://www.eml.st.dhs.gov/databases/.

T188 Whitt, D.B.; Jacobson, M.Z.; Wilkerson, J.T. Vertical mixing of commercial aviation emissions from cruise altitude to the surface. *Journal of Geophysical Research*, In Press.